TECHNICAL REPORT STANDARD PAGE

1. Title and Subtitle

Application of Mechanistic-Empirical Pavement Design Approach into RCC Pavement Thickness Design

2. Author(s)

Zhong Wu, Ph.D., P.E., and Moinul Mahdi, Ph.D.

3. Performing Organization Name and Address

Department of Civil and Environmental Engineering

Louisiana State University

Baton Rouge, LA 70803

4. Sponsoring Agency Name and Address

Louisiana Department of Transportation and Development

P.O. Box 94245

Baton Rouge, LA 70804-9245

5. Report No.

FHWA/LA.22/671

6. Report Date

December 2022

7. Performing Organization Code

LTRC Project Number: 19-1P

SIO Number: DOTLT1000271

8. Type of Report and Period Covered

Final Report

June 2019 – May 2022

9. No. of Pages

159

10. Supplementary Notes

Conducted in Cooperation with the U.S. Department of Transportation, Federal Highway Administration

11. Distribution Statement

Unrestricted. This document is available through the National Technical Information Service, Springfield, VA 21161.

12. Key Words

Roller compacted concrete, cracking, pavement performance, fatigue analysis, thickness design

13. Abstract

As a durable, economical, and low-maintenance concrete material, roller compacted concrete (RCC) is steadily becoming the preferred choice for many highway pavement applications. However, the current RCC pavement thickness design procedures are solely empirically based, not following the state-of-practice of the mechanistic-empirical (M-E) pavement design approach. In addition, the fatigue models used in the available RCC pavement thickness design procedures have generally been found to over-predict pavement fatigue damage under in situ heavy truck loading.

In this study, the field fatigue performance of RCC pavements were determined from an accelerated pavement testing (APT) experiment on six full-scale RCC pavement sections. Load-induced pavement responses and temperature-related strains were monitored using two embedded fiber-optical strain plates and verified using in situ non-destructive test results and finite element modeling. To further evaluate the performance of RCC fatigue cracking, a comprehensive beam fatigue test experiment was performed using 68 field saw-cut RCC slab samples from APT sections to investigate the fatigue behavior of in situ RCC pavements. This is the first research study to investigate the

fatigue behavior of field RCC beam samples prepared and constructed with a high-density asphalt-type paver and a vibratory roller. The results indicate that a well-compacted RCC pavement can achieve higher flexural strength and exhibit better fatigue life than conventional concrete pavement. Based on the beam fatigue test results and in situ fatigue performance of APT test sections, an RCC fatigue-life model was developed, providing a more accurate solution for estimating the allowable number of load repetitions of RCC pavements subjected to vehicular fatigue loading. This model was then calibrated into an RCC pavement fatigue design transfer function based on the APT performance observed, which could be used in RCC thickness design procedures to determine the optimum RCC design thickness and long-term fatigue performance of RCC pavements for roadway application. Finally, a M-E based RCC pavement thickness design procedure was proposed in this study. The proposed M-E design procedure was based on the current AASHTO Pavement M-E Design framework and applied the research findings obtained in this study. Following the proposed design procedure, a step-by-step RCC thickness design example was presented.

Project Review Committee

Each research project will have an advisory committee appointed by the LTRC Director. The Project Review Committee is responsible for assisting the LTRC Administrator or Manager in the development of acceptable research problem statements, requests for proposals, review of research proposals, oversight of approved research projects, and implementation of findings.

LTRC appreciates the dedication of the following Project Review Committee Members in guiding this research study to fruition.

LTRC Administrator/Manager
Zhongjie "Doc" Zhang, Ph.D., P.E.
Pavement and Geotechnical Research Administrator

Members
Christophe Fillastre
Mark Ordogne
Jeffrey Lambert
Xingwei Chen
Jason Lacombe
Patrick Icenogle
Brandon Buckner, FHWA

Directorate Implementation Sponsor
Christopher P. Knotts, P.E.
DOTD Chief Engineer

Application of Mechanistic-Empirical Pavement Design Approach into RCC Pavement Thickness Design

By
Zhong Wu, Ph.D., P.E.
Moinul Mahdi, Ph.D.

Louisiana Transportation Research Center
4101 Gourrier Avenue
Baton Rouge, LA 70808

The contents of this report reflect the views of the author/principal investigator who is responsible for the facts and the accuracy of the data presented herein.

The contents do not necessarily reflect the views or policies of the Louisiana Department of Transportation and Development, the Federal Highway Administration or the Louisiana Transportation Research Center. This report does not constitute a standard, specification, or regulation.

December 2022

Abstract

As a durable, economical, and low-maintenance concrete material, roller compacted concrete (RCC) is steadily becoming the preferred choice for many highway pavement applications. However, the current RCC pavement thickness design procedures are solely empirically-based, not following the state-of-practice of the mechanistic-empirical (M-E) pavement design approach. In addition, the fatigue models used in the available RCC pavement thickness design procedures have generally been found to over-predict pavement fatigue damage under in situ heavy truck loading.

In this study, the field fatigue performance of RCC pavements were determined from an accelerated pavement testing (APT) experiment on six full-scale RCC pavement sections. Load-induced pavement responses and temperature-related strains were monitored using two embedded fiber-optical strain plates and verified using in situ non-destructive test results and finite element modeling.

To further evaluate the performance of RCC fatigue cracking, a comprehensive beam fatigue test experiment was performed using 68 field saw-cut RCC slab samples from APT sections to investigate the fatigue behavior of in situ RCC pavements. This is the first research study to investigate the fatigue behavior of field RCC beam samples prepared and constructed with a high-density asphalt-type paver and a vibratory roller. The results indicate that a well-compacted RCC pavement can achieve higher flexural strength and exhibit better fatigue life than conventional concrete pavement. Based on the beam fatigue test results and in situ fatigue performance of APT test sections, an RCC fatigue-life model was developed, providing a more accurate solution for estimating the allowable number of load repetitions of RCC pavements subjected to vehicular fatigue loading. This model was then calibrated into an RCC pavement fatigue design transfer function based on the APT performance observed, which could be used in RCC thickness design procedures to determine the optimum RCC design thickness and long-term fatigue performance of RCC pavements for roadway application.

Finally, a M-E based RCC pavement thickness design procedure was proposed. The proposed M-E design procedure was based on the current AASHTO Pavement M-E Design framework and applied the research findings obtained in this study. Following the proposed design procedure, a step-by-step RCC thickness design example was presented.

Acknowledgments

Implementation Statement

This study presents DOTD design engineers and pavement researchers with an M-E based analytical framework with procedures for the evaluation of RCC pavement performance and thickness design that may be implemented for RCC-surfaced roadway applications in Louisiana.

Table of Contents

List of Tables

List of Figures

Introduction

Problem Statement

Roller compacted concrete (RCC) is a stiff, low-slump concrete mixture that is placed with a modified asphalt paving equipment and compacted by vibratory rollers. A recently completed accelerated pavement testing study showed that a relatively thin RCC (4 ~ 6 in.) pavement built over an 8.5-in. soil cement base can provide outstanding load carrying capacity with excellent field performance and construction cost savings over an asphalt pavement alternative for a rural low-volume roadway design in Louisiana, where heavy and overloaded trucks are often abundant. With a proper mix design, improved paving compaction methods and surface texturing techniques, RCC is steadily becoming the choice for many pavement applications as a durable, economical and low-maintenance concrete material. However, existing RCC pavement design procedures (e.g., the Portland Cement Association (PCA) method and United States Army Cops of Engineering (USACE) procedure) are only applicable for the thickness design of heavy industrial pavements with RCC design thickness of 8 in. or higher. Moreover, there are no mechanistic-empirical (M-E) structural pavement design procedures currently available for an RCC pavement design. As DOTD's pavement design approach is in the transition from the 1993 AASHTO design procedure to the newly-calibrated pavement M-E method, there is an urgent need to develop a M-E based thickness design procedure for RCC pavement applications in Louisiana.

Literature Review

RCC Pavement

RCC pavement is well recognized as a unique type of rigid pavement that is placed and compacted by similar construction equipment (i.e., asphalt pavers and vibratory rollers) that used for flexible pavement construction. The American Concrete Association (ACI) describes RCC as a comparatively stiffer blend of concrete mix with dense aggregate gradation and lower water content compared to conventional concrete mixture [1]. Over the years, RCC has proven to be a great success in the construction arena of pavement and dam application since this material typically performs well in cold climates and has lesser curing period than conventional concrete. Primarily, the use of this special type of concrete has amplified as a cost-effective and heavy load resistance construction material for typical road and street applications. The most frequent utilization of RCC can be seen in interstate shoulders, minor collectors, and parking areas. Moreover, recent advancement in the compaction procedure of RCC pavement boosted the use of it even more in the subdivision residential streets and arterial roadways [1]. Additional worthy uses of RCC include composite RCC pavements with asphalt, lanes designed for heavy vehicles, and road intersections [2].

The history of RCC pavement aligns with the advancement of vibratory roller used for flexible pavement construction. Since 1970s, this unique pavement construction technology promptly initiated in Canada and the United States. Soon after, many states in the United States as well as other countries also experienced the application of RCC in airport runways, dams, parking lots and several other constructions, as a sustainable, economic, and rapid construction materials [3]. The first experimental low volume RCC pavement was constructed by the US Army Corps of Engineers in mid 1970s' and the first pavement-duty application took place in Texas to construct an intermodal hub facility [3]. Now, considering only roadway application in the United States, the RCC usage as a pavement application has exceeded 16.9 million square yards since 1975 [4]. Predilection towards the RCC pavements even in countries with slighter rigid pavement construction practices is mostly because this special category of rigid pavement does not need any additional equipment necessary for rigid pavement construction rather similar process can be followed like flexible pavements. According to Pittman et al. (2012), financial benefits can be also achieved by constructing RCC pavement as revealed by the

life cycle cost analysis as construction and maintenance costs are lower than the rigid and flexible pavements [5].

An increased use of roller-compacted concrete pavements as an alternative was expected especially because of its construction convenience, reduced cementitious content, and better structural capacity [6]. As RCC is a zero-slump concrete, initial placement of the material is made using traditional asphalt or high-density paver. Later, a combination of vibratory roller or static roller is used to compact pavement surface. Overall, a dense layer is attainable using the process that can be launched to traffic loading earlier than the conventional rigid pavements [3, 7]. Another key benefit of RCC pavement is that it requires less rehabilitation and maintenance during its service life compared to widely used flexible pavements, such as permanent deformation (rutting) is not an observed distress in RCC pavement due to heavy traffic load.

Fatigue analysis is important for a rigid pavement design, as pavement is subjected to repetitive cyclic loadings from thermal variations and moving traffic. As a result, appearance of transverse and longitudinal surface cracks under repeated loading is considered as one of the primary distresses that influence maintenance periods and reduce the design life. For RCC pavement, the cracking distress becomes even more crucial since dowel bars, or steel reinforcement, are not used [8]. Fatigue life analysis on RCC pavement indicates that the design thickness might be different from conventional concrete pavement due to the variations of in situ properties [9]. However, currently the standard RCC pavement design practice is to apply any of the existing concrete pavement design methods including the American Association of State Highway and Transportation Officials (AASHTO) 1993 empirical design procedure as till date. Pavement ME design guidelines obtained by NCHRP report 1-37A does not include RCC pavement design in their software packages. Among the other available design methods, the RCC-Pave developed by Portland Cement Association and the StreetPave developed by American Concrete Pavement Association software are considered as the efficient and mostly practiced tools for RCC pavement [10-11]. Among these two, RCC-Pave is appropriate for designing pavements subjected to heavy truck traffic but having a minimal traffic group, whereas StreetPave is largely used for the pavement carrying mixed traffic. The strategy of Portland Cement Association can be also useful for designing RCC pavement overlaid with asphalt surfaces to provide additional smoothness. However, none of the currently available RCC design methods follow strictly the mechanistic-empirical pavement design approach.

RCC Material Properties

Institute for transportation (InTrans, Iowa State University) published a comprehensive report on RCC as a paving material. This report also contained thorough outline of current RCC pavement design as well as field performance. The authors recommended RCC pavement as a cost-effective solution to conventional concrete mostly due to its rapid opening to traffic and lesser cementitious content. Besides, unlike conventional rigid pavement, additional cost for steel bars is not required for this pavement construction. In case of field performance, RCC pavement provides excellent durability against freeze thaw cycles and chemical attacks even without an air entrainment agent. The lower cement and water content of RCC mix also offers a lower shrinkage coefficient that result in lesser shrinkage cracking just after pavement construction. According to this report, depending on paver and construction equipment RCC pavement surface thickness can be up to 10 in. [3].

Most essential property of plain concrete is compressive strength that is greatly dependent upon mixture density. The Portland Cement Concrete (PCC) strength can be decreased up to 50% for a 5% lowered mixture density [12]. Density also plays a significant role in laboratory and field performance of RCC material similar to plain concrete. There are several techniques established to measure RCC density in both field and laboratory. Just after the construction of RCC pavement, in situ density using nuclear gage can be measured according to American Society for Testing and Materials (ASTM) C1040 [13]. In laboratory, RCC lab-prepared sample density can be obtained by ASTM Standard of hardened concrete [14]. Usually, perfectly compacted RCC material achieves average compressive strength of more than 5000 psi. However, it should be kept in mind that the maximum dry density of any mixture content can be attained at an optimal moisture content. Most often, the highest compressive strength can be also observed for optimum moisture density. For determining the flexural strength of RCC ASTM C78 standard, using a simply supported beam under third-point loading can be employed. Occasionally this bending strength, also termed as modulus of rupture (MR), is obtained utilizing empirical relationships with density or compressive strength. The density and bonding of RCC mixes are comparatively higher resulting from its low water-cement ratio. Thus, the resulted modulus of rupture of RCC is usually also better, and averages more than 650 psi [8]. Additionally, a flexural strength of 1050 psi after three months can be easily reachable with proper mixture design and aggregate gradation. In properly constructed RCC pavements, minimal developed fatigue cracks are observed if the aggregates are densely packed. Another key property of any concrete mixture is its

modulus of elasticity that is defined as the materials ability to resist elastic deformation against an applied load. Laboratory investigation revealed that for a similar mix design elastic modulus of RCC is comparable or marginally greater than PCC mixtures [3].

Khayat et al. (2019) attempted to produce durable roller compacted concrete (RCC) mixes by ensuring better strength properties, workability, and performance in cold regions [15]. In this study, the authors developed a mix design procedure that involved proper aggregate gradation, fine to coarse (F: C) aggregates ratio to achieve better aggregate packing density. This study also introduced air entraining agent (AEA) into RCC mixtures to improve the salt scaling resistance and durability against freeze thaw cycles. Laboratory test outcomes indicate packing density of aggregate can significantly increase the performance of RCC pavement. The laboratory results while determining 28th day compressive strength of the specimens ranged from 5000 – 8400 psi that is greater than the minimum strength (3500psi) required for RCC pavement construction.

Lee et al. (2014) investigated the properties of roller compacted concrete specimens in the laboratory [16]. Their study had separate phases where three different cement contents with fly ash as a partial replacement (20%) were used to prepare six laboratory mixes. For all these stiff mixes, the authors kept the water content at approximately 5% and used similar aggregate gradations. In the laboratory, the RCC was compacted using a small vibratory roller to simulate the real field conditions and cylindrical shaped RCC specimens were obtained to test the strength properties. This study mainly focused on the use of RCC on bicycle roads and the minimum 28th day compressive strength was recommended as 21 MPa. This study also suggested to achieve the minimum strength the binder content should not be less than 250kg/m3. In the next phase of this study, a test RCC section was constructed by placing RCC with an asphalt paver and compacted with a vibratory roller. The author suggested that the applied field construction procedure was efficient enough to deliver a smooth and finished surface for bicycle riders.

LaHucik et al. (2017) conducted an experiment to evaluate the RCC properties obtained from in situ field samples as well as laboratory compacted specimens [17]. For both groups, the same materials and mixture design were followed. The primary intent of this study was to evaluate and make a comparison between the density and mechanical properties of field constructed RCC specimens with those of laboratory compacted samples. For field evaluation, specimens were collected from different RCC pavement projects in Illinois. The mostly used vibratory hammer along with the gyratory compactor had been used in this study for compacting laboratory specimens. The study concluded that a higher specified target field density is a crucial property that must be considered for

implementing RCC pavement projects. The study also recommended that prior laboratory evaluation of RCC mixes is necessary for achieving the desired performance of RCC pavement. Additionally, several field core results exposed that RCC pavement achieves lowered density in the bottom compared to the top of the slab. At the end of the study, hypothesis testing at 5% level of significance indicated that the strength properties of the RCC sample groups are significantly different. The authors reasoned that the compaction techniques and density variation might act a part in obtaining different compressive strengths. The result showed that the core samples collected from field has lower density (approximately 5%) than the laboratory samples and achieved less than 40% of the laboratory compressive strength. The authors recommended that a high-density paver and an extra layer beneath the RCC surface layer might be useful to achieve desirable field performance of RCC.

Khed et al. (2020) reviewed the laboratory determined strength of roller compacted concrete incorporating different waste materials and minerals [18]. It concluded that compaction effort on the RCC pavement is significant for its durability. With the improving interlocking of aggregates, the compressive and flexure strengths of RCC pavement enhances. It also concluded that the compressive strength of RCC specimen mainly depends upon the aggregate size, which decreases with the increasing aggregate size. Incorporation of coconut coir and sisal fiber in RCC pavement can additionally achieve a significant increase in ductility and strength.

Each construction material has its own coefficient of thermal expansion (CTE) that is defined by the fractional change in length of that material against unit temperature fluctuations. The significance and influence of coefficient of thermal expansion (CTE) as a design parameter is included in the new mechanistic-empirical pavement design process while predicting pavement performance including longitudinal and transverse cracks, joint deflection, and surface roughness. However, the value depends on the mixture constituents and relative humidity. Conventional concrete has a positive coefficient of thermal expansion [19]. Based on the investigation of several studies, a lower CTE value is recommended for a pavement structure to reduce the transverse cracking and joint faulting [20].

One of the earliest studies on CTE was conducted by Alungbe et al. (1992) to find out the impact of aggregate, water cement ratio, and cement content on the concrete CTE [21]. Their statistical analysis found that CTEs of three different aggregates were significantly different from each other. However, there was no significant difference between the CTE if compared based on the water/cement ratio and cement content.

Hossain et al. (2015) found a relationship between PCC strength and CTE where concrete with a higher flexural strength has lower CTE values [22]. The author recommended that an increasing slab thickness or by increasing the strength parameters of PCC, the percentage of transverse cracking can be reduced. According to Neville et al. (1996) among many factors, the coarse aggregate CTE has the most significant influence on the CTE of any type of concrete [19]. However, this influence is complex and a larger difference between the CTE of cement paste and aggregate can lead to a weak bondage in concrete. According to the authors, the CTE of cement pastes ranges can be as high as 19.8 $\mu\varepsilon$/°C. However, the CTE of plain concrete mixed using typical coarse aggregate used in pavement construction range from 7.4 to 13.1 $\mu\varepsilon$/°C [23].

Figure 1. Variation of CTE of concrete with moisture content
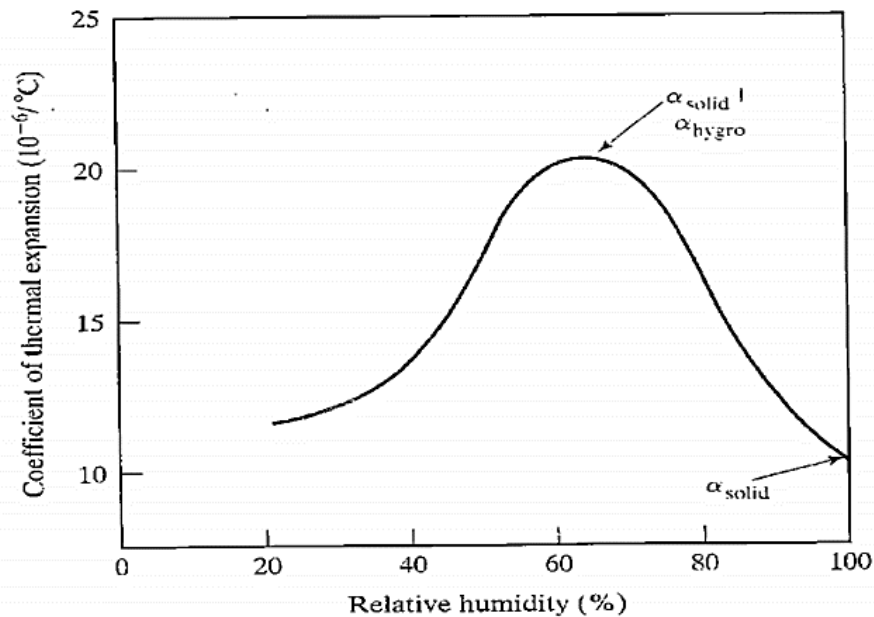
Another comprehensive study on CTE was conducted by Mallela et al. (2005) [24]. According to their results based on field collected cores of 663 PCC samples representing hundreds of test-section long term pavement performance (LTPP) programs all over United States, the general range of CTE values of PCC lies between 6.0 to 10.5 $\mu\varepsilon$/°C. However, concrete made from igneous aggregates got a lower CTE value (9.5 $\mu\varepsilon$/°C) than the concrete made from limestones (11.0 $\mu\varepsilon$/°C). Based on the performance investigation on the pavement test sections, the authors concluded that higher CTE and larger joint spacing significantly increased the possibilities of transverse cracking and mean joint faulting of rigid pavement.

However, the CTE is generally characterized by a constant value, but it can vary depending on the moisture presence in the mixture while performing the tests [25]. The maximum CTE of concrete can be achieved at approximately 65 % relative humidity whereas, at 100 % relative humidity, the CTE value is almost quarter lesser than the maximum one. However, the author suggested that while measuring this thermal property moist condition should also be considered to get actual range of CTE. The coefficient of thermal expansion is an essential material property to calculate the thermal stress due to temperature gradient (ΔT) in a pavement if the material's modulus of elasticity (E) is known:

$$\sigma \propto E * CTE * \Delta T \tag{1}$$

Where,

σ = Thermal stress

Shin and Chung (2011) conducted a study to evaluate the typical CTE values for PCC pavement [26]. Their sensitivity analysis on a mechanistic empirical pavement design indicated that the CTE value is highly sensitive while predicting the performance of rigid pavements. Therefore, either local calibration of the distress model or accurate measurement of CTE value is essential to produce an accurate design of concrete pavements. An HM-251 system produced by Gilson/Challenge technology was utilized to determine the CTE of the PCC mix in this study [26]. The HM-251 largely follows AASHTO T 336 specification and is divided into three distinct parts. The main concept of CTE came from the relationship between the change of strain for unit temperature difference and it can be estimated by the following equation for rigid pavement:

$$CTE = (((\Delta La / Lo))/\Delta T) \tag{2}$$

Where,

$\Delta La / Lo$ = observed strain in the specimen (change of the length of the specimen due to varying temperature),
ΔT = is the measured temperature change (increase = positive, decrease = negative).

Figure 2. Strain vs temperature plot to calculate CTE [26]
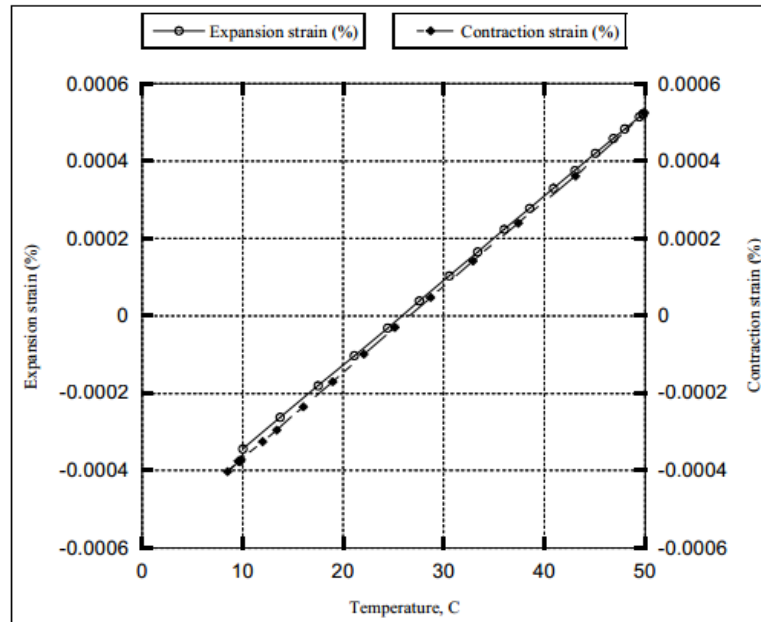
RCC Pavement Performance and Implementation in the U.S.

Generally, the maintenance requirement of RCC pavement is very little compared to flexible pavement. Load-induced fatigue cracking mechanism is the most observed distress in RCC pavement that is a combination of longitudinal and transverse cracking. While visually examining the critical locations by post-mortem trenches, results implicated that the critical location to initiate the fatigue cracks are either nearby the saw-cut joints or at the bottom of the slab [27]. Nevertheless, longitudinal and transverse fatigue cracking that appeared in RCC pavement can be easily treated as crack spalling is not generally observed. Mostly RCC pavement repair and maintenance are needed in a specific area where the placement or compaction was not mechanically done. However, to secure acceptable performance, the defected RCC material can be removed and replaced with new asphalt or concrete materials. The major drawback of RCC pavements is their performance against surface smoothness when compared to flexible or rigid pavements. The pavement smoothness or roughness (international roughness index) has long limited RCC applications for high-speed routes as riding comfort depends on vehicle speed. Typically, rigid pavement smoothness generally decreases with the appearance of longitudinal and transversal cracking, as well as the erosion beneath the foundation during the design period. However, RCC pavement smoothness is significantly

influenced by the placement, construction, and compaction procedure. Some researchers showed that, with the development of high-density pavers, improved smoothness of RCC pavement could be achievable [22]. However, considering smoothness as an important feature for high-speed roads, a few additional actions can be taken to improve the performance [27]:

- Upper limit aggregate size ≤ 0.5 in.
- Use high density paver for construction
- Construct thin RCC pavement ≤ 8 in.

A composite pavement structure with an overlay of thin (2 in.) asphalt layer of the RCC slab can also provide required surface smoothness and riding comfort. However, construction of an overlay can be avoided by using diamond grinding on RCC surface as it can provide additional smoothness. Recently, Chhorn et al. (2017) conducted a field evaluation of RCC pavement to examine the performance [28]. Here, the authors used five pavement trial sections of 580 m length. The key purpose of the paper was to analyze the characteristics of RCC pavement made with different maximum aggregate size under actual field conditions. Along with the standard mechanical tests, surface roughness properties were also studied. The result indicated that pavement constructed with 19mm aggregate had better surface smoothness in terms of International Roughness Index (IRI) than the pavement constructed with 13mm aggregates. However, the authors concluded that the smoothness of all the test sections was not decent enough for a pavement application where traffic flows with a higher operating speed. They also recommended that adequate compaction of RCC is the finest way to enhance the surface smoothness of the pavement during its service life. This study also revealed that up to a certain point, RCC pavement skid resistance increases if the mixture gets stiffer; however, too stiff mixture could result in a lower skid resistance of the pavement surface.

Virginia Department of Transportation constructed an 8 in. RCC pavement section that covered about 134,000 ft^2 and rebuilt an existing one with 6 in. RCC to observe the field performance [22]. These projects used 15% fly ash with the mixture to provide additional durability and sustainability to the pavement. Only a few cracks were observed in the pavement sections just after opening to the traffic, which was within 24-48 hours. The study observed the performance of the RCC sections for 1 year, and these did not show any distress other than a few transverse cracking. However, some longitudinal and transverse cracks were observed on the poorly formed construction joints. The authors recommended that to achieve acceptable performance from RCC pavement proper level of field compaction is obligatory. In addition, along with continuous curing to avoid early

cracks, saw-cut joints need to be cut deeper than one-fourth depth of the surface RCC layer.

As already discussed, RCC pavement is a sustainable alternative to conventional rigid and flexible pavement. RCC pavements are mostly implemented in the parking areas designed for heavy truck traffic. However, over the years, RCC is gaining its reputation for rapidly cured construction material that can be opened to traffic earlier than the PCC pavements. Nevertheless, the expected use of the pavement structure and the cost-effectiveness of RCC are generally the decisive considerations while selecting RCC over flexible or PCC pavement [29]. Currently, construction of RCC pavement is considered for local streets and arterials highways, as well as commercial parking spaces due to the advancement of construction and compaction practices [3]. In other words, the increasing implementation of RCC is a force that improves the required technologies with it. Donegan et al. (2011) listed the following typical application of RCC [30]:

- Military parking areas
- Truck resting areas
- Local streets and arterials
- Interstate shoulders
- Composite highway pavements with asphalt or concrete overlay
- Intersection approaches

Figure 3 shows different implementations of using RCC in pavement applications around the United States.

Figure 3. RCC application as shoulder and surface roads [31]

According to a report published by Zollinger (2015) significant improvement has been taking place for RCC pavement construction technologies, Figure 4 [31]. Mostly, development has been noticed related to the proper mix design of RCC with or without admixtures; use of heavy vibratory equipment to compact the road surface; and use of smaller aggregates and diamond grinding to achieve the required smoothness of the pavement surface. This paper not only summarized recent projectile growth of RCC projects, but also the types of construction equipment used and final surfacing techniques. It also provided a few case studies on some specific RCC projects like trial roads and commercial projects. The author concluded numerous benefits were achieved by utilizing RCC as a paving material on many projects such as less construction delay, less required maintenance, and early access of traffics, etc.

Figure 4. Increased Use of RCC (sqare yards) in the US [31]
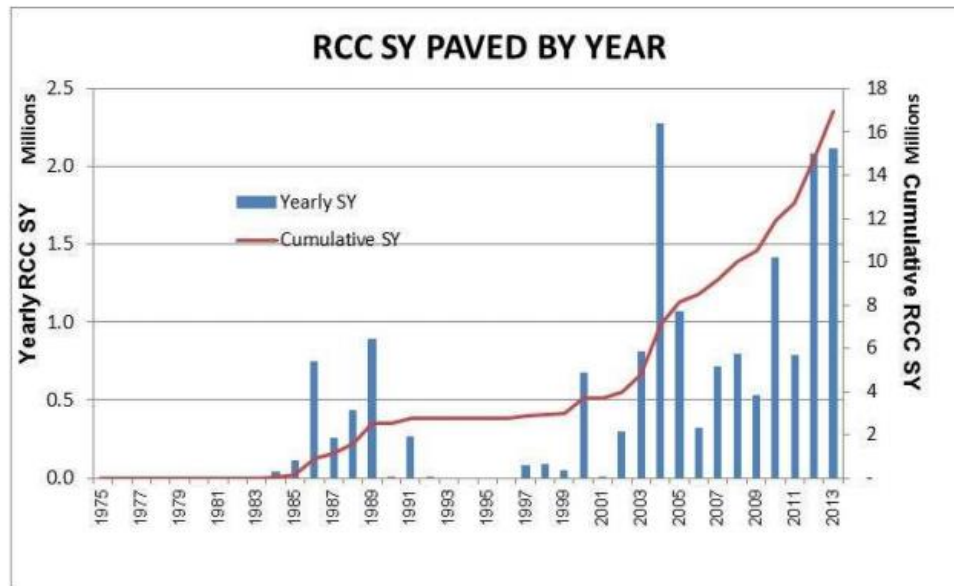
Until late 90s, RCC did not achieve enough recognition as a construction material. During that period, RCC had been employed only in 22 projects, and in terms of thousands of square yards, it was used less than 500 units. Later, from 2000-2010, the United States experienced a substantial use of RCC in several construction projects such as interstate shoulders, parking lots, and port applications. Until the last decade, a total of 9 million square yards of RCC material had been placed in more than 70 projects [5]. Currently, RCC application in pavement has a new dimension as low-medium volume roads also have been constructed. A recent survey reported more than 170 pavements have been paved with RCC covering more than four million square yards in between 2011-2013 [31].

The first RCC pavement was constructed in an industrial area of Lafayette Parish under the jurisdiction of Lafayette Consolidated Government (LCG). The project was introduced as a connectivity project, to connect several dead end roads to existing roadway facilities. There were three different locations, Decal Street, Sage Glenn Lane and Denbo Street, where the RCC pavement was constructed, shown in Figure 5. Each pavement section is approximately 220 ft. long by 28 ft. wide (two travel lanes). Each location was designed as a two-lane open ditch roadway. Four of the six tie-ins connected to standard concrete roadways and the other two tied into standard asphalt concrete roadway. Decal Street and Sage Glenn Lane were being used as dirt alley ways prior to construction, whereas Denbo Street location was an open field prior to construction.

Since these sections of roads did not exist, there were little problems with maintaining traffic.

Figure 5. Location of RCC Pavements
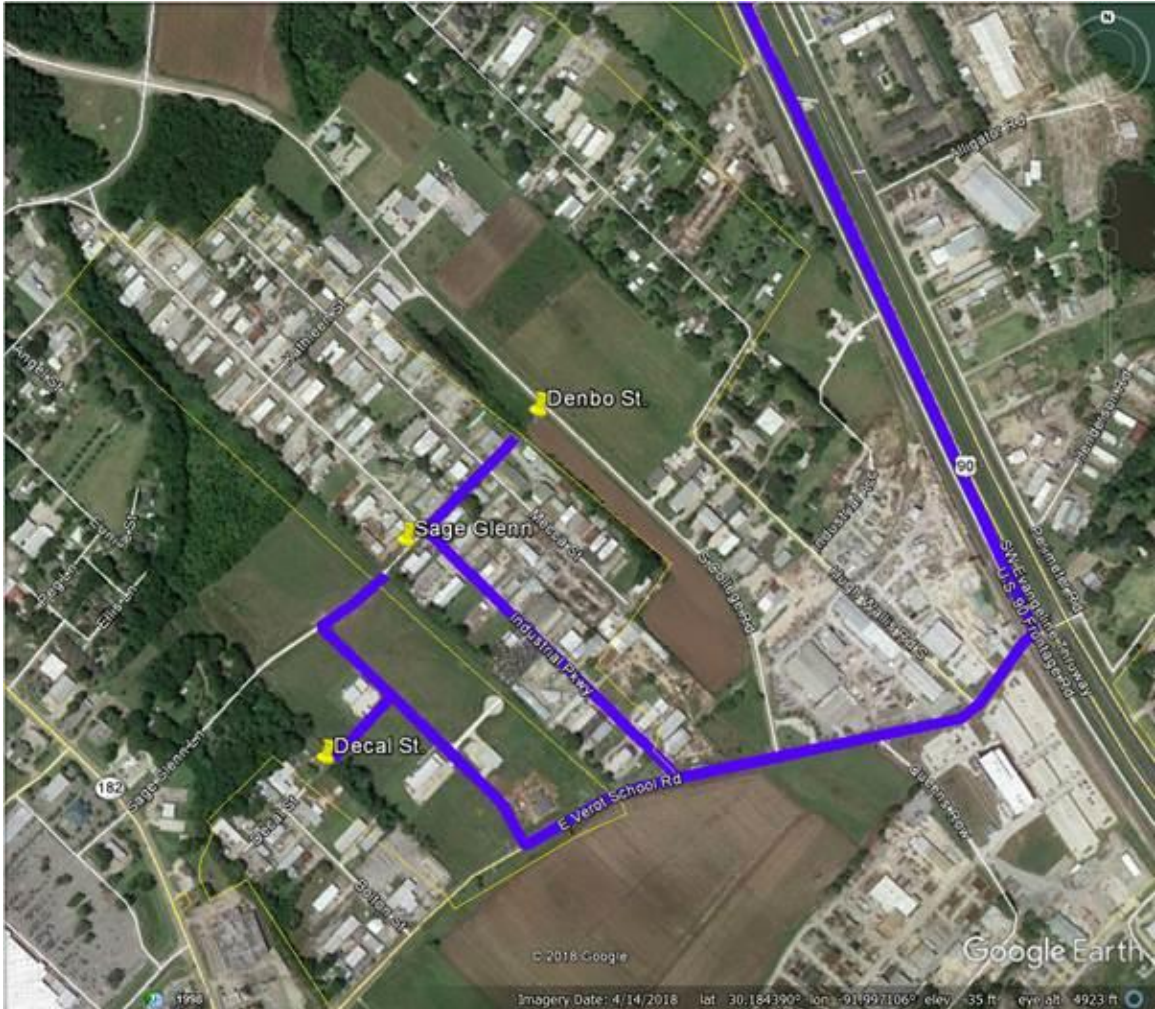
The construction for the project was carried out by Seima Construction under the supervision of LCG and LTRC. The preparation of the base layers began by removing the existing dirt alley and then treated the soil with 9 percent cement by volume for the 8-in. soil cement layer on Sage Glenn Lane. Denbo Street and Decal Street were treated with 9 percent cement by volume for 8-in. depth with an additional 3 in. of cement treated subgrade at 6 percent cement by volume. The base layers for all three lots were compacted to achieve 95 percent of the maximum dry density.

All three RCC pavement lots were constructed within a day using a set of specialized asphalt paving and RCC mixing equipment. Both lanes on each lot were placed at the same time. The concrete for the RCC pavement was produced in a central batch plant approximately 30 minutes away from the project site. The RCC mix was then transported to the jobsite in dump trucks. Ten dump trucks were used to minimize the time between mixing and compaction of RCC pavements. The 30 minute time limit for delivery specified in the construction specification was extended to 45 minutes due to the cooler than expected temperatures. Truck bed covers were used to avoid excessive moisture loss during transportation.

As a trial, the first 145 square yards (approximately 45 ft. of roadway) of RCC were placed and constructed on top of soil cement base layer to validate the design, rolling pattern, and method of construction using the same construction equipment. The trial section pay item consisted of placement, removal, and disposal of the RCC if the trial section was not acceptable. A high-density paver was used to place the RCC over the prepared base layer to achieve high initial density. A self-propelled smooth steel drum vibratory roller was used to achieve 90 percent compaction of the RCC pavement. The static roller was sufficient to meet the 98 percent compaction. Nuclear density gage was used to check the moisture and density right after the paver and after the compaction using vibratory roller. The in-place density ranged between 92-96 percent of the target density right behind the paver and increased to more than 98 percent after compaction. Finally, an admixture was added to the surface to allow a broom finish followed by the application of a curing membrane.

All RCC layers were placed in a single lift and there were no delays in transportation that required any cold transversal joint. However, transverse saw-cut joints were created to minimize or prevent possible randomly generated shrinkage cracking. Seven-hour wait time was required for early saw cutting to help prevent spalling damage during sawing operations. The saw-cut joints were cut 1/8th of an inch wide by 1/3rd of the pavement depth spaced at 10-ft intervals for all three-pavement sections. No joint sealing was performed on any of those saw cut joints. Figure 6 shows the construction of RCC pavements in Louisiana's first roadway application.

Figure 6. RCC pavements on Decal St., Denbo St. and Sage Glenn Ln.

(a) Rollcon High Density Paver

(b) Dump Truck Haul for Transportation

(c) Placement of RCC

(d) In-field density measurement

(e) Paving Operation

(f) Roller Compaction
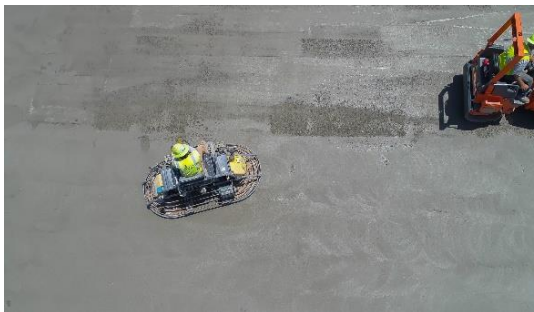
(g) Trowell Finish

(h) Final surface after curing and saw-cut

In April 2019, all the lanes were paved with a 6-in. RCC on top of an 8-in. soil cement base layer. According to the DOTD's roadway design specification, the minimum 7-day unconfined compressive strength for treated subgrade, cement treated base and soil cement base would be 100, 150 and 300 psi, respectively. To meet the specifications, the soil cement base layer used in Sage Glenn was treated with 9 percent cement by volume to the depth of 8 in. Denbo Street and Decal Street were initially treated with 9 percent cement by volume, but due to unforeseen issues in the field, both locations were restabilized with 6 percent cement by volume and increased the depth from 8-in. to 12-in. For drainage design purposes, all the lanes were designed for both open ditch and subsurface drainage.

Mechanistic-Empirical Rigid Pavement Thickness Design

Nearly, 94% of the roadways of the United States are paved with asphalt surfacing; however, rigid pavements are renowned for achieving better durability and design life [32]. The jointed plain concrete pavement (JPCP) is the most commonly constructed rigid pavement in the United States that usually contains a steel reinforcement mesh and is meant to hold firmly together to reduce the appearance of transverse cracks in the slab. Dowel bars and tie bars are used at all the joints of a pavement structure. Another type of rigid pavement is continuously reinforced concrete pavements (CRCP) that contain more steel reinforcement than JRCP but no regularly spaced transverse joints. Rigid pavement thickness design approaches can follow either an empirical design, where all equations that predict performance are based completely on observed responses of laboratory and field specimens that represent traffic and environmental loading; or, a mechanistic design method, a purely scientific approach that requires detailed engineered modeling of material, structural mechanics, and geometrics. Then again, a pure mechanistic approach is yet to attain a better prediction of pavement performance, but rather a combination of mechanistic and empirical known as M-E design procedure are mostly used.

The principle of pavement design depends on a variety of factors such as pavement type, failure modes, stresses in the pavement structure, traffic characterization, material properties, design strategy, etc. However, the basics of concrete pavement design consist of assuming a design life and calculating the number of load applications that a specific pavement system can sustain before failure. Based on the design purpose, variations in climate, traffic, and material conditions are also evaluated. The most widely used rigid pavement thickness design procedure was published in 1993 by AASHTO [33]. This

design procedure is specified in the Guide for Design of Pavement Structures by AASHTO, and was based on the empirical correlation by the AASHTO Road Test conducted near Ottowa, Illinois. However, the mechanistic-empirical design procedure is becoming a popular state-of-the-practice nationwide for rigid pavements since it uses both results from mechanical modeling and empirical performance observations to determine the most accurate thickness for pavement to satisfy its design period. Many states are currently using the PCA pavement thickness design procedure, or developed their state wise mechanistic-empirical procedure for the rigid pavement design like Florida Department of Transportation [34].

To attain a purely mechanistic design over the years, many attempts have been made to employ mechanistic variables such as stress, strain, or deflection in pavement design to complement the empirically monitored performance of a concrete pavement. One of the most used and earliest mechanistic-empirical analysis for highway design for plain concrete was employed in the zero-maintenance design concept by Darter (1977) [35]. This thickness design method was based on fatigue damage and it incorporated a relationship between fatigue life with the ratio of applied stress and concrete modulus of rupture to predict the traffic load and environmental stresses. The zero-maintenance fatigue equation was obtained by compiling results from previous beam fatigue studies into a single equation (3) with 50% probability of failure.

$$\text{Log Nf} = 17.67 - 17.61 * \text{SR} \tag{3}$$

Where,

Nf = maximum number of load repetitions prior to fatigue failure
SR = stress ratio

Initially, Darter (1977) used Westergaard's (1927) medium-thick plate theory to compute the critical stress [35]. Later, attempts were also made to improvise Westergaard's (1927) prediction methods by creating charts that included multiple wheel loads [36]. Now, mechanistic-empirical rigid design procedure followed the same strategy for determining the pavement responses. With the advances in finite element computer programs, the preferred method of rigid pavement stress prediction using finite element analysis has become the current practice.

The Portland Cement Association (PCA) also developed a largely accepted procedure that contained a tensile bending stress calculated from finite element analysis into a thickness design procedure. This procedure also analyzed the possible failure mechanism due to

erosion of the foundation of a pavement structure [34]. However, a major limitation of this study was that it did not consider the influence of temperature or moisture induced stresses. Later, along with NCHRP and Federal Highway Administration (FHWA), the AASHTO Joint Task Force on Pavements was assigned to develop an M-E based pavement design guidelines. Therefore, NCHRP Project 1-37A, development of the 2002 Guide for New and Rehabilitated Pavement Design was introduced in 1996 and the Mechanistic-Empirical Pavement Design Guide (MEPDG) was issued in 2008 [37]. This method enhanced the prevailing procedure by incorporating aspects such as steer-drive axle spacing, non-linear thermal variation along the slab, fatigue cracking and joint deflection predictions, climatic influences, and outputs of nationally calibrated models from test sites across United States and Canada. The mechanistic empirical procedure was ultimately accepted by AASHTO as the standard for pavement design, and AASHTO has made available standard guidelines for agencies to implement the procedure and perform local calibration of the distress models. The most recent version of the MEPDG design software is the AASHTOWare Pavement M-E Design Software, formerly known as DARWin-M-E, which automates the pavement design procedure outlined in the MEPDG. American Concrete Pavement Association's (ACPA) also developed a software named StreetPave based on the PCA thickness design method [11]. This software incorporates results from the AASHTO Road Test, more recent information from mechanistic empirical studies, and a newly updated fatigue model.

The mechanistic empirical pavement design software uses principles of engineering mechanics to find out the critical responses in terms of stresses, strains, and deflections in the pavement structure and uses these outputs to predict performance based on empirical correlations of the pavement over its design life. Here, traffic is characterized using site-specific traffic data and different load categories instead of equivalent single axle load (ESALs) that is used in AASHTO empirical design guideline. This traffic input accounts for steer-drive axle spacing, as well as the individual axle spacing on a tandem, tridem, and quad axle. Climatic responses, including the temperature profile and moisture throughout the pavement structure, are also determined internally through a mechanistic model termed as the Enhanced Integrated Climate Model (EICM). The general layers type that are integrated in the rigid pavement design software are concrete slab, asphalt stabilized base, cement treated base, other cement or lime treated layers, unbound base/subbase, and subgrade soils. The predicted results from the purely mechanistic models act as input to the empirical distress prediction models that correlate the detected responses to typical pavement distresses such as rutting, longitudinal and transverse cracking, joint faulting, and surface roughness. The empirical models to predict pavement

performance were calibrated using hundreds of pavement test sections, primarily from the LTPP database. One of the notable aspects of the pavement-M-E is the capacity to deal with a range of material inputs and their impact on pavement response to better reproduce the pavement distresses and improve design predictions. During the design inputs for pavement M-E design, designers can data based on three common levels.

- Level One: Inputs for a specific project based on direct testing or measurements. Example of level 1 data inputs can be required material properties (flexural strength) through direct laboratory testing.

- Level Two: The use of correlations to define the required inputs. An example of level two input is to determine the resilient modulus of subgrade from the California Bearing Ration (CBR) from empirical correlation.

- Level Three: Applying the default values to define the inputs. The example is the use of roadway truck type and truck type classification to determine the normalized axle weight and truck traffic distribution.

The sensitivity analysis of the design inputs can identify the most influential parameters for different climatic regions and traffic conditions. This will help pavement designers determine where additional effort is justified in developing higher quality and/or more certain input values. The following steps are generally considered during the analysis process for the rigid pavement thickness design.

- By defining layer arrangements, assemble a trial design for specific site conditions, material properties, traffic loading, and environmental conditions;

- Setting-up a design-criteria for acceptable pavement performance at the end of the design period (i.e., acceptable levels fatigue cracking, faulting and roughness);

- Selection of reliability level for each one of the distresses considered in the design;

- Computation of monthly traffic loading and seasonal climate conditions and adjustment of material properties in response to environmental conditions if needed;

- Determination of structural responses (stresses, strains and deflections) for each axle type and load for each month throughout the design period;

- Calculation of predicted distresses (e.g., fatigue cracking, roughness) based on the accumulated damage at the end of each month throughout the design period using the empirical performance models;

- Assessment of the predicted performance of the trial design for a reliability level. If the assumed trial thickness does not satisfy the performance criteria, the design (thicknesses or material selection) must be modified, and the calculations repeated until the design meet established criteria.

Current Practice of RCC Pavement Thickness Design

As discussed in the problem statement, pavement designers are using existing rigid pavement thickness design procedure or AASHTHO 1993 empirical design strategy for RCC pavement thickness pavement. These design approaches include the design procedure similar to the rigid pavement guidelines. However, as the performance and field study of RCC pavement revealed that the common distress mechanism in it is fatigue cracking compared to several other distress rigid pavement, extra focus is given to fatigue failure mechanism. Here, the main objective is to keep the pavements flexural stress caused by traffic loads and subsequent fatigue damage within allowable limits. Therefore, design traffic loading, RCC flexural strength, and the pavement structure became the crucial factors for thickness design of RCC pavement. As a result, RCC design thickness is a function of expected loads, concrete strength (modulus of rupture), and subgrade characteristics.

Portland Cement Association (PCA) has developed a thickness design procedure for RCC pavement subjected to heavy truck loading such as ports, terminals, industrial applications [2]. Their design approach involves the same basic assumptions that a pavement structure can withstand a definite amount of loading for certain loading cycles without failure. As the critical stresses of rigid pavements are resulted from bending, fatigue damage associated with bending stress generally governs the thickness design strategy. This kind of damage is important to investigate because it can arise from the stresses caused by a specific load lower than the strength of the material. Repeated stress levels can degrade material property with time and cause fatigue failure. However, other than the fatigue damage, this method also employs erosion analysis to crosscheck RCC thickness design. Same as fatigue, total damage due to erosion is also calculated as a ratio between the expected numbers of repetitions to the allowable number of repetitions of the same axle load. The principle of erosion damage in pavement arises from erosion of foundation support and joint faulting. It also evaluates potential of a pavement to fail due to pumping near the joints. However, as saw cut joints of RCC is not prone to joint

faulting or pumping as much as the rigid pavements, erosion model is mostly derived from the foundation and surface thickness layer characteristics.

RCC pavement thickness design principle is slightly different from the conventional rigid pavement as the general thickness design of RCC pavement is mostly governed by fatigue damage. Here, primarily the fatigue damage is estimated by calculating critical stresses for every loading category. The critical location can be on top or bottom of the slab subjected on the time (day or night) and traffic loads. Later, based on the stress ratio (ratio between the critical stress and modulus of rupture, MR) the highest possible number of loading cycles (Ni) for each axle category is determined. Pavement fatigue damage associated to each axle category for a given condition in the design life that is measured from the ratio of actual number of load repetitions (ni) against the allowable number of repetitions (Ni) is calculated. The cumulative damage caused to the pavement by fatigue, Df, is given by the following relationship, where all type of load categories is considered in the design life:

$$Df = \sum ni/Ni \tag{4}$$

At the end of the design period, the sum of the total fatigue damage should be less than or equal to 100%. If the sum of the damage is higher than 100%, a thicker concrete thickness should be assumed and the whole process must be repeated until the fatigue damage reaches equal or less than 100%. For designing RCC pavement, a software named RCC-PAVE has been developed that used the PCA pavement thickness design principle. When using this method for RCC pavement design, maximum bending strength or the modulus of rupture and the assumed thickness of the RCC surface layer are the major factors that influenced the design life. However, one of the major limitations of this software is that the PCA fatigue model was based on data derived from concrete beam fatigue tests conducted in the early 1950s and 1960s and did not consider the construction procedure of RCC pavement [38]. The following three equations are termed as PCA fatigue equations (5, 6, 7) that are currently being used in the RCC-PAVE software:

$$Log\ Nf\ =\ 11.737 - 12.077 * SR;\ for\ SR\ \geq\ 0.55 \tag{5}$$

$$Nf\ =\ \left(\frac{4.2577}{SR - 0.4325}\right)^{3.268};\ for\ 0.45\ <\ SR\ <\ 0.55 \tag{6}$$

$$Nf\ =\ unlimited;\ for\ SR\ \leq 0.45 \tag{7}$$

Where,

Nf = maximum loading cycles till failure
SR= stress ratio

The most primitive thickness design procedure of RCC pavement was conducted by Construction Technology Laboratories (CTL) in 1987 [39]. The design approach of CTL followed the same strategy like PCA rigid pavement design. Their proposed procedure also required determination of allowable pavement stress based on the number of total load applications and prediction of actual pavement stress due to the designed traffic loading. A trial thickness was considered as the selected design thickness if the predicted pavement stress is less than the allowable pavement stress. For mixed traffic, loading the procedure developed in this study also can be applied. The primary parameters affecting thickness design of concrete pavements are concrete flexural strength and concrete fatigue behavior. The CTL RCC fatigue relationship constructed by Tayabji and Okamoto (1987) was applied into the thickness design procedure of RCC pavement in this report [39, 40]. The authors conclude that RCC has much similar properties like conventional concrete and taking RCC fatigue curve into consideration, other rigid pavement design procedure can be followed.

American Concrete Pavement Association (ACPA) attempted to improve the rigid pavement thickness design procedure by including a reliability term in their fatigue model. They established their fatigue model based on available published PCC fatigue data of existing studies [41]. They proposed this ACPA PCC fatigue model as an alternative to the fatigue design curve published by Portland Cement Association (PCA). This model later was incorporated in StreetPave and PavementDesigner software and it is now also used for RCC pavement thickness design [42].

$$LogNf = [-(SR^{(-10.24)} Log(1 - P))/0.0112]^{0.217} \qquad (8)$$

Where,
Nf =the allowable number of load repetitions
SR= stress ratio
P = probability of failure = (1-Reliability)

The design strategy by Dellate of a composite pavement system comprising of an asphalt overlay over RCC pavement structure was also the same as the PCA rigid pavement design procedure [43]. This study only considered fatigue cracking as performance studies shown very little tendency for joint and crack faulting of RCC pavement. The fatigue behavior of RCC has been assumed to be similar to PCC and PCA fatigue

equations based on different stress ratios used while calculating allowable number of repetitions for fatigue damage.

Fatigue Behavior of Rigid Pavement

Wohler (1860) was the first to study fatigue effects scientifically on a metal specimen [44]. Later, Bauschinger (1886) demonstrated that material response against a static loading is different from the responses observed against a cyclic loading condition [45]. Paris et al. (1961) used fracture mechanics theory to explain the crack growth during cyclic loading [46]. However, with the development of closed-loop servo-hydraulic loading systems (i.e. material testing system), advanced understanding of fatigue behavior increased to a drastically higher level.

During the service life, a pavement experiences repetitive loading from traffic and thermal variations. Keeping that in mind, fatigue tests on construction materials are conducted with application of cyclic loading that is less than the maximum bending strength of the material. For concrete, usually flexural-fatigue test is often performed as a direct tensile stress is difficult to apply. Three-point or four-point bending tests are the most preferred procedure to evaluate the fatigue behavior of notched or normal beam specimens. In some special cases where fatigue behavior requires a direct tension fatigue test, fatigue tests can be carried out on compact square or disc-shaped tension samples. Developed based on the principles of Wohler, the most widely used procedure for fatigue analysis and fatigue life prediction for concrete is the stress life (S-N) curve, obtained by plotting the number of load repetitions/cycles to failure (N) corresponding to stress ratios (SR) on a logarithmic scale. In this strategy, fatigue tests are considered as stress or load control testing where the stress ratio is expressed in terms of the ratio of the maximum stress applied to the maximum bending strength of the material obtained from static tests.

The S-N approach, universally used in concrete fatigue tests, is generally preferred for rigid materials as they did not display a large response to applied stress. The stress-life curve of concrete has also been utilized as a design criterion while designing concrete pavements. In 1974, the design S-N fatigue curve used by the Portland Cement Association (PCA) was created by combining fatigue curves obtained from conventional concrete samples from previous studies. However, initially the use of S-N fatigue curve developed in PCA method generated some unlikely outcomes. Soon after, minor adjustment of the fatigue analysis was made and until now, the modified S-N curve is being used to predict fatigue life of concrete [34].

Several research has been conducted to investigate the behavior of RCC beam and slab specimens. Most of these studies only aimed to develop a fatigue model for RCC to calculate RCC pavement fatigue damage, whereas some of these attempted to revise the well-established rigid fatigue models by incorporating properties of RCC mixes. Before conducting experiments on RCC fatigue life, this study reviewed prior experiments and recorded the results in this section.

Park et al. (2020) used 1m x 1m RCC slab specimen obtained from field to evaluate the fatigue behavior of RCC pavement considering field variability [47]. Initially, 144- x 4- x 0.2-m RCC pavement test sections were constructed in South Korea. Later, to obtain the slab specimen, several 20 m sections were cut from the test section. The fatigue equation for the RCC slab specimen was developed using the theory of Wohler's equation and the obtained result showed better performance while compared with PCC fatigue equation. In the case of static load test on RCC slab section, all the slab failed due to four directional bottom-up cracks. A constant fatigue stress ratio (f_{max}/f_{min}=0.2) was kept throughout the fatigue testing as the minimum applied stress on pavement structure will not be zero. The obtained fatigue (equation 9) found from the study is as follows with an R^2 value of 0.802:

$$Log\ N\ =\ 11.668 - 12.511SR \tag{9}$$

> Where, N = the allowable number of load repetitions
> SR = stress ratio

Sengun et al. (2021) investigated the fatigue behavior of three different RCC mixes based on beam specimens [48]. The authors replicated the field compaction procedure of RCC in the laboratory on a short scale by creating 200cm x 85cm x15cm sections. Both vibratory plate compactor and small-scale vibratory hand roller were used to compact the RCC mix in a plate shaped mold, Figure 7. As a drawback of this study, the authors were not able to consider the influence of base and subgrade to the field performance of RCC pavement. Later, fatigue behavior of the collected beam specimens (100 x 150 x 350 mm) was evaluated by third-point flexural fatigue loading at five different stress ratios. The ratio between maximum and minimum loading during fatigue cycle was kept constant (0.2) to avoid additional variability. In this study, Weibull's graphical approach is preferred to incorporate the reliability into the RCC fatigue design curves. The authors concluded that considering fatigue reliability, the S-N curve developed by ACPA and PCC is more conservative compared to the design curve of RCC developed in this study. This study also concluded that RCC mixture with better fatigue life tends to act more

brittle compared to the other mixtures. It also developed a combined fatigue model considering all three mixtures other than, developing three separate fatigue curves for different RCC mixes:

$$S = 0.911 - 0.047 \, log \, N \tag{10}$$

Where,
N = the allowable number of load repetitions
S = stress ratio

Figure 7. Preparation of RCC beam specimens.

Adamu et al. (2018) considered five types of RCC mixtures to evaluate the fatigue performance of RCC pavement [8]. Four out of the five mixtures had crumb rubber or silica as a partial replacement of fine aggregate. Results showed that both crumb rubber and silica could improve the fatigue life of RCC pavement. For fatigue testing, RCC beams of 100 x 100 x 500 mm size were prepared in the laboratory and tested under third-point loading. This study was more interested into the S-N curve for RCC mixture comparison to determine the fatigue life of different mixtures and thus testing was conducted at three predetermined high stress ratios (0.7, 0.8, and 0.9). Fatigue stress ratio while applying cyclic loading (f_{max}/f_{min}) was kept constant to 0.1. Total 6 samples were used to develop the following S-N relationship for a controlled RCC mix where N and S have the conventional definition.

$$Log \, S = 0.1016 - 0.046 \, Log \, N \tag{11}$$

Tayabji and Okamoto (1987) from Construction Technology Laboratories, Illinois developed the earliest fatigue curve that was later used for RCC thickness design as discussed earlier [40]. For this study, four test panels were constructed with four RCC mixture design. Later, a total of 20 sawed beams (five beams from each section) collected after 70 days of test section construction were used to develop a relationship between stress ratio and loading cycles based on Wohler's principle. For flexural fatigue testing the applied stress ratios were ranged from 0.50 to 0.95. The mixture with higher flexural strength gave better resistance to fatigue loading for low stress ratios compared to the other mixtures. The cyclic load was applied with a hydraulic actuator and the loading frequency was maintained at 10 Hz. To prevent impact loading, a minimum static force of 10 percent of maximum applied load was maintained in each load cycle. The following S-N relationship presented in Figure 8 is also known as CTL RCC fatigue curve.

Figure 8. RCC design fatigue curve developed by CTL [40]
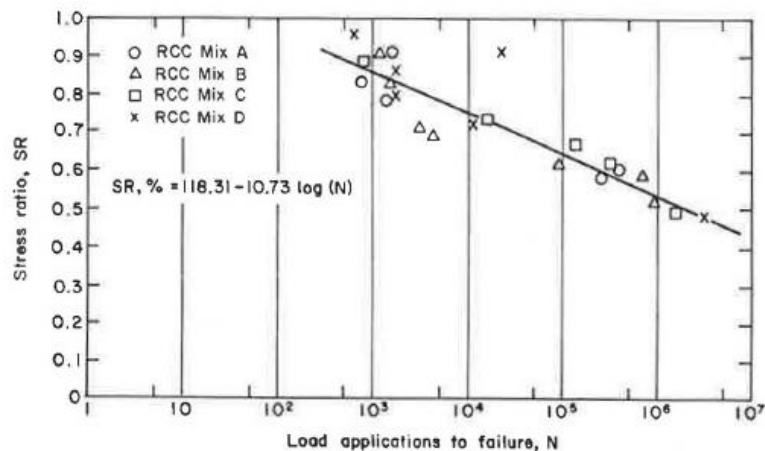
A comparison between the PCC fatigue model and RCC fatigue model showed that RCC has better performance under fatigue loading than conventional concrete.

Okamoto (2008) in another study performed fatigue tests on 37 beam specimens of dimension 100x100x400 mm^3 and 44 specimens of size 150x150x750mm^3 from three different RCC mixtures [49]. In this study, the effect of different aggregate types (limestone, dolomite, etc.) and varying beam specimen sizes on fatigue behavior were investigated. It was stated that both different aggregate types and different beam sizes produce almost similar fatigue relationship of stress ratio and number of cycles to failure.

Roden (2013) published an interim report for ACPA proposing a new fatigue model for RCC pavement [7]. For the development of this new fatigue model, reliability levels were

incorporated on 141 RCC fatigue beam data collected from the literature. First, all published fatigue data representing separate RCC mixtures and different beam sizes were recorded and adjusted by a size factor to allow conversion, a 6-in. x 6-in. beam size [40, 49]. After the conversion, McCall's model was used to combine all the fatigue data into a single model. Later, the new ACPA RCC fatigue model and the existing fatigue models were compared, and the effect of the pavement thickness was explained. However, this model later was not allowed to be the benchmark for RCC thickness design based on fatigue cracking though it complied all the previously published RCC fatigue data and presented a comprehensive methodology to improve RCC thickness design.

Sun et al. (1998) studied the influence of fly ash on the RCC fatigue performance based on a laboratory compacted beam specimen (100 mm x 100 mm x 400 mm) [50]. Focusing on that, four fatigue models for RCC mixes with and without fly ash content were developed. The loading frequency for the testing was in between 5-8Hz. The RCC beam fatigue model with zero fly ash content developed in this study is presented below.

$$SR = 0.936 - 0.0693 \, log \, N \tag{12}$$

The authors recommended that RCC and fly ash RCC (FARCC) pose excellent fatigue performance and the fatigue strength of RCC gives 40-50% higher values when compared to PCC.

Reviewing the existing literatures on RCC fatigue, it can be concluded that all the authors viewed fatigue damage as the key failure mechanism of an RCC pavement. However, other than the fatigue curve proposed by CTL and Park et al. (2020), all other curves used laboratory RCC specimens by simulating RCC field compaction procedure and failed to consider RCC pavement construction variability [47]. However, CTL RCC fatigue design curve did not consider the advanced vibratory equipment's to construct RCC test sections and is somewhat outdated. Considering the high variability in the fatigue performance, a major limitation of the study conducted by CTL and Park et al. (2020) is that the developed fatigue models were based on a limited number of specimens and did not incorporate any reliability in the developed models [47]. Moreover, considering only a specific modulus of rupture while determining the RCC fatigue strength is also a major limitation of the reviewed studies.

Accelerated Pavement Testing (APT) and Instrumentation

The construction of Arlington Test Road in 1919 was the very first accelerated pavement testing (APT) facility in the United States [51]. It was constructed to observe the plain concrete performance under heavy truck loading. Gradually, many other APT facilities like the Maryland Test Road, Bates Experimental Road, and the Western Association of State Highway Officials Road Test began to test road sections employing simulated or real traffic conditions [51]. The core idea of accelerated pavement testing is to observe the field performance of the test sections under applied traffic loading. Varieties of instruments are currently being used by different state agencies to develop and validate different pavement performance models for pavement test sections. An additional instrumentation strategy for this type of test section can help to examine in situ response and the material properties against thermal and/or traffic loading. Table 1 below lists the different APT facilities and the instrumentation strategy all over the United States.

Table 1. Different APT facilities in the United States

Facility	Measured Pavement Response	Strain Gage Used
NCAT pavement Test Track	Horizontal strain, vertical strain, temperature, pressure, and moisture	CTL
Ohio Research Institute	Horizontal strain, vertical strain, temperature, pressure, and moisture	Dynatest
Florida DOT	Horizontal strain, temperature, and pressure, moisture	Tokyo Sokki
PRF, LTRC	Horizontal strain, vertical strain, temperature, pressure, and moisture	Tokyo Sokki
MnRoad	Horizontal strain, vertical strain, temperature, pressure, and moisture	Dynatest, Tokyo Sokki
Kansas State	Horizontal strain, vertical strain, temperature, pressure, and moisture	Texas Measurement (TMK)
Cal Trans	Temperature and moisture	-

To obtain meaningful results from APT, it is necessary to record the dynamic pavement responses against different critical parameters such as strain, deflection, moisture and temperature [52]. However, while some of these instruments measure the response accurately, others require incessant adjustments to collect reliable data consistently during APT testing. Nevertheless, to measure meaningful pavement responses under APT

loading, projection made by pavement instrumentation must be precise and accurate [53]. Several considerations are given priority while selecting a sensor that is not limited to its frequency, noises, and weather resistance capabilities. The suitability of sensors on an APT system mainly depends on two factors: (1) measurement of pavement response under normal trafficking, and (2) measurement of pavement response under anticipated failure [52].

Moreover, understanding and converting the pavement response data generated strain gages towards a meaningful dataset, which is also challenging [54]. Recently, due to developments in electronics, advanced fiber optic sensors are adapted as the most effective way of collecting dynamic response from APT system [55]. All the characteristics of sensors must be thoroughly investigated to make sure that probable responses will not exceed the sensor's highest operational capacities. Additionally, prior to installation sensor operation must be verified and calibrated, and prior to gage deployment must be tested for its functionality [56-58].

Sok et al. (2018) evaluated the initial pavement responses developed in an RCC slab resulting from thermal and moisture variations [59]. A full-scale test section of RCC pavement under actual environmental conditions was monitored. Then, the pavement critical responses, temperature variation along the depth of slab, and coefficient of thermal expansion (CTE) of RCC were measured and analyzed. The results showed that the CTE of RCC is 10.8 $\mu\epsilon/°C$ and shrinkage strain of the pavement is lower when compared to rigid pavements. Also, the initial stress developments in the RCC pavement slab were highly influenced by the thermal-induced stresses. The study also recommended assuming a constant value of CTE while calculating the stress development in the slab as the CTE of the RCC mixture did not show any variation with time.

Objective

The objectives of this research included:

- Determine in situ load-induced and temperature-related pavement responses, investigate pavement failure mechanism and structural performance, and quantify the equivalent axle load fatigue damages for RCC pavements under accelerated pavement testing;

- Conduct laboratory beam fatigue tests using in situ saw-cutting RCC slab specimens and develop a new fatigue damage model for the use of thickness design and performance evaluation of RCC pavements; and

- Propose a mechanistic-empirical pavement design procedure for the thickness design of new RCC pavements.

Scope

To achieve the objectives, RCC pavement sections were instrumented with fiber-optical strain plates and tested under the ATLaS30 loading. In situ transverse strain responses of RCC slabs due to wheel loading and temperatures were measured. The APT pavement performance of test sections were evaluated based on crack-mapping, nondestructive testing, and finite element modeling. For laboratory experiment, 68 RCC field beams were saw cut from the test sections and tested using the beam fatigue and flexural strength testing protocols. Laboratory density tests were also performed. Laboratory test results were used to develop a RCC fatigue model with a capacity of incorporating the reliability into a pavement design. Load transfer factors were also determined for RCC pavements using a numerical modeling approach. Finally, field performance and laboratory experiment results were employed to propose a mechanistic empirical pavement design procedure for RCC pavement thickness design.

Methodology

This study consisted of three basic analytical steps: performance evaluation of accelerated pavement testing of RCC test sections, development of an M-E based fatigue damage model using in situ saw-cut beams from RCC test sections, and application of M-E approach into RCC pavement thickness design.

Accelerated Pavement Testing

Description of APT Test Section

Six full-scale RCC pavement test sections were constructed using normal highway construction equipment and procedures at the Louisiana Pavement Research Facility (PRF) site in Port Allen, Louisiana. Figure 9 presents the plan view and pavement layer thickness configurations of the six test sections. Specifically, both section 1 and section 4 were placed with an 8-in. RCC layer, while sections 2 and 5 had a 6-in. RCC, and a 4-in. RCC was used for section 3 and 6. Each section was about 13 ft. wide and 71.5 ft. long.

Figure 9. RCC test sections
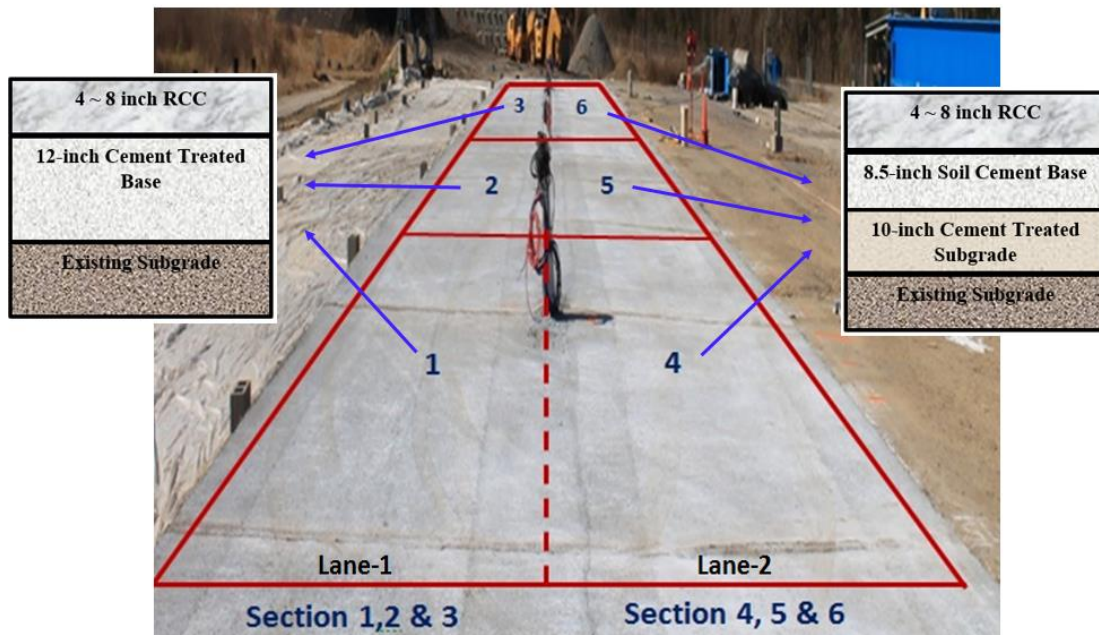
All RCC layers were constructed and paved in single lift using a high-density paver and compacted by a vibratory steel drum roller. The RCC mixture was produced and supplied by a continuous flow pugmill. During the construction, transverse saw-cut joints were created on each RCC test section to minimize or prevent possible randomly generated shrinkage cracking. It should be noted that the APT loading on four RCC sections (Sections 2, 3, 5, and 6) in Figure 9 has been completed in another LTRC project. More details on RCC mixture design and pavement construction can be found elsewhere [27]. The APT experiment of this study was focused on the two 8-in. RCC sections (i.e., Section 1 and Section 4) shown in Figure 9.

Strain Plate Instrumentation

Both 8-in. RCC pavement test sections (i.e., Section 1 and 4) were instrumented with an innovative strain plate for measuring the wheel load and temperature induced strain responses of RCC pavement. As shown in Figure 10, each test section was retrofitted with a thin polymeric plate positioned perpendicularly to the loading direction. The plate was instrumented with fiber optic gages and fixed inside a thin saw cut in the RCC layer with a slow curing epoxy glue. Figure 11 shows the installation of the fiber optic strain plate.

Figure 10. RCC Pavement Test Section and the ATLaS30 Device
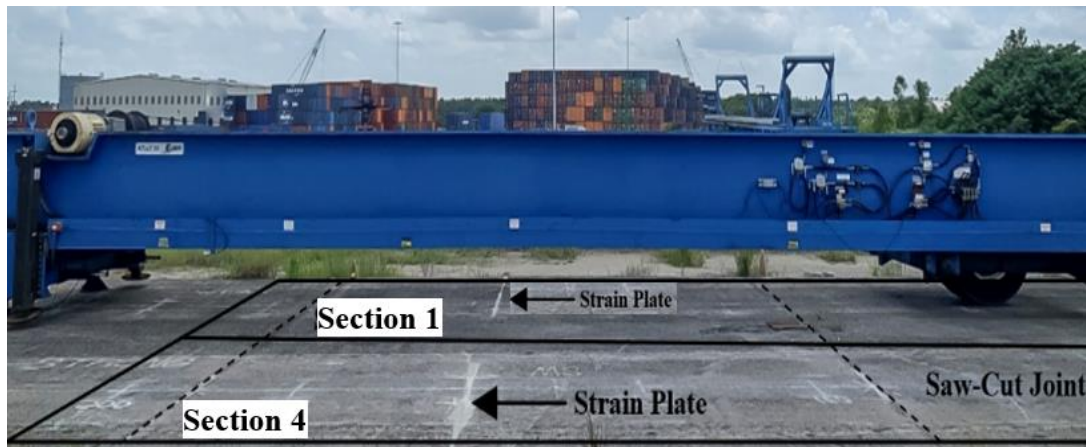
Figure 11. Installation of fiber optic strain plate in RCC pavement test section

(a) Saw cutting

(b) Cleaning of saw cut

(c) Installation

(d) Pouring epoxy

The plate width and thickness are 30 in. and 0.2 in. with a height of 8 in. to fit the thickness of the RCC layer at each test section. Each plate has 16 fiber optic strain gages and three temperature gages at different depths. The sensors were positioned apart along with the plate to measure critical strains under dual tire accelerated loading. Figure 12 shows the layout of the strain and temperature gages on the plate: five transversal strain gages and three vertical strain gages 0.2 in. below the top of the plate; five transversal strain gages and three vertical strain gages 0.2 in. above the bottom of the plate; and three temperature gages at the top, mid depth, and bottom of the plate. This will allow the measurement of vertical and transverse strains in the upper and lower parts of RCC layer under accelerated loading along with the temperature profile throughout the RCC slab.

Figure 12. Strain plate dimensions and sensor locations correspond to wheel load
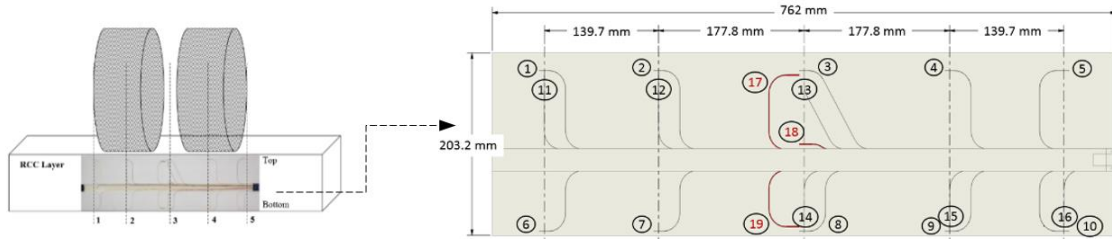
The fiber-optic strain gages working principle is based on the white light polarization interferometry technology. This technology uses a signal conditioner to sense the path length difference inside a Fabry-Perrot interferometer of a known cavity length and delimited by two dielectric mirrors. With proper calibration, the path length difference can be related to strain and temperature measurements.

A data acquisition system (i.e., Opsens DAQ hardware) equipped with eight channels was used to collect the data of the 19 gages on one plate. For this experiment, instrumentation data was collected using Opsens built-in cloud based software, and the raw data files at a 500 Hz collection frequency were saved into separate folders/subfolders according to the test date, dual tire load, repetition, section number, and data type.

After installation, several validation tests were performed shortly to ensure good quality strain measurements. The strains measured by different sensors showed similar shapes and amplitudes under similar loading conditions.

APT Loading and In Situ Measurements

A heavy vehicle load simulation device (ATLaS30) was used for the accelerated loading of RCC test sections in this experiment. The ATLaS30 wheel assembly models one-half of a single axle and is designed to apply a dual-tire load up to 30,000 lbf by hydraulic cylinders. With a computer-controlled loading system, the weight and movement of traffic are simulated over a 40 ft. long loading area in bi-directional mode at a top speed of 6 mph.

In situ tests including the falling weight deflectometer (FWD) and walking profiler test were conducted at different locations along the pavement test section on both loaded and unloaded areas. In addition, an ARRB Walking Profiler G2 was used to measure the centerline profilers of the finished RCC surfaces.

Instrumentation data and surface profiles were collected periodically during the loading experiment. The instrumentation data includes the tensile and vertical strains at various locations on the fiber-optical strain plates due to the wheel loading and temperatures. In addition, surface crack mapping and distress survey were conducted at different load repetitions.

Development of RCC Fatigue Model and Laboratory Experiment

Experimental Design

The main objective of the laboratory experimental design was to perform laboratory fatigue test on in situ saw-cut RCC beam samples and develop a new RCC fatigue model with the consideration of construction and pavement structural variations and true pavement fatigue performance. This study also investigated the variation of RCC in situ flexural strength due to the varying field compaction effort.

Figure 13 shows the overall laboratory experimental design that had been adopted in this study to develop an RCC fatigue model.

Figure 13. Work flow for RCC fatigue model development
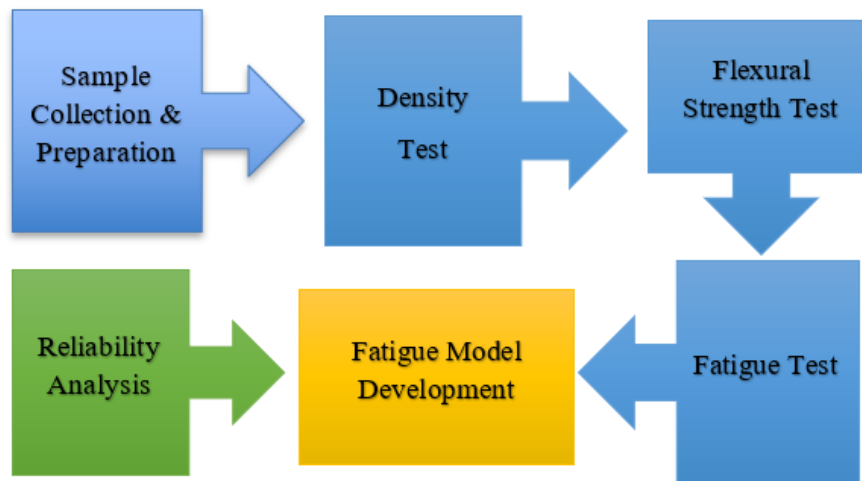
Sample Preparation

As shown in Figure 9, six RCC pavement test sections were constructed at the PRF sites. According to current Louisiana practice, two base designs were utilized, a 150 psi unconfined compressive strength (UCS) cement-treated base (CTB) with a thickness of 12 in. and a 300 psi UCS soil-cement base with a thickness of 8.5 in. over a 10-in. cement treated subgrade. The 10-in. cement treated subgrade contains a cement content of about 4 percent, or just enough to provide a dried stable working platform in which to build the stronger base. Over each base, 4-, 6-, and 8-in. RCC pavement sections were constructed, as shown in Figure 14. The soil-cement base is considered to be stronger than the cement-treated base and is recommended to be used for low to medium volume roadways in Louisiana; whereas, the cement-treated base is more suitable for low-volume roadway application.

Figure 14. RCC pavement structure

(a) Strong   (b) Weak
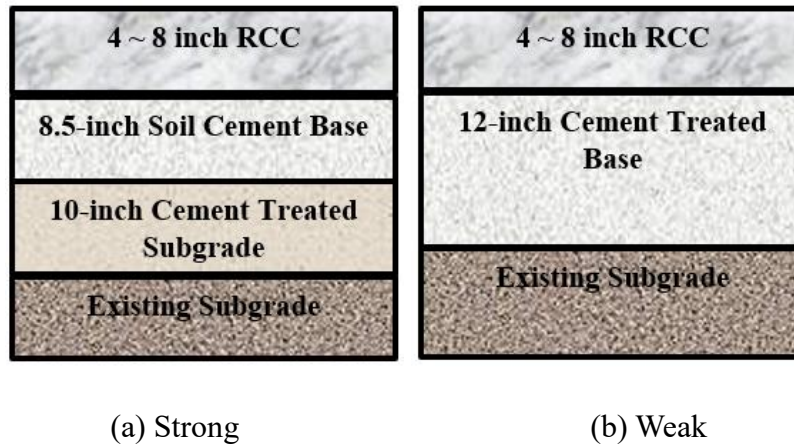
A total of 68 beams (34 from both strong and weak test section) were collected from the RCC test sections with 4 in. and 6 in. surface thickness. At first, a saw cut machine was used to cut and extract the beams from field test sections, shown in Figure 15 (a,b). Later, a laboratory wet saw machine shown in Figure 15(c) had been used to further reshape the collected beams in a rectangular size, 4 in. x 4 in. x 14in. (100 mm x 100 mm x350 mm), to satisfy the specimen size requirements of ASTM C78/78M standard.

Figure 15. (a) RCC beams collection using core cutter (b) Field RCC beams (c) Resizing of beams according to standard using a wet saw (d) Prepared beam specimens for testing

(a)
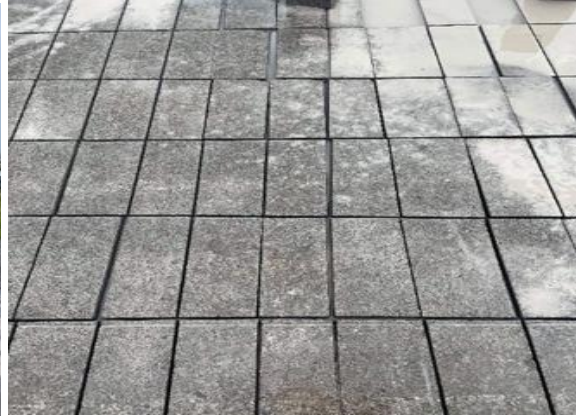
(b)

(c)

(d)

After trimming and resizing during sample preparation, if a beam failed to meet the standard of 4 in. thickness, it was discarded from laboratory testing. That is why few beams from 4-in. test section qualified for the requirement, and 6-in. sections were mostly preferred as it was easy to satisfy the minimum specimen size requirement of third point loading testing.

Density and Specific Gravity Testing

As the pavement structure beneath the RCC surface layer of the two-testing section was different, it was anticipated that the specimens from both sections might have dissimilarities in density due to unique compaction effort. So, at the very beginning of the

laboratory testing, the density of each beam was calculated. For that, initially bulk specific gravity of each of the specimen was measured in laboratory using the principles of ASTM C642-13 (hardened concrete) and AASHTO T166-11 (asphalt) standards as there is no standard developed for RCC materials [14, 60]. According to ASTM, the bulk specific gravity of a material is defined as the ratio of the mass of a specific absolute volume of the material, excluding the mass of water within the pores to the weight of an equal volume of distilled water. The bulk density is then calculated by multiplying the bulk specific gravity of each sample with the unit weight of water.

Figure 16. Density and specific gravity testing of RCC specimen

According to ASTM, this test is useful to match the required specifications for using concrete and to show variations from place to place within a mass of concrete. Bulk specific gravity can be calculated from the following equations:

Bulk specific gravity, $SG = A/(B - C)$ (13)

Bulk density, $\rho = \rho w \; x \; SG$

Where,
A= mass of the oven dry specimen in air, lb.
B= mass of the saturated surface dry specimen in air, lb.
C= mass of specimen in water at 25 ±1°C (77 ±1.8°F), lb.
ρw= density of water, pcf (62.4 pcf).

Flexural and Fatigue Testing

After measuring the density of each collected sample, flexural strength tests of RCC specimens were conducted in a servo-hydraulic loading system according to ASTM C78/78M standard [61]. ASTM C78/78M defined flexural strength of a specimen as the maximum resistance to bending. In other words, assuming linear-elastic behavior of concrete, calculated stress in the tensile face of a beam specimen at the maximum bending moment during a standard test method is termed as flexural strength or modulus of rupture. This material property can be also determined from the compressive strength of concrete from an empirical relationship. However, in this study it is measured using the following formula, where the dimensional properties are known, and the ultimate load is collected from Material Testing System (MTS).

$$f = PL/(bd^2) \tag{14}$$

> Where,
> f = flexural strength (modulus of rupture), psi
> P = the ultimate load, lb.
> L = the span length, 12-in.
> b = the average width of the specimen at the fracture
> d = the average depth of the specimen at the fracture

Generally, to specify the limits of the stress/load controlled flexural fatigue test, at the beginning of third point loading testing, static flexural strengths of the RCC samples need to be determined. In this phase, a total of 24 beam specimens (12 specimens from each section) were subjected to Material Testing System (MTS) machine to obtain the ultimate flexural strengths. During flexural testing, the load should be applied to the specimen continuously and without any shock. The load shall be applied at a constant rate to the breaking point. According to the ASTM standard, the loading rate shall be applied constantly to increase the maximum stress on the tension face between 0.9 and 1.2 MPa/min (125 and 175 psi/min) until rupture occurs. The loading rate can be calculated using the following equation:

$$r = (Sbd^2)/L \tag{15}$$

> Where,
> r = loading rate, lb/min,
> S = rate of increase in maximum stress on the tension face, psi/min,
> b = average width of the specimen as oriented for testing, in.
> d = average depth of the specimen as oriented for testing, in. and

L = span length, in.

It should note that this study applied a constant loading rate that maintains a constant stress of 150 psi/min for all the test specimens in order to avoid unnecessary variability in test results.

In the subsequent phase of third point loading testing shown in Figure 17, a total of 44 field RCC beams (22 from each section) were used for fatigue testing. The stress levels considered for fatigue testing were 0.9, 0.8, 0.7, 0.65, 0.6 and 0.55. The lower levels of the stress ratio (0.55, 0.6, and 0.65) were initially applied to find out the fatigue strength of the field RCC beams. Since the fatigue test was time consuming, two criteria were carefully chosen as the termination condition, whichever occurred earlier (a) complete failure of sample; (b) loading cycle reached 2 million. If a sample reached 2 million cycles, it was assumed the stress ratio is the fatigue strength as a percentage of static flexural strength. To achieve 2 million cycles at 10Hz, a specimen needs to be tested for almost four days without any interruption. The loading mode was selected as stress control and a sine wave load was applied at a frequency of 10 Hz.

Figure 17. (a) Cracked specimen due to flexure (b) Cyclic loading at MTS (c) Failure of a specimen under cyclic loading (d) Obtained cycles to failure at SR = 0.9

(a)   (b)
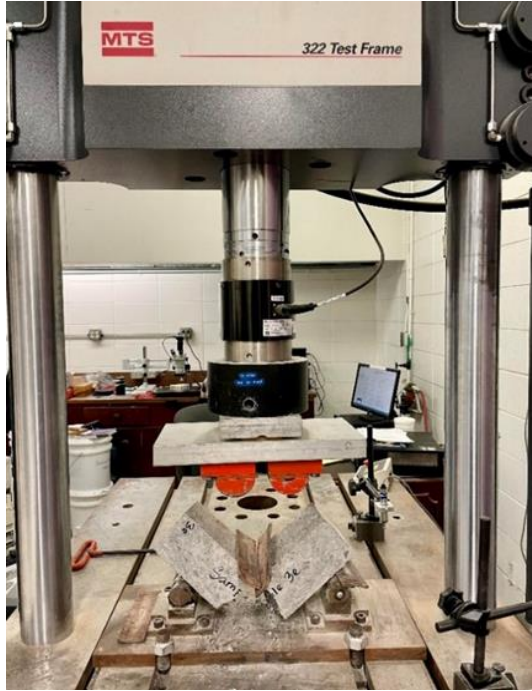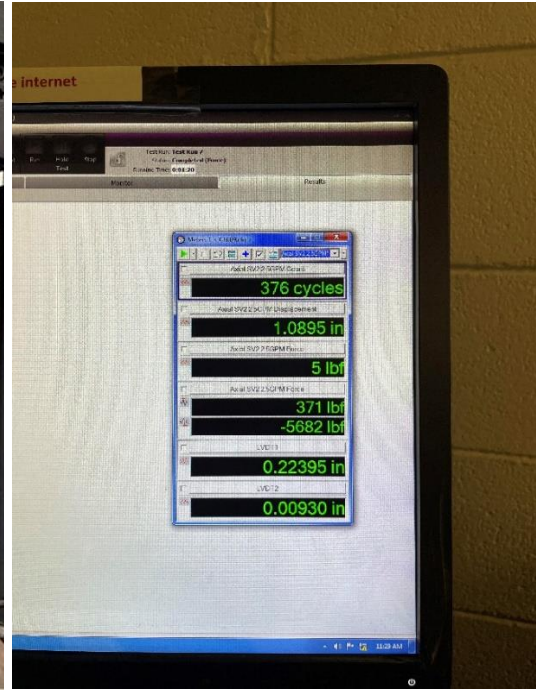
(c)   (d)

One of the critical inputs for beam fatigue testing is the input of absolute end levels which just only depends on the flexural strength of the beam sample. From preliminary flexural strength test results, it was observed that the flexural strength of field RCC samples varied significantly along with the pavement location. Using an average flexural strength value for the determination of absolute end levels for the fatigue testing seemed unreasonable. The absolute end levels are defined as the maximum and minimum loading during a fatigue loading cycle. Since it is impossible to test one beam sample under both flexural and fatigue, extra efforts were taken to extract two adjacent beams from each location along with the pavement test section. While testing for the fatigue life of each sample, the average flexural strength of the adjacent beams was used to determine the absolute end level-1 (f_{max}) and absolute end level-2 (f_{min}). These absolute end levels are defined as the maximum and minimum load that is applied to the sample as the limits of cyclic loading:

$$P_{(ultimate)} = (f_{average} \, bd^2)/L \qquad (16)$$

$$P_{max} = SR * P \; ultimate \; (specimen) \quad (17)$$

$$P\_min = R * P\_max \qquad\qquad\qquad\qquad (18)$$

Where, P_(ultimate) = the ultimate (maximum) load, lb

f_average = the average flexural strength of the adjacent beams, psi,

fmax = maximum load in a cycle, lb.

fmin= minimum load in a cycle, lb.

SR = stress ratio

R= ratio between maximum and minimum stress in a loading cycle (fmax/fmin)

Previous studies showed that the ratio (R) between the maximum and minimum loading in a fatigue cycle was usually taken in the range from 0.1-0.25, and the influence of the ratio is comparatively less when the value is less than 0.25 [38]. For this study, this ratio was taken as 0.2 to reduce the impact load during fatigue testing.

Application of M-E Approach into RCC Pavement Thickness Design

Due to the current RCC thickness design methods being empirically based, this study proposed a mechanistic-empirical (M-E) based design procedure for RCC pavement thickness design. Figure 18 presents the proposed M-E based design framework for an RCC pavement thickness design.

Figure 18. Proposed RCC Pavement thickness design framework
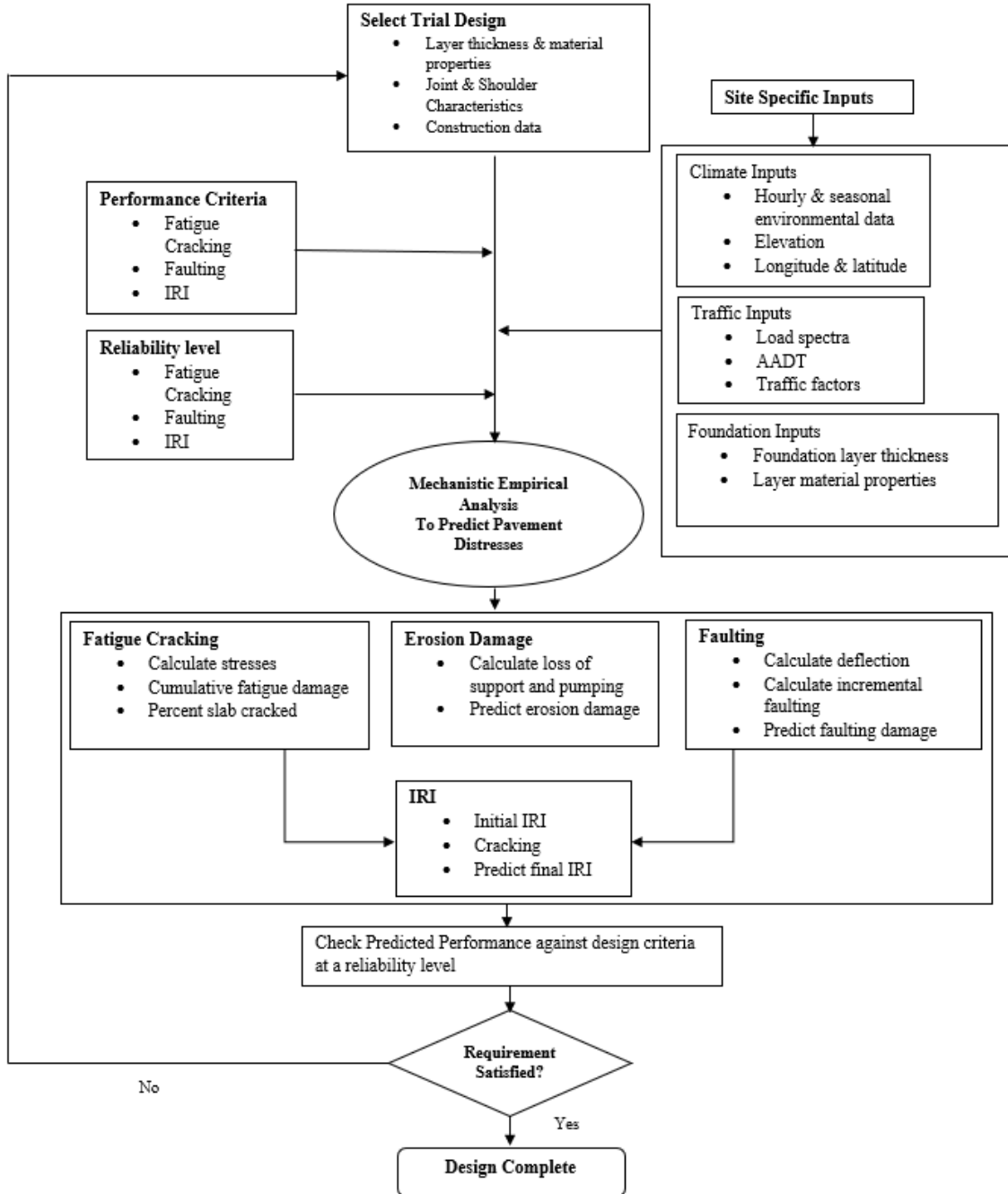
The proposed procedure incorporates a mechanistic component (load/stress/deflection) with empirical observations, including results from the accelerated pavement testing of different RCC pavement sections, to establish an RCC pavement thickness design. The procedure will evaluate the traffic stream with load spectra and assesses each load and axle type separately. This will allow for more detailed traffic input. This detail can

dramatically influence design thickness as heavy axle loads have a significant effect on loading. Another important consideration in the proposed procedure is the effect of temperature, moisture, and seasonal variation of material properties. The temperature and moisture variations across the depth of pavement cross section result in pavement deformation that influences the pavement performance significantly. Therefore, the deformation caused by each of these factors must be taken into consideration.

The mechanistic portion, which consists of evaluating critical stresses and deflections, will be based on a finite element analysis. The critical stresses and deflections will be used to develop design tables and charts based on general pavement design knowledge and empirical pavement performance and research.

The empirical portion contains different components like fatigue, erosion and smoothness. The fatigue analysis simply evaluates the fatigue of the RCC pavement. An empirical fatigue model, based on the APT results, will be recommended as the fatigue model for the design procedure of RCC pavement, and another empirical model will be proposed to estimate the percent fatigue cracking. The erosion analysis evaluates the potential for a concrete pavement to fail by pumping, erosion of the foundation support, and/or joint faulting, and is based on corner deflections. An erosion model will be proposed to consider the erosion related pavement damage. The model will evaluate the work done by the pavement system as a function of corner deflection; pressure at the slab-foundation interface; concrete modulus of elasticity and Poisson's ratio; slab thickness; and modulus of subgrade reaction. Conceptually, a thinner pavement has a shorter deflection basin than a thicker pavement, and therefore, will "punch" into the subbase faster. Finally, the International Roughness Index (IRI) model will be proposed based on the fatigue cracking, initial IRI and site factors to predict the smoothness of RCC pavement over the entire design period.

Discussion of Results

The results presented for discussion were obtained from both laboratory and APT measurements, including the fatigue testing, nondestructive testing, instrumentation data, surface crack mapping, and forensic trenches on failed RCC test sections. In addition, the fatigue performance of RCC pavements were analyzed in detail, which has led to the development of fatigue equations for RCC pavement structures.

Results from Accelerated Pavement Testing

The accelerated loading test started on Section 4, followed by Section 5, Section 6, Section 3, Section 2, and Section 1 in a time sequence order (Figure 9). Each test section was loaded by an incremental loading sequence of 9, 16, 20, 22, 25, and 27.5 kips. Table 2 provides a list of different dual-tire load magnitudes with the corresponding loading repetitions applied on each RCC section along with distresses observed at the end of APT testing. Note that, for Sections 1 and 4, due to having a relatively thick RCC slab thickness (i.e., 8 in.), only limited numbers of loading were applied. For this experiment, a test section was considered to have failed when 40% of the trafficked area of a section developed visible cracks (e.g., longitudinal, transverse, and alligator cracks) more than 1 ft./ft^2.

Table 2. APT loading passes and test section distresses

Half Axle Load (kips)	RCC Pavement Test Sections					
	Section 1	Section 2	Section 3	Section 4	Section 5	Section 6
9	178500	108,000	73,000	178,500	112,000	78,500
16	278500	265,000	73,000	178,500	404,000	392,500
20	270500	108,000	50,000	228,500	398,000	78,500
22		108,000		78,500	108,000	78,500
25		106,000		78,500	487,000	78,500
27.5					241,850	
Total Passes	727,500	695,000	196,000	742,500	1,750,850	706,500
Estimated ESALs (x10^6)	9.9	19.4	2.7	16.2	87.4	19.2

Fatigue cracking (%)	10.6	53.5	46.8	20.4	40.9	41.0
Slab Settlement (in.)	<0.1	0.3	0.15	<0.1	0.15	0.2
ΔIRI (in./mi.)	32.7	219.8	94.2	51.3	75.6	108.9

In this study, the predicted ESAL numbers were computed using an equivalent axle load factor (EALF) multiplied by the corresponding number of load repetitions under a certain ATLaS30 axle load. The EALFs for different ATLaS30 axle loads were estimated based on the AASHTO's rigid pavement equations as follows [62]:

$$\log(EALF) = 4.62\log(18+1) - 4.62\log(L_x + L_2) + 3.28\log L_2 + \frac{G_t}{\beta_x} - \frac{G_t}{\beta_{18}} \tag{1}$$

$$G_t = \log\left(\frac{4.5 - p_t}{4.5 - 1.5}\right) \qquad \beta_x = 1.00 + \frac{3.63(L_x + L_2)^{5.20}}{(D+1)^{8.46} L_2^{3.52}}$$

Where,

L_x is the load in kip on different axles;

L_2 is the axle code, 1 for single axle, 2 for tandem axles, and 3 for tridem axles;

p_t is the terminal serviceability, which indicates the pavement conditions to be considered as failures; and

D is the slab thickness in inches.

RCC Pavement Test Section Performance

At the end of the APT experiment, four sections (Sections 2, 3, 5, and 6) were continuously loaded and found to have reached their respectively pavement service lives, as evidenced by the extensive surface cracks and significant surface roughness shown in Figure 19. The two 8-in. RCC sections 1 and 4, however, were not loaded to failure due to a concern of possibly extremely long loading time.

Figure 19. RCC pavement condition at the end of testing

The crack development under different load repetitions at different stages were recorded in this study for all RCC pavement test sections. After initial cracking was noticed in the sections, an FWD test was performed and the backcalculated subgrade moduli (MR) at different stations was determined. Based on the backcalculation results, it was noticed that cracking initially developed at the area of lower subgrade moduli. Figure 20 shows

the cracking development under different load repetitions on the RCC test sections. Detail information regarding the cracking development can be found in LTRC final report 12-7P [27].

Figure 20. Crack mapping of RCC test sections
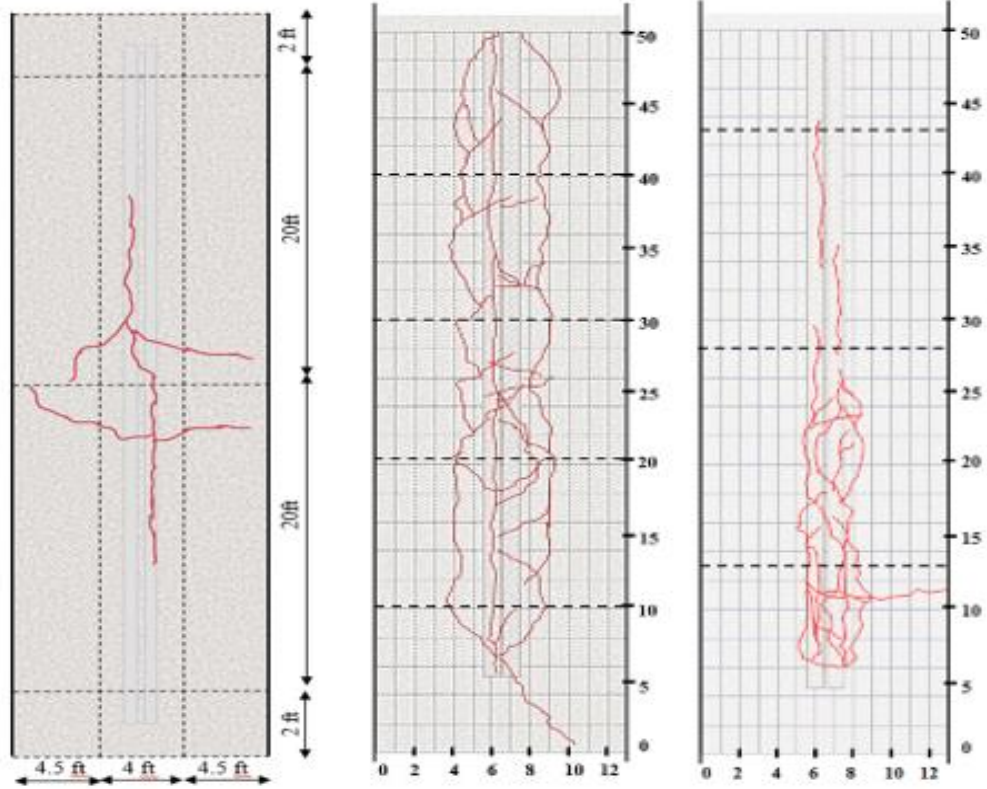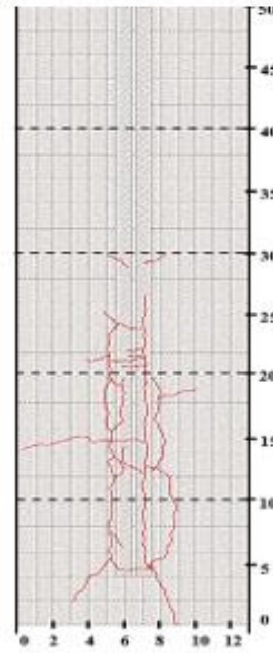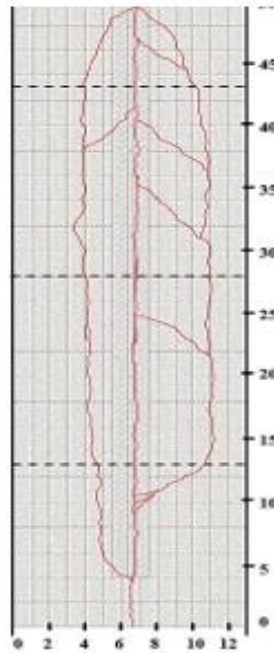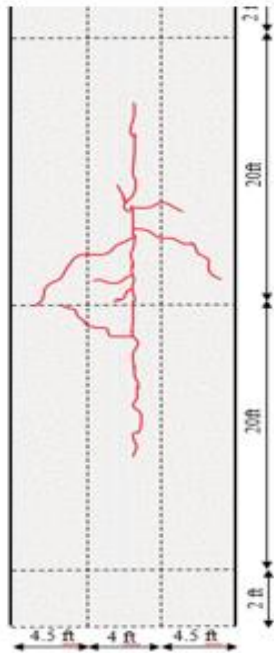
As the induced wheel loading was applied bi-directionally on the test sections, joint faulting was not anticipated. However, pumping of fines was observed through saw cut joints and cracks, which resulted in slab settlement, Figure 21. Later, to verify the observed distresses in the RCC sections, post-mortem results on the failed RCC pavement sections were evaluated.

Figure 21. (a) Observed pumping (b) Observed slab settlement

(a)   (b)

The post-mortem trench observation showed that the longitudinal cracks under the wheel path are mostly bottom-up cracking, as shown in Figure 22. Likewise, all the sections had voids underneath the RCC layer caused by the loss of material due to erosion and pumping, Figure 22 (b). This void can lead to the slab settlement. The post-mortem results also revealed that initially transverse cracking occurred at the saw cut joints that propagate along the slab.

Figure 22. Cracking mechanism

(a) Bottom up cracking   (b) Voids   (c) Cracked Saw cut joint
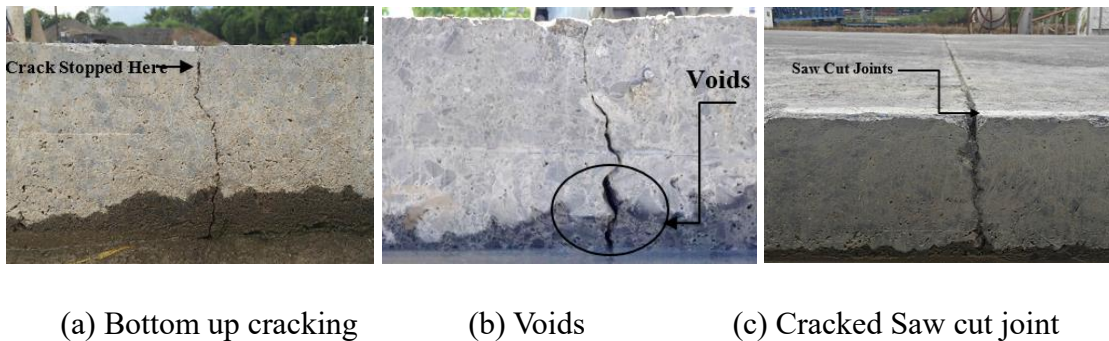
Instrumentation Measurement Results

Both load induced and temperature induced pavement responses were investigated during the APT experiment. Before collecting the instrumentation data, the fiber optic plate installation was verified to check the uniformity of the pavement structure. FWD tests were performed on both the RCC pavement test sections to study the uniformity of pavement structures before and after retrofitting the fiber optic plate. Table 3 shows the change in average deflection at the center of the FWD load plate (D0) before and after the plate installation at the installation location under 9 kip FWD load. There is no significant change observed at the center deflection indicating no substantial damage on the pavement structure.

Table 3. FWD deflection under the load plate before and after plate installation

	Before plate installation	After plate installation	%difference
	Average D0 (mils)	Average D0 (mils)	
Section-1	2.72	2.83	3.89%
Section-4	2.91	3.01	3.32%

Strain responses were also recorded under FWD loading at different load magnitudes. Figure 23 shows the strain basin at the bottom of the RCC layer under 16 kips FWD load at different locations (stations A, B, and C). As can be seen from the figure, installation of the fiber optic plates did not cause any weakening or strengthening of the pavement structures and behaved as an integral part of the RCC pavement test section. The results also confirm that the strain basin patterns were the same for a FWD loading plate positioned on either side of the strain plate. Same responses were observed at the top transverse sensors and under different load magnitudes. This indicates that a good bonding of the epoxy with the RCC layer was achieved and the plate was able to transfer the applied loads to the entire strain plate indicating continuity of the RCC pavement layer.

Figure 23. Strain basin at the bottom of RCC layer under FWD loads
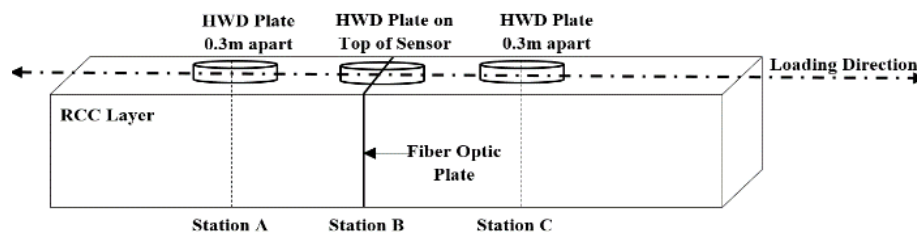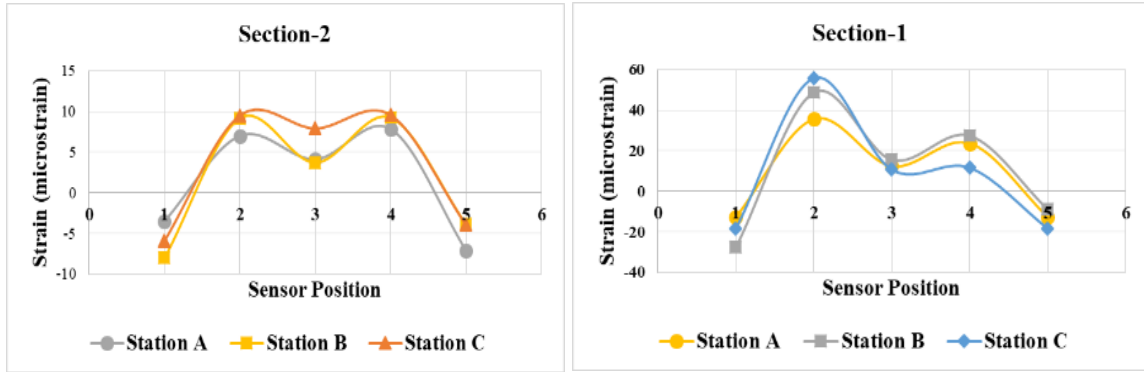
Load-Induced Pavement Responses

In this study, load-induced strain responses were recorded at 8-in. RCC sections under four different load magnitudes (9, 16, 20, and 25 kip). The recorded data was used to produce strain basins under different loading conditions. Figure 24 shows the typical strain output patterns in both top and bottom of RCC layer under 4 passes of a bi-directional dual tire loading. As shown in the figure, for the transversal strains (top and bottom), compression was observed at the upper and tension at the lower part of the slab due to the bending behavior of the RCC layer. The strain responses also indicated that the strain relaxation time between the first two consecutive passes was not enough for full strain recovery. That was because of the installation of a fiber optic plate near one end of the pavement section where the wheel turns its direction. Another major observation from the strain responses shows that the two peak strain values under bi-directional loading were not always identical. This is due to the fact that the pavement had a slope from north to southbound and due to the pavement slope, ATLaS30 hydraulic system can not maintain the same load level in both directions. The difference between the two peaks was not significant in most of the cases and can be considered negligible. However, for such cases, the average of the two peak values were considered during analysis. More typical strain responses can be referred to Appendix A.

Figure 24.Typical strain responses under ATLaS30 dual tire load at the bottom and top sensors
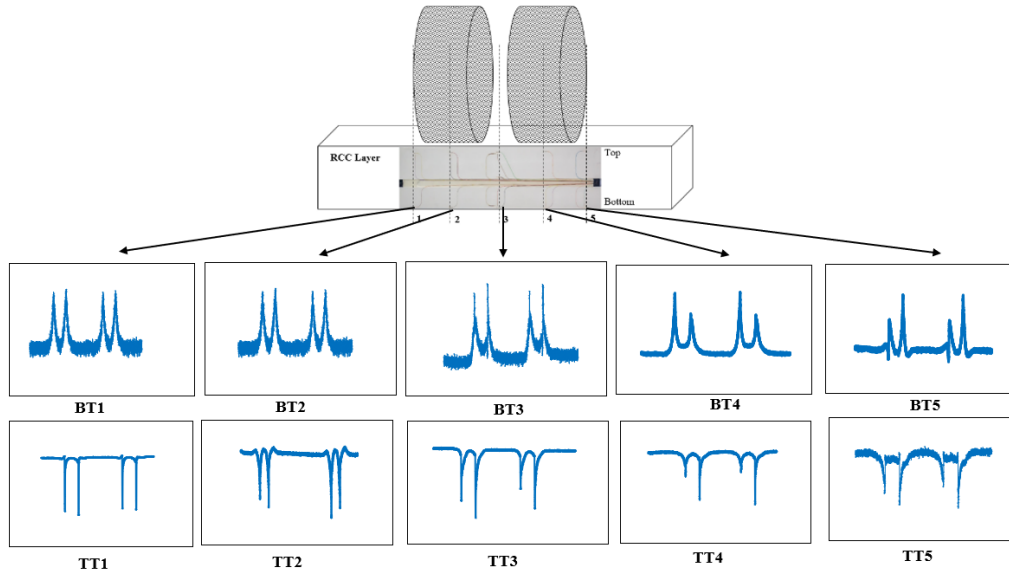
The strain data collected with the plate was either negative (compression) or positive (tension). As shown in Figure 25 for the transversal strains (top and bottom), compression was observed at the top and tension at the bottom due to the bending flexural behavior of the RCC layer. It was observed that the critical compressive strain at the top of the RCC layer occurred at Section 3 (middle of dual tire loading), whereas the critical bottom tensile strain occurred at the middle of each individual tire at Section 2 or 4. Similar strain basins were observed under dynamic loading and different load magnitudes.

Figure 25. Strain basin at top and bottom of RCC layer under ATLaS30 dual tire loading
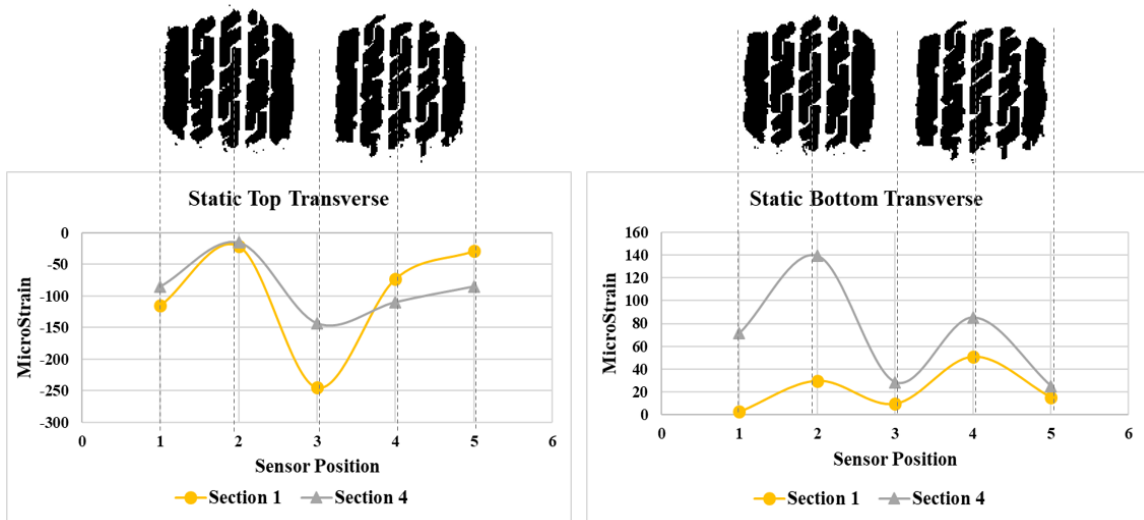
It was also observed that Section 1 exhibits less critical tensile strain compared to Section 4 for the same loading and weather conditions. According to the pavement structure, Section 1 was supposed to be a weaker section compared to Section 4 due to having a weaker base support resulting in higher tensile strain at the bottom. However, based on field core samples, it was reported in the previous study that Section 1 was built thicker than the designed thickness [27]. That explains why Section 1 has less tensile strain compared to Section 4. The FWD surface deflection under the FWD plate also showed that Section 1 had less center surface deflection compared to Section 4.

Furthermore, the pavement responses under static and dynamic loading conditions were investigated at the top and bottom of the RCC layer under different ATLaS30 dual tire loading, Figure 26.

Figure 26. Pavement strain responses under different ATLaS30 load magnitude
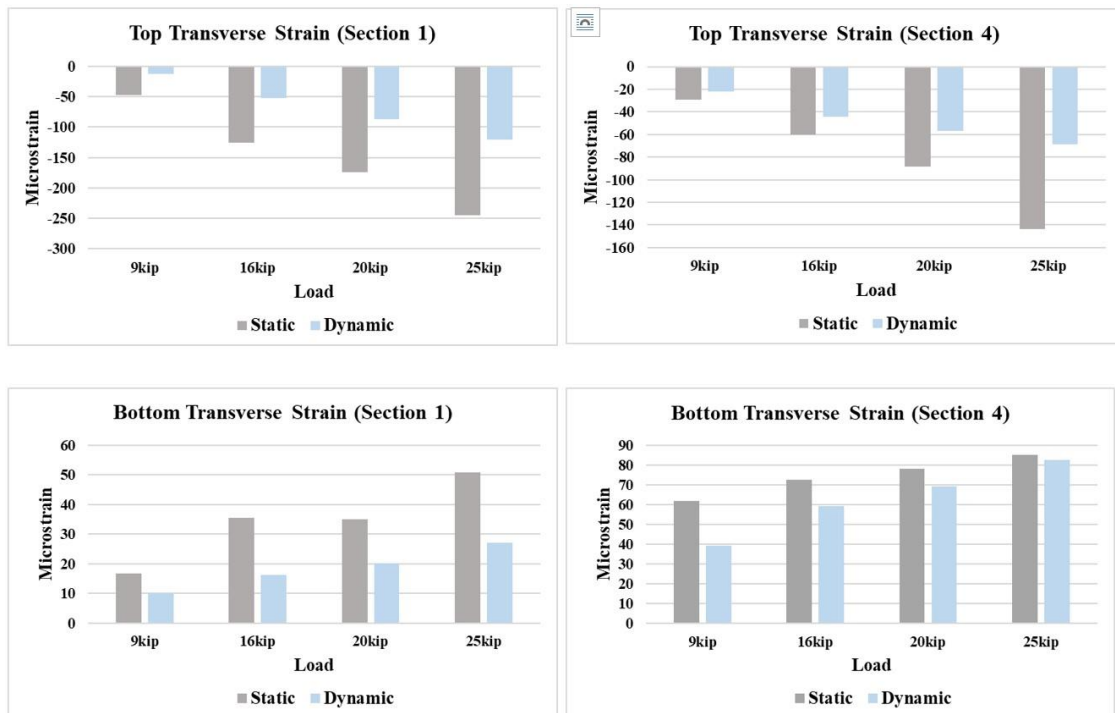
For both, static and dynamic loading, the compressive strains at the top of the RCC layers showed an increasing strain with the increase of the load level, as well as a decreasing strain with the increase of the RCC layer thickness. Similarly, the tensile strains at the bottom of the RCC layers showed an increasing strain with the increase of the load level, as well as a decreasing strain with the increase of the RCC layer thickness. The dynamic

pavement responses were observed to be lower than the static loading for the top and bottom of both pavements.

Temperature Induced Pavement Responses

It is very important to consider curling stress and moisture warping in RCC pavement thickness design, because curling stress may be quite large and cause the slab to crack when combined with only very few number of load repetitions. For day-time curling condition, compressive curling stresses are induced at the top of the slab whereas tensile stresses occur at the bottom; or vice versa for night-time curling condition. The moisture gradient in concrete slabs also results in additional warping stresses. The temperature related stresses also largely depend on the coefficient of thermal expansion (CTE), hourly and seasonal temperature, moisture variation, and effective built-in temperature gradient that exists in the slab at zero-stress time. To quantify the temperature related damage, local temperature gradients need to be studied and considered in the damage analysis for RCC pavement especially for mechanistic-empirical design procedure.

Temperature readings along the depth of RCC slabs were recorded during the APT study and the temperature profile exhibited the non-linearity of the temperature distribution along the slab, Figure 27. The daily temperature gradients recorded over the entire study ranged between +18°C to -9.5°C.

Figure 27. Temperature profile along the depth of RCC slab
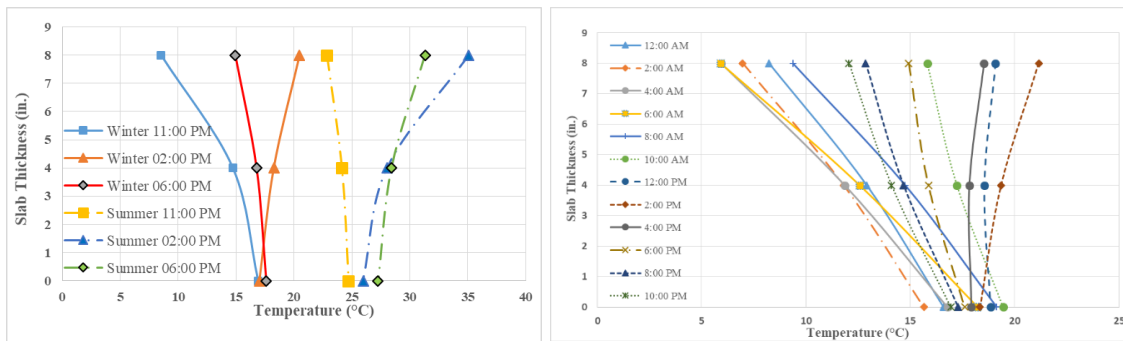
The coefficient of thermal expansion (CTE) of RCC test sections were measured from the recorded strain responses without any kind of wheel loading. Though CTE is a material property, recorded data from both the sections were used to measure considering it an in situ property and investigated the variations due to pavement structure. Figure 28 below shows the typical static strain change in the transverse direction due to temperature and

moisture fluctuations for both the RCC test sections and the slope of the curves is identified as the RCC thermal expansion coefficients.

Figure 28. Static Strain response with temperature variation in a 24-hour cycle (a) Section 4 Top Transverse (b) Section 4 Bottom Transverse (c) Section 1 Top Transverse (d) Section 1 Bottom Transverse
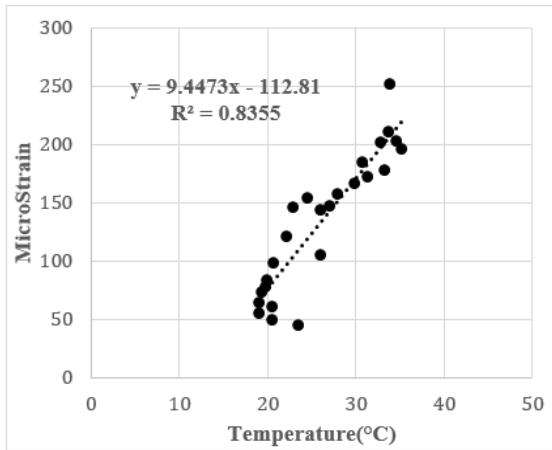
(a)
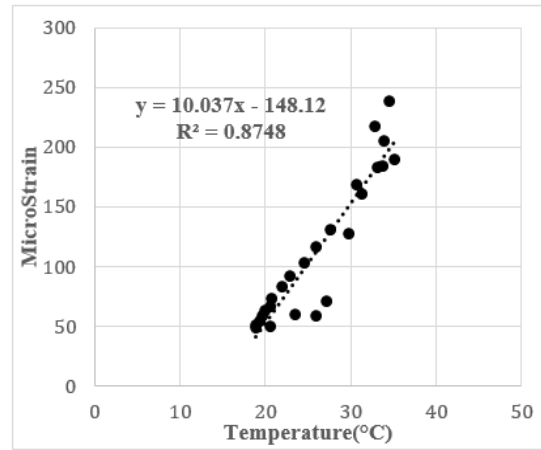
(b)
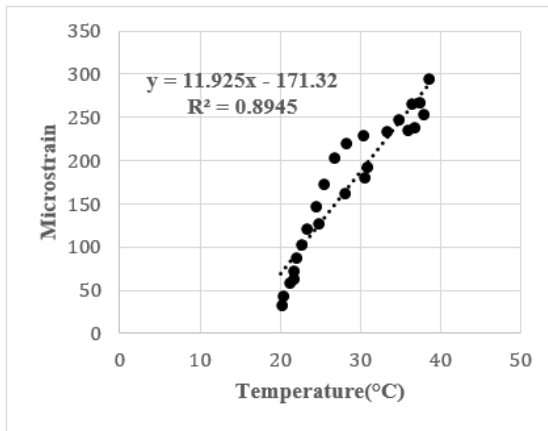
(c)
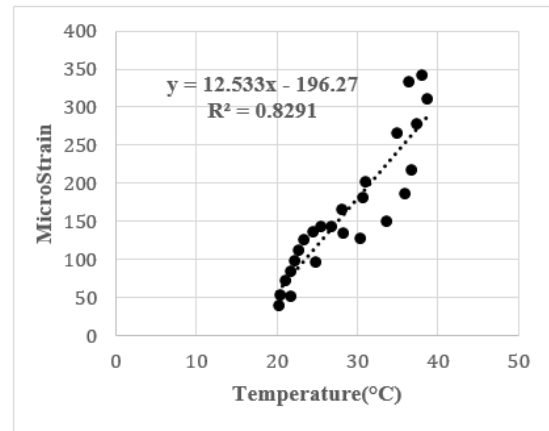
(d)

According to the strain responses from Figure 28 shown considering both sections, the in situ thermal expansion coefficient values for RCC slabs ranged from 9.44 µε/°C to 12.53 µε/°C (5.0 µε/°F to 7.5 µε/°F). However, Section 4 illustrates lower CTE value (9.44 µε/°C to 10.04 µε/°C) compared to Section 1 (11.93 µε/°C to 12.53 µε/°C), which implies strain response in this section against thermal loading is lower. All the equations shown in the figures also got higher goodness of fit values. The substantial difference observed in

thermal expansion coefficient between Section 1 and Section 4 could be due to the construction variability or the slab restrain. Section 1 had an open edge with no edge support and was more exposed to the moisture condition. The combined effect of load and temperature was validated by a finite element model in the next section where the measure response by the APT study was compared with a model with similar geometric properties.

Laboratory Testing Results of RCC Beams

Variation of RCC Beam Flexural Strength

As stated earlier, a total of 24 field saw-cut beam samples were tested for flexural strength using third point loading setup prior to the beam fatigue testing. Equal number of samples (12 each) were collected from both test sections to investigate the field compaction variability. After the density test and flexural strength test of the samples were conducted, a clear distinction between the results of weak and strong section was observed. The results are also in line with the 28-day compressive strength results obtained from the field core samples during the construction phase. As the material composition and construction practice was the same for both sections, the only difference was the density resulting from compaction effort. It was intended to confirm if the flexural strength of the two sample groups were significantly different. To achieve that objective, a one-tailed t-test was conducted (considering the equal variance of two sample groups) to examine the following hypothesis:

- Null hypothesis (H_o): Mean of the flexural strength of strong section = Mean of the flexural strength of weak section;

- Alternative hypothesis (H_1): Mean of the flexural strength of strong section $\neq$ Mean of the flexural strength of weak section.

The two-tailed t-statistics result showed that the null hypotheses can be rejected at a significance level of 1% based on the obtained p-value of 0.0007 (<0.01). In other words, there is not sufficient evidence to conclude that the mean flexural strength of two test sections is equal. Therefore, it is evident that compaction effort (density variation) might have a crucial impact to the flexural strength of the RCC samples as the mix design was same for both test sections. However, other variables (i.e., time and temperature during

construction, moisture content, etc.) may also have an impact on the flexural strength results. Table 4 shows the results of two test sections during this phase of the study.

Table 4. Results of density and flexural strength testing

Measured Parameters		Strong Section	Weak Section
Density (pcf)	Average	152.1	149.6
	Range (max-min)	150.2-153.4	145.6-151.1
Flexural Strength (psi)	Average	1020	870
	Range (max-min)	850-1240	710-1075

While the t-test established that density variation might have an impact on RCC flexural strength, it was essential to develop a link between them. Figure 29 shows the correlation between the density and flexural strength utilizing the lab test results. It displays a strong positive relationship based on the goodness of fit value ($R^2 = 82\%$). Here, the illustrated linearly positive relationship shows that with the increase in density, the RCC flexural strength also increases. This relation was generated using 23 out of the 24 samples that were tested for flexural strength. One sample from weak section was discarded as the failure was due to a premature crack outside of the middle section.

Figure 29. Relationship between flexural strength and measured laboratory density
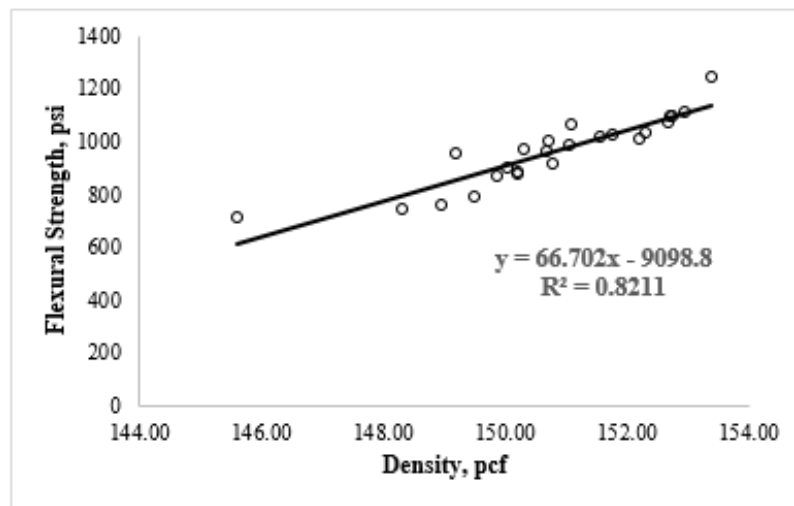
All the 24 specimens used in flexural testing had different densities. It was clear that dissimilarities in density might play a role during the testing for fatigue life. To

contemplate that, as stated in the experimental setup, for each sample during fatigue testing, absolute end levels 1 (P_{max}) and 2 (P_{min}) were calculated based on the average flexural strength of the adjacent beams. Such a strategy aimed to reduce the inconsistency of S-N relationship subjected to the varied density of RCC field beam samples.

Beam Fatigue Results

As described in the methodology, 44 beam fatigue tests were performed in this study. The testing factorial and beam fatigue test results are presented in Table 5. From the results shown in Table 5, it can be observed that as the stress ratio increased up to 0.65, the RCC beams can withstand 2 million fatigue cycles. Thus, based on the literature, it can be concluded that the obtained fatigue strength or the fatigue endurance limit of the collected RCC beams was 65% of the static flexural strength [48, 63-65].

Table 5. Fatigue Testing Results

Section	Stress Ratio	No. of Samples	Total loading Cycles
Strong Section	0.55	2	+2 million
	0.60	2	+2 million
	0.65	2	+2 million
	0.70	6	985330, 102205, 301194, 423386, 308012, 256836
	0.80	5	2023, 5937, 2560, 5741,10801
	0.90	5	531, 563, 666, 784,1983
Weak Section	0.55	2	+ 2 million
	0.60	2	+ 2 million
	0.65	2	+ 2 million
	0.70	6	37608, 523285, 80832, 106424, 555551, 594785
	0.80	5	1781, 7472, 6524, 7086, 2020
	0.90	5	298, 376, 594, 712, 1229

As the previous section revealed, the flexural strength of the strong section is significantly different than the weak section. It was necessary to perform an additional hypothesis test to check if the fatigue life of the strong section is significantly better than the weak section. Therefore, one tailed t-test was performed for each stress ratios considering unequal variance of two sample groups to examine the following hypothesis at 5% level of significance:

- Null hypothesis (H$_o$): Mean of the fatigue life of strong section - Mean of the fatigue life of weak section ≤ 0

- Alternative hypothesis (H$_1$): Mean of the fatigue life of strong section - Mean of the fatigue life of weak section > 0.

The p-value obtained from the hypothesis testing were 0.21, 0.46, and 0.22 for stress ratio of 0.7, 0.8, and 0.9, respectively. All the obtained p-values were greater than the significance level (0.05) of the hypothesis tests. Therefore, the null hypothesis cannot be rejected. In other words, there is not sufficient evidence to conclude that the strong section produces better fatigue life than the weak section.

Development of RCC Fatigue Model

Development of S-N Curve. The S-N approach was utilized to investigate the fatigue performance of RCC beam samples. The S-N curve for any rigid material represents the relationship between the applied stress ratio, and the number of load cycles applied till fatigue failure of the specimen [44, 66]. The equation for S-N relationship is commonly expressed in the following form:

$$Log\ Nf\ =\ A\ -\ B * SR \tag{20}$$

　　　　　Where,
　　　　　SR = stress ratio
　　　　　Nf = number of cycles to failure
　　　　　A, B = regression coefficients

Initially, S-N relation was examined for the beam samples collected from each test section and then a final fatigue curve was developed utilizing all the sample results. Nearly two-thirds of the prepared beams (32 specimens: 16 from each section) were used to develop the fatigue curve. The remaining 12 specimens were used for defining the fatigue strength of the RCC field specimen at 2 million cycles. Figures 30 (a) and 30 (b) illustrate the S-N relation for the samples collected from the strong section and weak section respectively. The results for these two cases are then combined and shown in Figure 30 (c). All three S-N curves show a strong relationship between the stress ratio and loading cycles to failure. From the combined results as shown in Figure 30 (c) the final fatigue model developed for this study can be expressed as follows:

Log Nf= 15.499 – 14.493*SR　　　　　　　　　　　　　　(21)

Figure 30. S-N relationship from the lab fatigue test for: (a) Strong section (b) Weak section (c) Combined

(a)

(b)
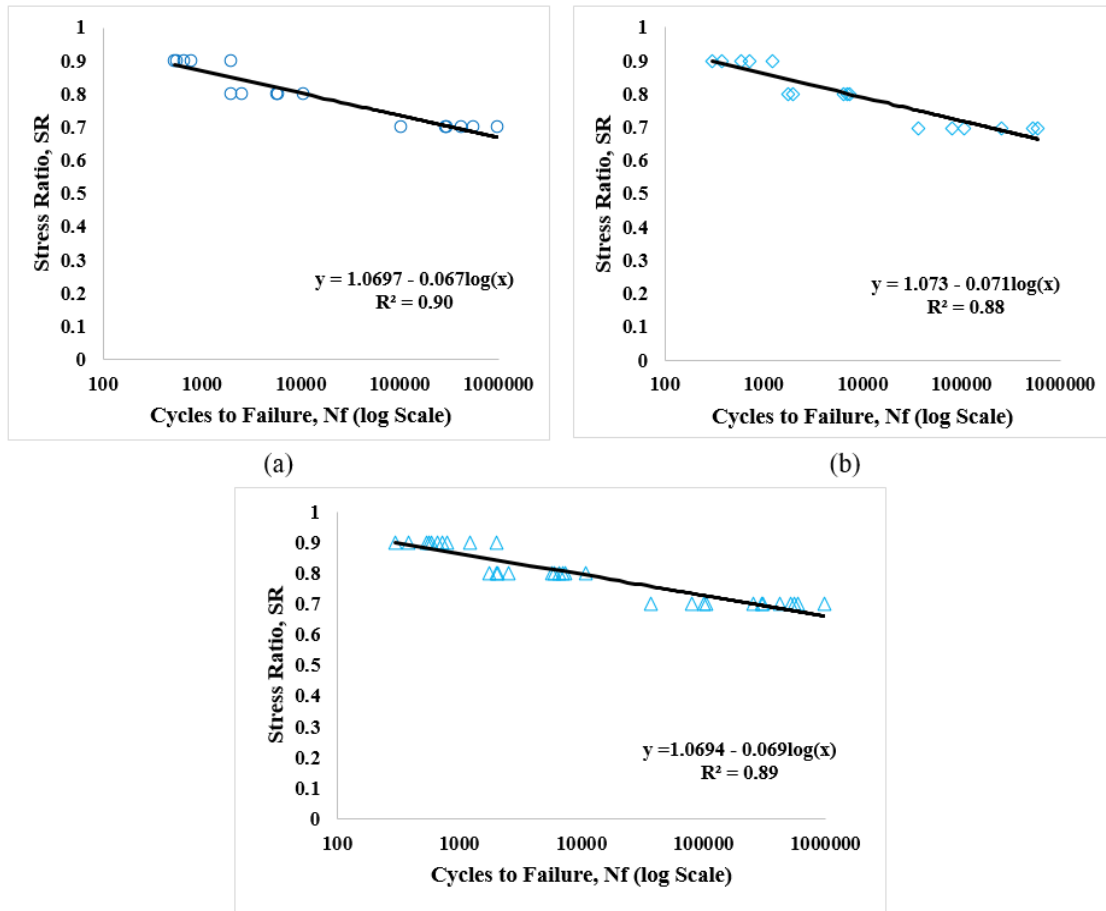
Reliability of the S-N Curve. The fatigue test results shown in Figure 30 indicate that the fatigue life data are generally scattered and different from each other even at the same stress ratio. This is caused by the uncertainty of the fatigue behavior of RCC materials including the variation of the beam density. It is commonly assumed that any design curves related to material strength are always subject to statistical variability. Probabilistic reliability theory is an effective way to deal with this uncertainty in the result. The American Society of Testing and Materials (ASTM)'s Special Publication 91-A provides three statistical analysis models for analysis of fatigue testing data: normal distribution model, lognormal distribution model, and Weibull distribution model. The Weibull distribution model is generally considered to be the most suitable model for describing the fatigue life distribution of concrete type material [67, 68]. In this study, the Weibull distribution model is used in the reliability of the developed S-N curve. A similar

Weibull distribution approach was also employed by the Sengun et al. (2021) study [48]. The Weibull's cumulative distribution function (CDF) is shown in equation 22:

$$F(x) = 1 - e^{\wedge}(-(x/\lambda)^{\wedge}k) \; ; \; \lambda \geq 0, k \geq 0 \tag{22}$$

Where,

λ and k are the scale and shape factors.

The following relationship between reliability and probability of failure can be obtained if we substitute $R = e^{\wedge}(-(x/\lambda)^{\wedge}k)$ and probability of failure, P= F (x), in the cumulative distribution function (CDF):

$$P = 1 - R \tag{23}$$

Based on the referred Weibull approach, various failure probability curves for field RCC beams were constructed and presented in Figure 31 (a). For each stress ratio, (SR), the number cycles, (Nf), are plotted against the probability of failure, P in a semi-log scale. The obtained shape and scale factors, (k, λ), of Weibull distribution for stress ratios 0.7, 0.8 and 0.9 were (0.376, 155825.7); (17.836, 115679.9); and (102.4, 97798.69) respectively. As expected, the predicted number of load repetitions increased as the probability of failure increased.

Figure 31. (a) Failure probability curves (b) The developed S-N curves at different reliabilities
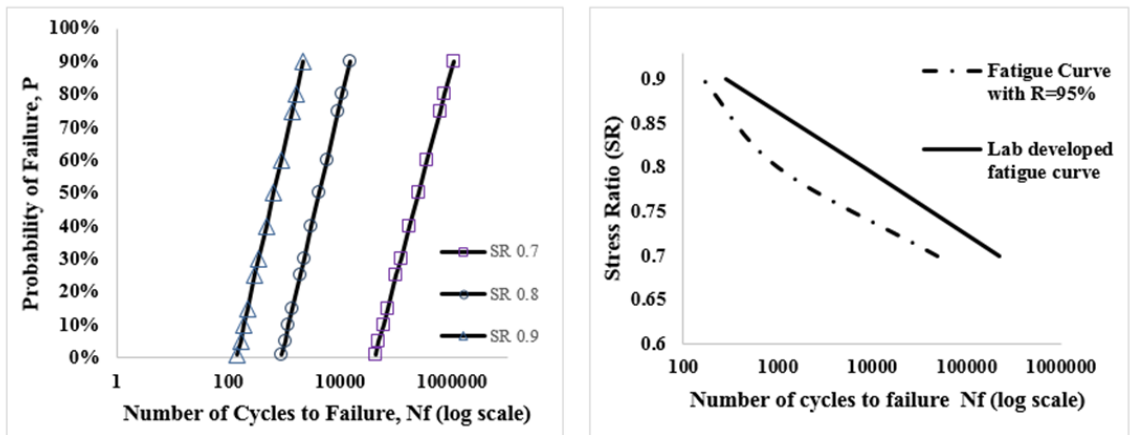
(a)   (b)

For pavement design purposes, the typical range of probability of failure ranges from 1% to 50% (26, 27). Figure 31 (b) shows the comparison of the developed RCC fatigue curves using raw laboratory data and at 95% reliability (P=5%) based on Weibull's distribution. Since the developed model is sensitive to both SR and probability of failure,

this model satisfies the objectives of this study and would be suitable for implementation for RCC pavement design.

Evaluation of the Developed RCC Fatigue Model

Figure 32 shows the plots of stress ratio versus the number of cycles to failure of the fatigue model developed in this study along with the current StreetPave fatigue model and models developed from existing studies at a reliability level of 50% [41, 48, and 50]. In this figure, the typical Portland Cement Concrete (PCC) fatigue curve based on Darter's zero maintenance concept is also compared with the developed fatigue model [35]. Though lab developed, fatigue curves are assumed to have 50% reliability; here, the developed curve is plotted based on 50% reliability by Weibull's approach. As shown in the figure, the developed RCC fatigue curve will generally suggest a longer service life for a given condition, and number of load repetitions compared to other models currently used for PCC and RCC fatigue life prediction. The obtained result from this study is also complemented by a study conducted on RCC fracture property that showed RCC mix had better fracture property that can lead to better fatigue life compared to plain concrete. It also suggests that a higher stress ratio can be allowable for a given number of load repetitions in design, indicating more optimized thickness requirements for RCC pavements in roadway applications. Figure 32 also illustrates that, while comparing with the developed model, the RCC fatigue model developed by Sun et al. (1998) and Sengun et al. (2021) are more conservative in predicting RCC fatigue life at higher stress ratio [48, 50].

Figure 32. Comparison of developed RCC fatigue curves with other curves at 50% reliability
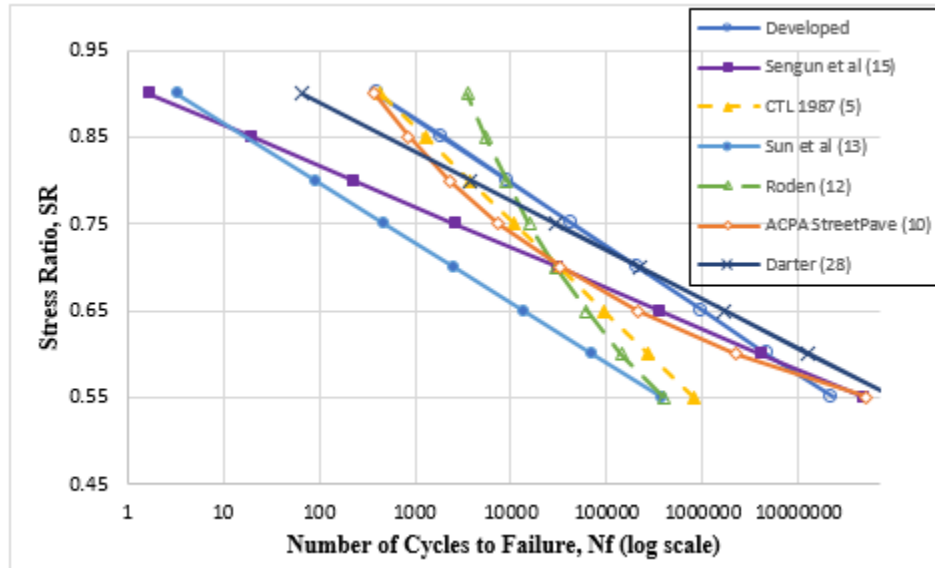
To further evaluate the applicability of the developed RCC fatigue model, the APT field test results (4) were utilized to predict the RCC in-field fatigue performance. In the APT study, six pavement test sections were loaded to failure under fatigue cracking by an incremental loading sequence till 50% of the loaded area is cracked. For the fatigue analysis, fatigue damage was calculated for all the RCC test sections considering 50 % of the loaded area cracked corresponds to cumulative damage of unity. The fatigue model at 50% reliability was considered for the damage calculation as previous studies suggested that fatigue models at a 50% reliability could be used to predict the in-field performance [69].

Table 6 shows the prediction of cumulative fatigue damage using different RCC fatigue models for failed RCC test sections tested under accelerated loading. For the total damage prediction, the in-site critical stresses under different loading magnitudes were predicted using a finite element (FE) model developed using finite element software ABAQUS and verified through field instrumentation results. The predicted critical stresses were then used to determine the stress ratio for each load magnitude. Based on the field strength results, an average flexural strength of 800 psi and 850 psi was considered for the weak and strong sections respectively. As it can be seen from the results, the developed fatigue model at 50% reliability predicts the APT field performance very well whereas all other fatigue model fails to predict the RCC fatigue life. Especially at higher load levels, all the other fatigue models predict a very low number of allowable

load repetitions. However, in the APT study, it was observed that the RCC pavement can withstand heavier loads up to 50-kip single axle loading for a significant number of passes [27]. The higher prediction of cumulative damage on 6-in. RCC over CTB base is also justifiable based on the APT field performance since this pavement test section cracked severely and 60% of the loaded area was cracked at the end of the APT loading.

Table 6. Fatigue performance of RCC test section under accelerated loading

RCC Test Sections	Cumulative Fatigue Damage			
	Developed RCC fatigue model	ACPA *StreetPave* Fatigue model	ACPA RCC fatigue model	Sengun et.al RCC fatigue model
6-in RCC over soil cement base (Section 5)	1.03	5.37	15.08	3.42
6-in. RCC over CTB base (Section 2)	1.39	8.67	6.77	16.18
4-in RCC over soil cement base (Section 6)	1.10	6.82	5.22	13.33
4-in. RCC over CTB base (Section 3)	1.01	6.07	3.66	14.31

Based on the performance prediction results, it can be observed that the RCC fatigue model developed in this study can provide a more reasonable and optimized design thickness against the fatigue failure criterion. To further understand the applicability of the developed fatigue model into RCC pavement design, the developed fatigue model was added into the Pavement Designer/StreetPave design framework to allow a comparison of design thickness results for typical road traffic.

Four different load spectrum categories termed as residential, collector, minor arterial and major arterial were considered for this comparison. The following assumptions were made in the designs, Table 7.

Table 7. Input parameters for RCC pavement design

Design life	20 years
Traffic growth rate	2%
Directional distribution	50%
Design lane distribution	100%
Percent Slab Cracked at the end of design life	15%
Edge Support	With shoulder
Composite subgrade, k	300 pci
RCC modulus of elasticity	4000 ksi
RCC Poisson's ratio	0.15
RCC flexural strength	700 psi

Figure 33 shows the required percent decrease in thickness for an RCC pavement using the developed fatigue model compared to PCC Designer/StreetPave prediction for different traffic load spectra. While comparing the pavement design thickness, it was observed that, by replacing the developed fatigue equation in place of ACPA, fatigue model can lessen the minimum thickness requirement in RCC pavement design. A thickness reduction ranging from 7-18% was observed for different design alternatives indicating a good structural capacity of thinner RCC pavement. This outcome is also in agreement with the APT test results, where it was observed that a thin RCC can be a good design alternative for low to medium volume roadways.

Figure 33. Comparison of RCC pavement thickness design
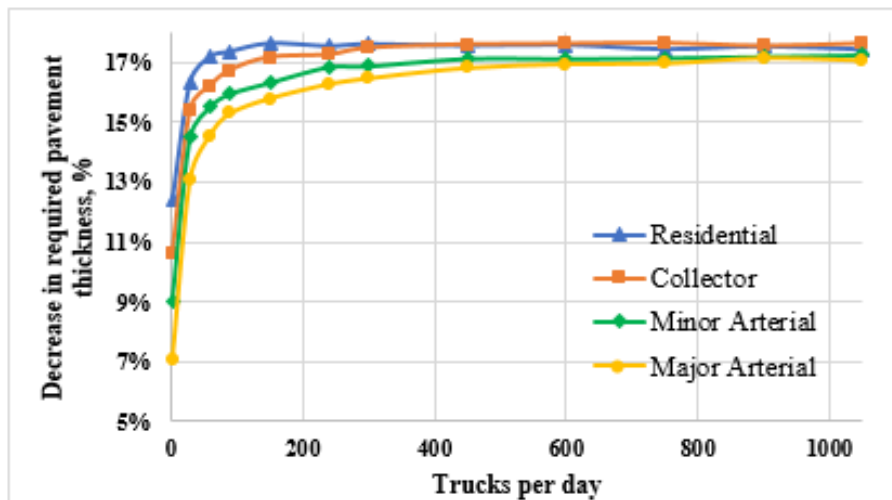
Pavement Designer/StreetPave also considers the erosion criterion in RCC thickness design based on the PCA method. This criterion limits the erosion of materials underlying the pavement caused by deflections resulting from repeated loading along edges and joints (pumping). This paper mainly focuses on the fatigue performance of RCC pavement, and the erosion damage was not considered for thickness design consideration. Moreover, the RCC erosion damage needs to be further evaluated for design purposes since improved base conditions can reduce the erosion failure potential significantly.

Numerical Simulation and M-E Application of RCC Pavement Thickness Design

Finite Element Modeling and Axle Load Equivalency Factors

The measured in situ strain results from this study were used to calibrate a finite element model for RCC pavements. Using the FE predicted results and developed RCC fatigue model, an artificial neural network (ANN) was built to rapidly estimate the load equivalency factor of different RCC pavement structures subjected to different axle loading conditions.

Development of Finite Element Model. A finite element (FE) model was used in this section to investigate the structural behavior of RCC pavements under accelerated loading. In this model, similar geometric and thermal properties as the APT sections were used. For developing this FE model, ABAQUS software was utilized. Many previous researchers have been shown that an FE model can be a useful tool to predict pavement stresses under different loading conditions. Hasan and Jalali (2018) investigated the behavior of asphalt pavement for different locations of tire loading [70]. In this study, they considered the pavement structure as a viscoelastic material. Yijuan et al. also employed finite element approach to build a mechanistic-empirical prediction model for joint spalling distress in concrete pavements [71]. For this simulation of the pavement structures, researchers usually adopted a meshing technique with more mesh numbers concentrated in the loading area.

In this study, the FE model was built considering the field conditions of Accelerated Loading Facility (ALF) sections. The model contains two lanes and three slabs in each lane. Each slab is 20 ft. long and the width of each lane is 13 ft. These three RCC slabs were divided by equally spaced two saw-cut joints. The tire prints in this model were 12

in. x 12 in. and located in the middle of the slab. Figure 34 shows the detailed geometry of the joints, which is 1/4 in. in width and 8/3 in. in depth. Two boundary conditions are applied in this model: (1) the bottom of the model was fully constrained and (2) the side of the model is applied with roller boundary condition, shown in Figure 34.

Figure 34. (a) Detailed geometry of FE model with tire print (b) Saw cut joint in FE model (c) Mesh of FE model (d) Boundary conditions of FE model
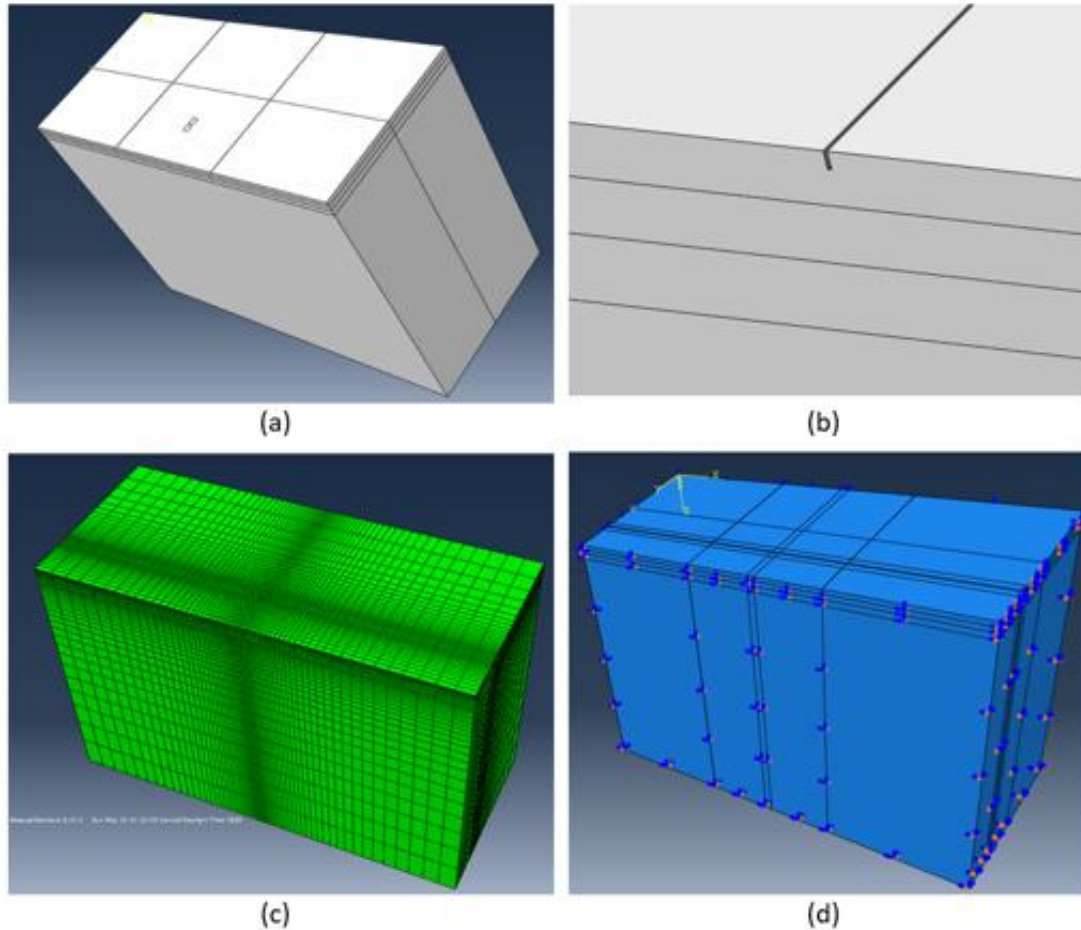
During simulation, four layers were designed for Section 1 from top to bottom: RCC layer, soil cement layer, cement treated base, and subgrade. The material parameters of each layer of the adopted FE simulation are listed in the Table 8 below.

Table 8. Material properties for FE simulation

Layer Materials	Elastic Modulus (ksi)	Poisson's ratio	Coefficient of thermal expansion (με/°C)
RCC	4000	0.15	9.5 με/°C
Soil cement layer	300	0.25	
Cement treated layer	150	0.25	
Subgrade	11	0.3	

The FE model developed in this study was a simple elastic model and the material properties were considered based on the back-calculation results shown in previous sections. For the temperature effect, a constant CTE of 9.5 με/°C was considered for Section 1 to match with the in situ responses. Initially, the FE model prediction results were compared with KENSLAB software. It can be observed from Figure 35 that the result from the analysis matches well between the two softwares. However, the ABAQUS FE model has its advantages in precision with more elements applied and nonlinear thermal loading. The saddle shape in the stress or strain curves can be simulated, which was also observed in the field-tested data in Figure 35.

Figure 35. Comparison of FE model with KenPave based on stress at the top of the pavement
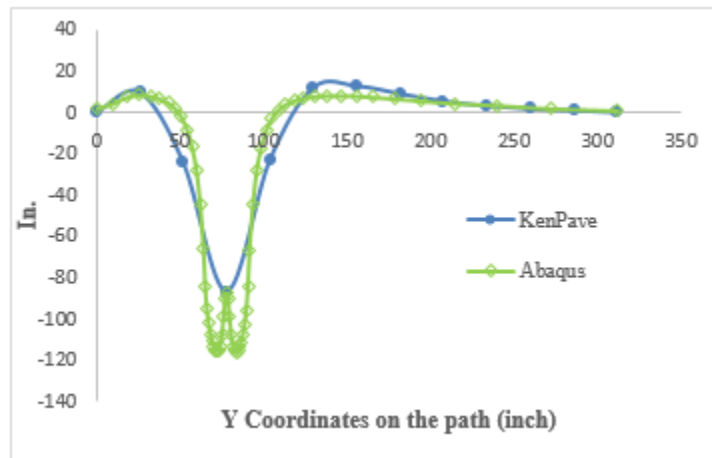
Two analysis steps were included in the FE numerical simulation. In the first step, the temperature measured from the field was applied as boundary conditions on the top and bottom surface of the RCC slab. As a result, the slab was curling or wrapping due to the thermal gradient.

Later in the second step, duel-tire load was applied with the existing temperature and strain distribution obtained from the previous step. The strain results from the two steps are used to calculate the strain response and verified with the instruments responses. The strain responses at the top and bottom RCC layer on the two RCC test sections with four tire load levels were predicted and plotted against the measured responses collected from the APT study.

Figure 36. Measured vs predicted strain response under accelerated loading in Section 1 (a) Bottom Transverse Strain (b) Top Transverse Strain

(a)

(b)
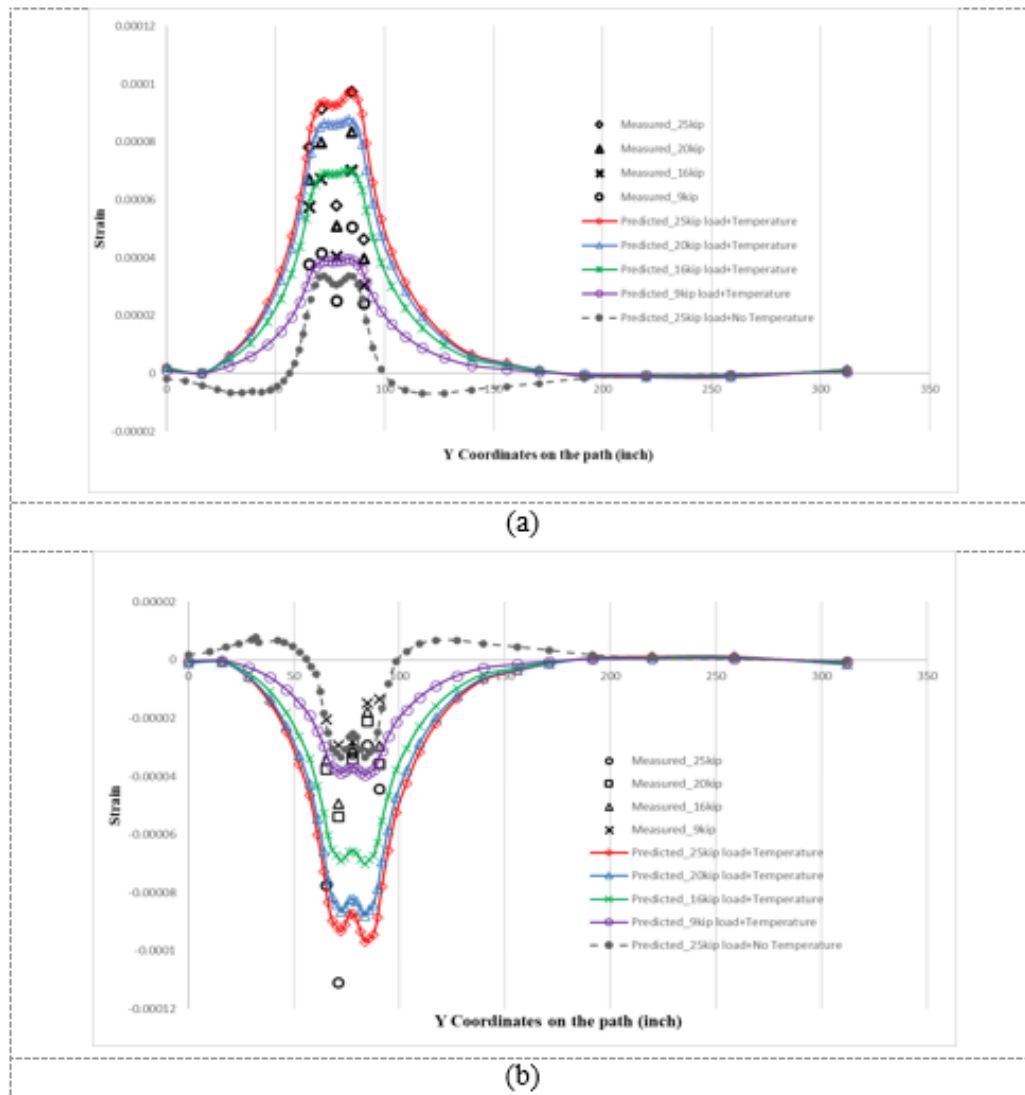
From Figure 36, it can be observed that the FE simulation results matched very well with the measured bottom transverse responses, especially for the critical transverse strain

located under the tire loading area. The simulation results also fairly matched with the measured top transverse responses with some outliers, Figure 36. Because of the top sensors are located just 0.2 in. below the surface, the measured strain values showed a lot of fluctuations under accelerated loading due to the Poisson's effect. The slight difference in the measured versus predicted strain basin could be also due to the anisotropic behavior of the RCC layer or the epoxy used for the installation. The simulation results also showed that there is clear difference between the predicted and measured strain response for 25 kip loading if the thermal properties were not considered.

ANN model for LEF Prediction. AASHTO first introduced the load equivalency factor (LEF) for both flexible and rigid pavements used in the AASHTO pavement design guides [62]. Since the LEFs were developed based on the AASHTO Road Test results obtained over fifty years ago, many studies have reported those LEFs are no longer applicable for the current pavement structures and truck load configurations. Some recent studies tried to develop equivalency factors for different axle loads and configurations using the mechanistic-empirical pavement design principles [72, 73]. Other studies estimated the load equivalency factors based on pavement deterioration curves from the pavement management data. Without knowing the true pavement responses and damage, the developed load equivalency factors may be only applicable for a network pavement performance evaluation, and not suitable to be used in a pavement design.

Once the FE model was validated against the APT field measured responses, it was further used to investigate the critical structural responses for various RCC thicknesses, RCC moduli, base thicknesses, base moduli, subgrade moduli and axle load levels. Based on the FE predicted critical stresses, the allowable repetitions to fatigue failure (Nf) was calculated for each case using a recently developed RCC fatigue model from the APT study [27].

In order to obtain the LEF of various load levels and configurations with any given RCC model, an artificial neural network was built in this study to calculate allowable repetitions to fatigue failure. A two-hidden-layer ANN model with 10 neurons in each layer was designed in Matlab. The input layer has 8 parameters and the calculated Nf is set as output (Table 9).

Table 9. Matrix of input and output for ANN training

Input	Output
RCC modulus (ksi) RCC thickness (in.) Base modulus (ksi) Base thickness (in.) Subgrade modulus (ksi) Axle load (kips) RCC flexural strength (psi) Percentage of reliability (%)	numbers of cycles to failure

The allowable repetitions to fatigue failure for a given axle load were then correlated to the repetitions to failure from a standard 18 kip single axle load (half axle represents ATLaS30 dual tire loading) using equation 24.

$$LEF\_fatigue = (N\_18/N\_axle) \tag{24}$$

A set of 1,548 samples obtained from numerical simulation were applied to train this ANN. The Levenberg-Marquardt algorithm was adopted to approach the training. The 70%, 15%, and 15% of the data were applied in training, validation, and testing procedures.

With the trained ANN model, the influence of subgrade modulus, RCC thickness, RCC/base modulus ratio, and RCC modulus were investigated. Figure 37 shows the LEF calculated an 8 in. RCC over 8.5-in. soil cement base by trained ANN model with multiple load levels from 14 to 50 kips. The prediction results show that with the increase of subgrade modulus and RCC thickness, the LEF will decrease significantly, especially for axle loads over 35 kips (Figure 37). The RCC modulus and modulus ratio (E1/E2) between RCC (E1) and base (E2) were also investigated. It indicates that an increase in both E1/E2 and RCC modulus will result in larger LEF for heavy loads, and the ANN model is capable to simulate these varying structural conditions.

Figure 37. Influence of model parameters on LEF

(a)

(b)

(c)

(d)
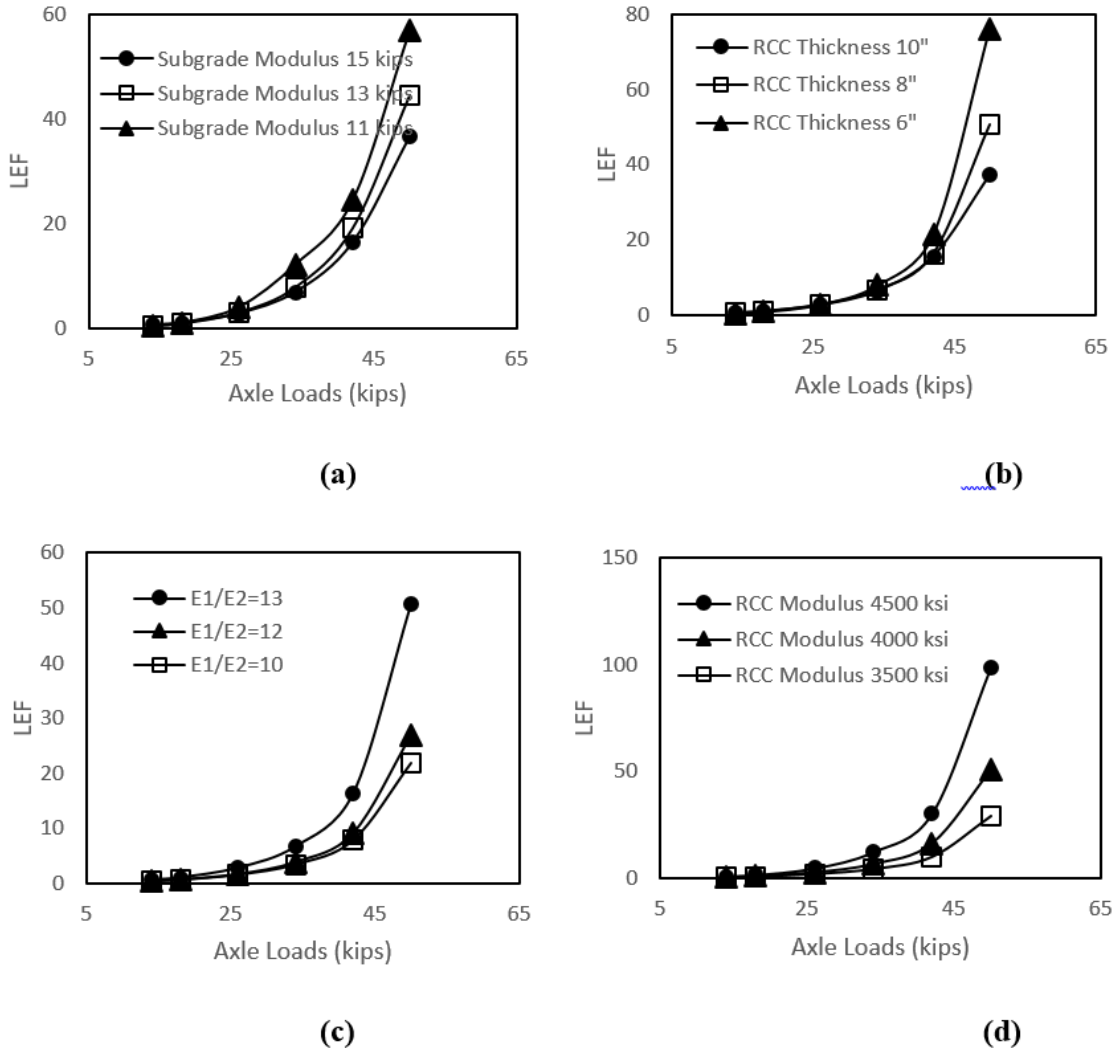
Since the critical stress generally occurs at the edge of the slab in actual roadway conditions under different axle configurations, the FE model can be further modified for edge loading under different full axle configuration (single axle, tandem axle, and tridem axle) to identify the critical stresses on the edge of the RCC pavement sections. Based on the modified FE predicted result, another ANN model can be developed to account for the actual traffic loading on RCC pavement structure for a low volume roadway with heavy trafficking.

LEF for ATLaS Dual Tire Load. Based on the ANN prediction, the fatigue based LEF along with the AASHTO and 4th Power-law LEF values are included in Table 10 for both RCC sections. From the LEF calculations, it can be seen that the heavier single axle (20 and 25 kips) does significantly more damage than the standard 18 kips single axle load. Previous APT studies under ATLaS30 dual tire loading indicated that both AASHTO and 4th Power-law over predict the damage for heavier single axles.

Table 10. Load equivalency factor for ATLaS dual tire load

	Load (kips)	LEF (Fatigue Based)	LEF (AASHTO)	LEF (4th Power)
8-in. RCC over 8.5-in. Soil Cement Base	9	1	1	1
	16	6.653	10.100	9.988
	20	16.329	25.651	24.386
	25	50.634	68.157	59.537
8-in. RCC over 12-in. Cement Treated Base	9	1	1	1
	16	7.61	10.100	9.988
	20	19.51	25.651	24.386
	25	56.08	68.157	59.537

In general, the LEF is usually higher for pavements with lower structural capacity because heavy axle loads are more destructive to less robust pavement structure. As it can be seen from the table, the fatigue based LEF results for Section 2 is higher than the results from Section 1 in spite of having the same RCC thickness. The reason is mainly because of having weaker base support on Section 2 compared to Section 1, indicating more damage will occur under similar load conditions. This also supports the APT performance observed in the field. The proposed mechanistic framework is capable in determining the LEF for different pavement structures, whereas both AASHTO and 4th Power-law cannot account the effect of thickness and stiffness of the pavement layers.

Since RCC pavement is suitable to be used as a design alternative for the heavy load trafficking pavements, overlooking the influence of the pavement structure in damage quantification can provide an inaccurate assessment of the design service life. Inaccurate evaluation of the damage from heavy axle loads will also lead to an either over designed RCC pavement layer or early failure of the pavement, which will cause unnecessary expenditures. The outcome of this study will be beneficial to accurately predict the true pavement life of RCC pavements subjected to heavy trafficking.

Proposed RCC Pavement M-E Design Procedure

The general objective of a mechanistic-empirical (M-E) pavement design procedure is to provide the highway community with a state-of-the-practice method based on M-E principles for the design and analysis of new and rehabilitated pavement structures. The mechanistic portion refers to the application of the principles of engineering mechanics, which leads to a set of rational, theoretical-based, predicted critical pavement response (strains, stresses, deflections, etc.) as a function of traffic and climatic loading. The empirical part is indicated by defined relationships between the critical pavement response parameter and field-observed distress. This means that the design/analysis procedure calculates pavement responses (stresses, strains, and deflections) and uses those responses to compute incremental damage over time. The procedure empirically relates the cumulative damage to observed pavement distresses.

Due to the absence of a fully developed M-E design procedure, the current RCC pavement thickness design is solely empirical or following the developed jointed plain concrete pavement (JPCP) design procedure available in the current AASHTOWare PMED [74]. Obviously, a direct use of the developed JPCP M-E design procedure for an RCC pavement design is neither suitable nor practical. This is because (1) both the mix design and construction practice between RCC and JPCP pavements are different, and (2) RCC pavements do not consider any steel dowel bars in joints [74]. Therefore, an M-E based RCC pavement thickness design procedure has been proposed in this study.

The proposed M-E design procedure for RCC pavement is generally compatible with mechanistic-empirical framework as those of JPCP design in the current AASHTOWare PMED and thus adaptable into the design framework. M-E design procedures require an iterative approach by the designer. The designer must select a trial design and then analyze the design in detail to determine if it meets the established performance criteria. The performance measures include fatigue cracking, faulting, and smoothness prediction. If the trial design does not satisfy the performance criteria at a given reliability level, the design should be modified and reanalyzed until the design does satisfy the criteria. The designs that meet the applicable performance criteria at the selected reliability level are then considered feasible from a structural and functional standpoint and can be further considered for other evaluations.

The proposed M-E pavement design procedure for RCC pavement contains the following five major steps:

1. Establish target performance criteria for all the typical distress observed in RCC pavement at the given reliability level to obtain an acceptable performance during the whole design period;

2. Select a trial design for a specific site considering all the required inputs (i.e., materials properties, subgrade properties, projected traffic spectra, and climate conditions);

3. Mechanistic evaluation of the inputs of step 2 to obtain structural responses (i.e., critical stress, and deflection) for each different axle type and environmental conditions using finite element model;

4. Calculate accumulated damage and predict the distresses using empirical transfer functions (i.e., fatigue cracking, erosion, faulting during design life); and

5. Compare the projected performance of the trial design with the target performance at the given reliability level based on pavement functional class. If the projected performance fails to satisfy the target performance criteria for each distress, and perform the whole procedure by revising the RCC thickness until the design satisfy the established criteria (i.e., using the iteration method).

General Design Inputs. Design life— Expected pavement design life in years.

- Construction & Traffic Opening Month— Selecting the construction month is important because it is related to the early pavement failure. Selecting hot months will result in higher "zero-stress" temperatures and wider crack opening. The traffic-opening month is also a sensitive input because it determines the RCC strength at which traffic is applied to the pavement.

- Traffic— Traffic data is one of the key data elements required for the analysis and design of pavement structures. For example, wander in traffic loading reduces the rate of fatigue damage accumulation on slabs, thus decreasing required slab thickness. Other factors such as traffic loading, wheel spacing, dual tire spacing, and traffic distribution have significant effects on pavement design. Thus, the traffic data should be carefully investigated for the RCC pavement design. The full axle load spectra for single, tandem, tridem, and quad axle will be considered along with other traffic data such as average daily truck traffic (ADTT), percent truck, operational speed, monthly

adjustment factor, traffic growth, hourly distribution, wheelbase, axle configuration, and traffic wandering need to be considered during RCC pavement design.

- Climate— Environmental conditions have a significant effect on the performance of rigid pavements. Factors such as precipitation, temperature, freeze-thaw, and depth-to-water table affect pavement and subgrade temperatures and moisture content. In turn, these factors directly affect the load carrying capacity of the pavement layers and pavement performance. All the key environmental factors will be considered and the EICM step will be used to yield the necessary information such as hourly temperature, moisture distribution, zero-stress temperature, annual freezing index, number of wet days, freeze-thaw cycle, and relative humidity values for use in the design analysis.

- Pavement Structure— A RCC pavement structure could consist of an RCC slab, base layer of different types, subbase, compacted subgrade, natural subgrade, and bedrock. Defining a trial design for RCC pavements involves defining all the pavement layers and material properties for each individual layer, including subgrade. Depending on the input level, a different amount of information is required for all the layers. The initial thickness selection and design inputs can be altered until the desired distress levels are achieved. The geometric dimensions (slab length and lane width) of the slab also play an important role in the pavement design analysis.

- Material Properties— General properties such as layer thickness, modulus of elasticity, flexural strength, poisons ratio, coefficient of thermal expansion, and thermal conductivity will be used for the RCC pavement design. Additionally, RCC mix related properties such cement content, water/cement ratio, aggregate type will also be used to calculate the zero-stress temperature, ultimate shrinkage at a specified relative humidity. The seasonal variation of the material properties is also an important factor and the EICM step will be linked to estimate seasonal variations based on changing moisture and temperature profiles through the pavement structure.

Structural Response Model. Proper structural response modeling of a new pavement structure and the interpretations are considered as a core of the M-E design procedure. These models are essential to perform the mechanistic part of a pavement design such as calculating critical stress, strain, and displacement in a pavement system due to both traffic and environmental loading. The models assume a pavement as multi-layer elastic structure to calculate responses that are then used in the damage models to accumulate damages as a monthly basis over the design period. The following factors should be considered during the analysis:

- Pavement Structure— Slab size, shoulder type, slab base interface;

- Load configuration— Axle type;

- Load level— Different load magnitude based on axle type; and

- Temperature gradient— The effects of mean monthly temperature gradient, permanent curl/warp, and monthly variation in warping expressed as the effective temperature difference.

Because thousands of responses are required for any design, an ANN-based pavement prediction model is usually developed using the responses collected from FE model that can compute accurately and instantly the critical stress and deflection based on the trained results. For simplicity, a suite of prediction equations proposed by Lee et al. (1997) [75], based on concrete pavement's equivalent-stress concept, can be used as an alternative to compute the critical stress and deflection in design.

Performance Indicators and Distress Prediction Model. More specifically in a JPCP design, the AASHTO PMED includes a set of transfer functions and regression equations that are used to predict various JPCP performance indicators considered. Those important JPCP performance indicators are: (1) mean joint faulting, (2) joint load transfer efficiency (LTE), (3) load related transverse slab cracking, (4) International Roughness Index (IRI) - pavement smoothness and (5) joint spalling (embedded into the IRI prediction model).

Based on the field performance and laboratory experiment results in this study, the following performance indicators are recommended for an RCC pavement thickness design:

    a. Load related fatigue cracking
    b. Cracking related erosion and faulting
    c. Smoothness and IRI

(a) Load related fatigue cracking— All cases that produce significantly different stresses must be evaluated separately in the fatigue analysis to obtain accurate results. The general expressions for fatigue damage accumulations considering all the critical factors for RCC fatigue cracking is as follows:

$$Fatigue\ Damage = \sum n\_(i,j,k,l,m,n)/N\_(i,j,k,l,m,n) \tag{25}$$

      Where,

      n_(i,j,k....)= applied number of load repetitions at condition i,j,k,l,m,n

N_(i,j,k....)= allowable number of load repetitions at condition i,j,k,l,m,n
i = pavement age; j = month; k = axle type; l = load level; m = temperature
difference; n = traffic path

The applied number of load applications is the actual number of axle type (k) of load level l that passes through traffic path (n) under each condition (age, season and temperature). The allowable number of load applications is the number of load cycles at which fatigue failure is expected and is a function of the stress ratio, which is the ratio between applied stress and RCC flexural strength. Once the allowable load repetitions are computed and the design traffic is known, then the level of fatigue damage can be calculated by summing damage from each damage increment.

Fatigue damage of 1.0 did not necessarily guarantee that the pavement section had failed. Thus, a relation between various fatigue damage levels to the percent of slabs cracked in the field has been developed. Utilizing APT test section cracking development, a transfer function for RCC fatigue damage was established in this study, shown in equation 26. Here, the cracking model form is similar to the one provided in rigid pavement M-E pavement design guidelines; however, both longitudinal and transverse cracking were considered in this model [37]. The utility of a cracking model is to translate the mechanistically calculated fatigue damage into observed field fatigue cracks.

$$CRK = 1/(1 + 1.15 * FD^{(-1.63)}) \qquad (26)$$

Where,

CRK= Percent area cracking

FD= Fatigue damage

To better illustrate, the proposed cracking model is fitted into a non-linear regression curve; shown in Figure 38 (a). Here for 100% fatigue damage, the observed fatigue cracking is 46.5%. When the damage is very small (i.e., < 0.001), the RCC surface would not expect to show any visual cracking. However, if the damage increases to a significant value (i.e., > 0.1), visible fatigue cracking may be expected to grow. Figure 38 displays the efficiency of the non-linear cracking model by measured vs predicted cracked area. Here, the measured and predicted cracked area (%) shows a significant correlation with a goodness of fit value (R2 = 89%).

Figure 38. (a) Cracking model (b) Accuracy of the model
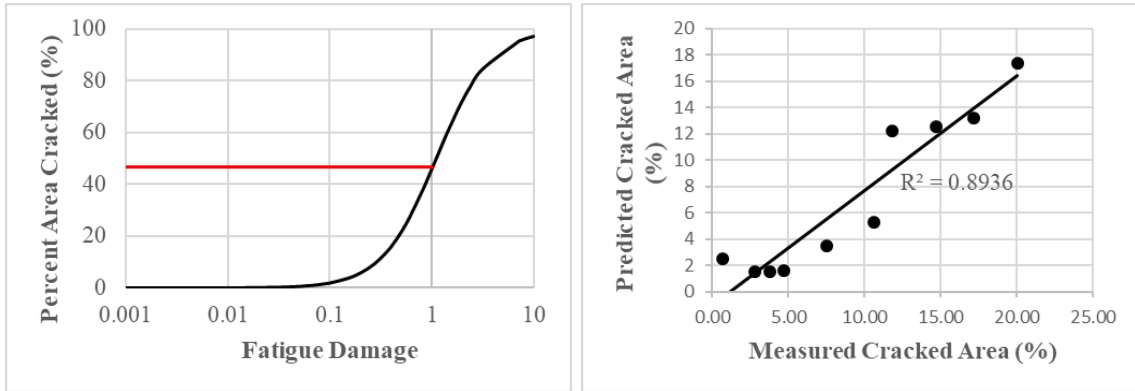
(a)   (b)

(b) Cracking related erosion and faulting— It is important to consider erosion damage for RCC pavement design as it leads to loss of support resulting in cracking of slab and potential faulting at the saw cut joints. The factors affecting erosion are the presence of water, rate of water movement beneath the RCC slab, erosion potential of the support layers, magnitude and number of load repetitions, and slab deflection. A model to consider all these factors mechanistically is still not available today. However, PCA method and pavement M-E both have empirical based procedures to account for the potential for erosion that addressees the aforementioned factors. For the RCC pavement design method, the effect of loss of support on fatigue cracking and joint faulting will be considered to account for the erosion related damages.

To consider the effect of loss of support in the development of fatigue cracking, the erosion width or void under the RCC slab will be determined based on the empirical model developed by PCA. In this case, the criterion, shown by equation 27 is termed as power or rate of work by which any axle load causes corner deflection and pressure at the slab foundation interface [76].

$$P = 268.7 \, (p^2/hk^{(0.73)}) \tag{27}$$

$$LogNe = 14.524 - 6.777 * (C1 * P - 9)^{0.103} - LogC2 \quad when, C1 * P > 9$$

$$Ne = unlimited \quad when, \quad C1 * P \leq 9$$

$$C1 = 1 - (k/2000 * 4/h)\,^2 \text{ and, } C2 = (0.06 \text{ for } NS \text{ and } 0.94 \text{ for } WS) \tag{28}$$

$$Erosion = 100 * \sum(C2n\_i)/N\_i \tag{29}$$

Where,

N_e= Allowable number of repetitions

P = Rate of work or Power

The faulting potential at the saw cut joints will also be predicted using an incremental approach developed by ACPA. The faulting model incorporated in Pavement M-E will be evaluated and calibration parameters will be adjusted suitable for RCC pavements.

$$Fault = Erosion^{(0.25)} * [\ 9.75873 * 10^{(-4)} * (PR)^{(0.91907)} + 0.0060291 + JS^{(0.54428)} - 0.016799 * Drain] \tag{30}$$

Where,

Fault= Mean transverse undoweled joint faulting (in.)

Erosion= Percent erosion damage

PR= Annual precipitation (in.)

JS= Transverse joint spacing (ft.)

Drain= 1 (w/ edge drains) or equal to 0 (w/o edge drains).

(c) Smoothness and IRI— An empirical IRI model for RCC pavement has been developed based on the limited APT test results, equation 31. This model will be further evaluated to be used in the RCC pavement design. Originally, other than initial IRI value, pavement M-E rigid pavement guideline uses cracking, faulting, and spalling for JPCP to predict IRI. However, in this study, it was not possible to incorporate the factors other than fatigue cracking. As an alternative to the currently developed model, the pavement M-E national calibrated model for smoothness can be incorporated for predicting smoothness for RCC pavement design when all the other parameters are known, equation 32.

IRI model developed based on limited APT cracking data:

$$IRI = IRI_0 + 4.4 * CRK \tag{31}$$

$$IRI = IRI_0 + C1 * CRK + C2 * SPALL + C3 * FAULT = C4 * SF \tag{32}$$

Where,

IRI= the predicted IRI, in/mile

IRI0 = Initial pavement IRI, in/mile

SPALL= Spalling

SF= Site factor

C1, C2, C3, C4= calibration co-efficient

Failure Criteria and Design Reliability

In the next step, the total damage for each distress category needs to be calculated and predicted at the end of the design period. According to pavement M-E, the distress prediction can be made in an incremental approach where the total design period is divided into separated time periods. In case of RCC M-E design, at the end of the design period, pavement distress can be predicted using individual distress prediction empirical models.

The outputs of the pavement M-E design are the predicted distress at the end of the pavement design life. Therefore, initially the critical levels of pavement distresses allowed by the agency at the selected level of reliability need to be defined by the users. Similarly, to perform an RCC pavement M-E design in an iterative process, a target performance criteria of the major distress should be established. Based on the established performance, the whole thickness design process will be evaluated. As M-E design performance criteria are closely related to a pavement type, the following criteria shown in Table 11 can be recommended for RCC pavement. As this study recommended RCC pavement as a cost-effective solution to low-medium volume roadways, the design criterion for faulting and initial IRI are specified by reviewing the guidelines of Louisiana low-medium volume roadways [77]. Other criteria were recommended based on the observations of this study. Reliability level can be considered as 90% for low-medium roadways, however, based on the pavement functional class the level can be adjusted.

Table 11. Design performance criteria for RCC M-E design

Performance Criteria	Limit
Percent Fatigue Cracked Area (%)	40%
Erosion Damage (%)	< 100%
Faulting, in.	0.25
Terminal IRI (in./mile)	300

A large amount of uncertainty and variability exists in pavement design and construction, as well as in the application of traffic and environmental loading. A design reliability for the individual pavement distress model can play a crucial factor during RCC pavement design. Reliability also can be incorporated while predicting the distresses during pavement design life. Over the years, there have been several strategies while utilizing reliability in concrete pavement design. In pavement M-E, reliability shifts the transfer

function curves, which relate the accumulated calculated pavement responses to the predicted pavement performance. However, for RCC pavement, reliability levels based on functional classification can be selected as shown in Table 12 below.

Table 12. Reliability for different roadway facilities [37]

Functional Classification	Reliability Level	
	Urban	Rural
Interstate	95%	95%
Principal Arterials	90%	85%
Collectors	80%	75%
Local	75%	70%

If the predicted performance at a reliability level fails to meet the design performance criteria at the end of the design period, the RCC thickness should be increased until the predicted performance satisfies the criteria.

Design Example for M-E Based RCC Pavement Thickness Design

A M-E based RCC pavement thickness design is presented in this section considering all the fundamental concepts of pavement M-E design criterion. The following systematic procedure will be considered to predict the pavement performance during the RCC thickness design.

- Step 1: Process input parameters

- Step 2: Determine saw-cut joint spacing

- Step 3: Determine deterioration of saw-cut joint stiffness and joint LTE

- Step 4: Determine loss of support along slab edge

- Step 5: Determine structural responses under traffic and environmental loading

- Step 6: Determine damage for each design increment

- Step 7: Determine pavement performance at the end of design life

This design example sets the following performance criteria recommended in this study for RCC thickness design procedure at 50% reliability. Though it is challenging to achieve RCC surface smoothness, initial IRI is assumed as 100 in./mile for terminal IRI prediction.

- Percent fatigue cracked area (%) = 40%

- Erosion damage (%) < 100%

- Mean transverse joint faulting, in. = 0.25 in.

- Terminal IRI (in./mile) = 300 in./mile

The pavement in the design carries an ADT of 10,000 with 10% truck traffic. For traffic inputs, the calculations for structural responses are performed based on stress equivalent concept developed by PCA design procedure. Similar traffic input was considered as the current pavement M-E traffic input. To calculate the allowable traffic, the fatigue model developed in this study at 50% reliability based on Weibull's approach was considered. Other design inputs are shown below.

Table 13. Design inputs for the example problem.

Inputs		
Design Input	Design Period	20 years
	Road Category	Low-Volume Road
Material Properties Input	RCC Modulus of Elasticity	4000 ksi
	RCC Poisson's Ratio	0.15
	RCC Flexural Strength	650 psi
	Subgrade Modulus	300 pci
Environmental Input	Coefficient of Thermal Expansion of RCC	$4.2*10^-6$ /°F
	deltaT	0° F
Traffic Input	ADT	10000
	%Truck	10%
	Traffic Growth Rate	2%
	Directional Distribution	50%
	Design Lane Distribution	100%
Pavement Structure Input	Width	13 ft.
	Crack Spacing	15 ft
	Shoulder	Tied
	RCC Trail Thickness	5 in.

According to the equivalent stress prediction models [75], the critical stresses due to wheel and environmental loadings were calculated for the different axle load distributions. The current pavement M-E traffic spectra was adopted for the analysis.

The intermediate files from pavement M-E software were utilized to get the traffic spectra details and also the environmental information such as average precipitation, temperature gradient, etc. The joint spacing was determined based on the previously mentioned method and used as a design input. After all the given inputs, the distresses during the pavement service life were predicted at the trial 5 in. RCC thickness. At 5 in. RCC thickness, the pavement failed due to faulting. Later the design criteria met at 5.45 in. of RCC thickness. The fatigue and erosion damage along the pavement age is shown in Figure 39 below. More details of the fatigue and erosion damage estimation can be found in Appendix B.

Figure 39. Damage accumulation of RCC pavement
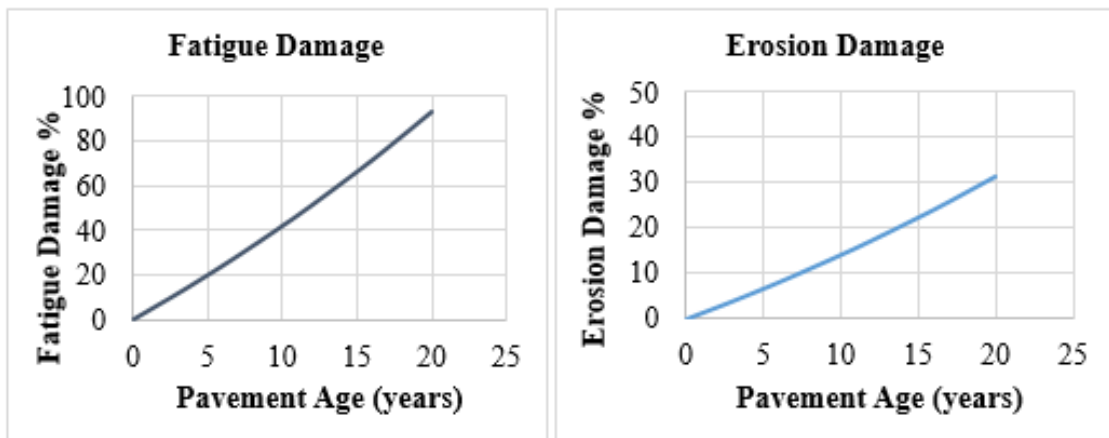
Based on the damage analysis, the pavement performance was predicted for the entire pavement design life based on the proposed performance prediction models. The results can be shown in Figure 40 below.

Figure 40. Design example distress charts

Pavement Area Cracking

Faulting

IRI
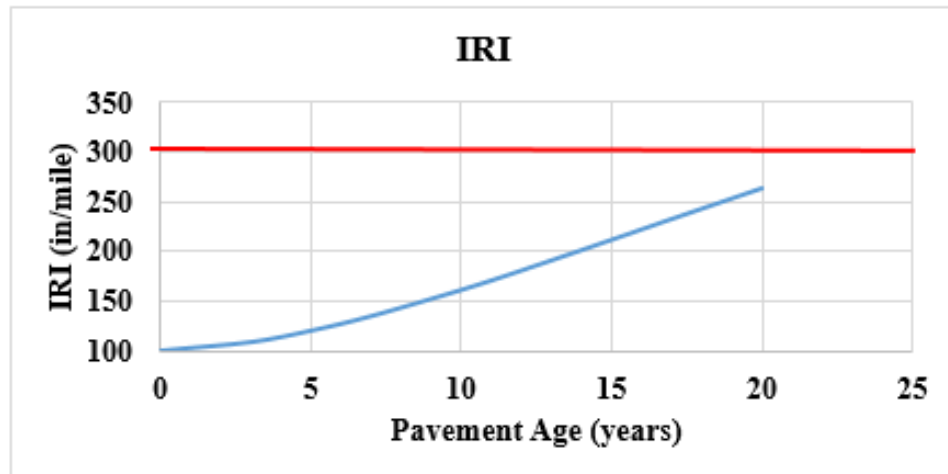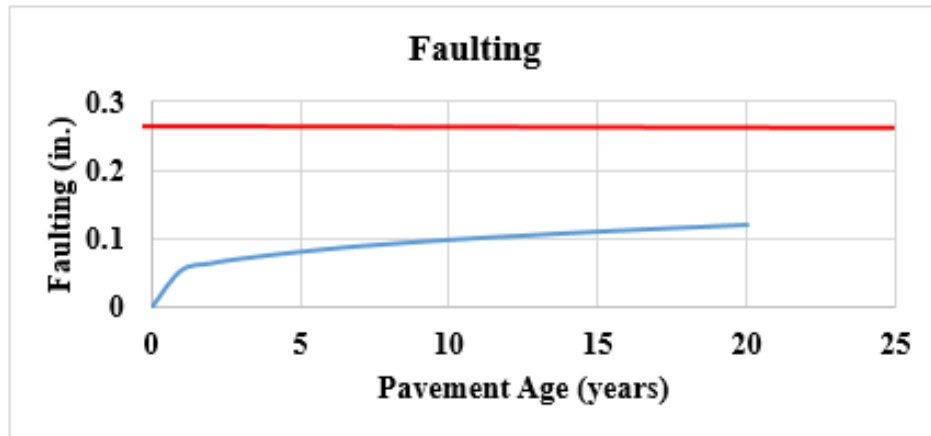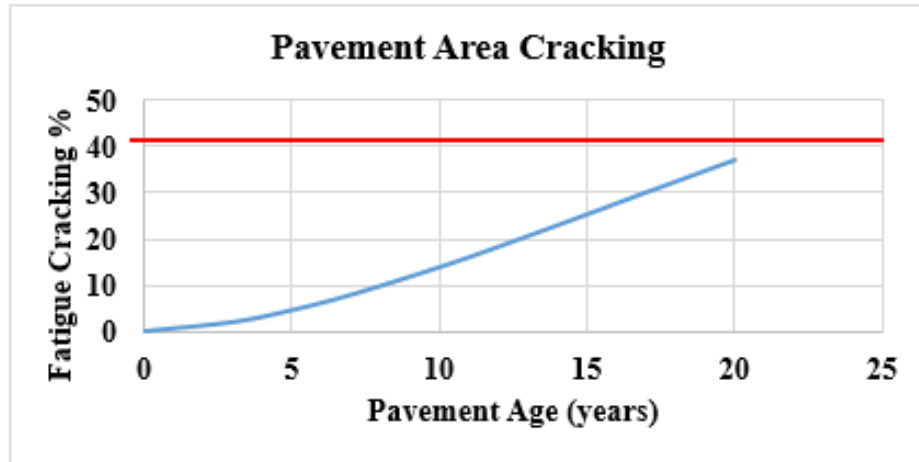
It can be seen from the figures above, all the distresses at the end of design life are within the recommended threshold value indicating the pavement passed the design criterion.

However, pavement design is a complex process that involves many uncertainties, variabilities, and approximations like truck axle loadings many years into the future, materials variability, etc. Even though mechanistic-empirical concepts provide a more rational and realistic methodology for pavement design, a consistent and practical method to consider these uncertainties and variations is needed so that a new pavement can be designed for a desired level of reliability. The developed fatigue model in this study with a reliability component will be very useful in RCC pavement design to meet the applicable performance criteria at the selected reliability level from both structural and functional standpoints.

Conclusions

With a proper mix design, improved paving compaction methods, and surface texturing techniques, RCC-surfaced pavement is steadily becoming the choice for many transportation agencies as an economical, durable, and low-maintenance design alternative for roadways experiencing large heavy and overloaded truck trafficking. In this study, the performances of six full-scale RCC pavement sections were evaluated under an APT experiment and a laboratory fatigue model was developed using in situ RCC beam samples. Finally, based on the observed APT performance and fatigue model prediction results, a M-E based RCC pavement thickness design framework was proposed.

The following specific observations and conclusions can also be drawn from this study:

APT Performance

- All six RCC test sections (i.e., including three RCC slab thicknesses 4, 6, and 8 in.) exhibited outstanding load carrying capacity and excellent structural performance. Four sections (Section 2, 3, 5 and 6) were previously loaded to a fatigue pavement failure evidenced by more than 40% of the trafficked area developed various surface cracks. However, the two 8 in. RCC sections (Section 1 and 4) were not loaded to a failure due to a concern of possibly extremely-long loading time required.

- In situ distress survey results indicated that the performance indicators related to pavement service life for RCC-surfaced pavements include the fatigue cracking, slab differential settlement at joints or cracks and extremely rough surface. Post-mortem trench results further revealed that the fatigue cracks generally initiated from the bottom of an RCC slab specially at a weaker foundation support location under the slab. It was also observed that the thicker RCC slabs could develop a wider fatigue-cracking pattern under dual tire loading compared to relatively thin RCC slabs.

- Due to the difference in RCC pavement construction, conventional concrete strain sensors were found not suitable for RCC pavement instrumentation. The conventional concrete sensors are prone to easily get damaged or disoriented during the roller compaction of RCC slabs. The fiber optic sensors, on the other hand, proved to be easy to retrofit in RCC pavements and were able to capture the complete strain distribution of the RCC slab under different load magnitudes.

- The fiber optic strain results were used to examine the complete load-induced pavement strain response distributions of two 8-in. RCC slabs under different dual-tire load magnitudes of ATLaS30. The instrumentation results revealed that: (1) for the same load magnitude the dynamic RCC pavement strain responses were generally smaller as compared to those under static loading; (2) the critical (maximum) dynamic compressive strains near the top of an RCC pavement were found located in the middle of a dual tire print; whereas, the critical bottom tensile strains (i.e., associated with the bottom-up pavement cracking) were observed directly occurred beneath the center of individual tires.

- To quantify temperature related stresses and strains, the coefficient of thermal expansion (CTE) of RCC test sections were determined from the recorded temperature-induced strain responses. The measured CTE values for in situ RCC slabs were varied from 9.44 to 12.53 $\mu\varepsilon/°C$ with a daily slab temperature gradient ranged between $+18°C$ and $-9.5°C$.

Laboratory Fatigue Model Development

- The developed fatigue model (i.e., an S-N curve) in this study is marked as the first research study to investigate the fatigue behavior of field RCC beam samples compacted with high density asphalt paver and compacted with a vibratory roller.

- The developed model was found agreed very well with the APT experimental results. This can be attributed to the in situ saw-cut RCC beams used in the laboratory beam fatigue tests of this study.

- A positive-trended, strong linear correlation was observed between the static flexural strength and measured density among the saw-cut RCC beams, indicating a higher in situ compaction can result in a greater flexural strength, which can lead to a longer RCC pavement fatigue life

- The current practice of RCC pavement thickness design utilizes the fatigue models developed about 30 years ago or produced for conventional concrete roads. Incorporating the developed fatigue model in the RCC pavement design implies that, the required RCC thickness can be less than that is recommended by current RCC design guidelines provided by ACPA and PCA.

M-E RCC Pavement Thickness Design

- The proposed M-E design procedure investigates several major important factors in the RCC pavement thickness design. The fatigue performance has shown to be very sensitive to vehicle class distribution, primarily the percentage of FHWA Class 5 to 8 trucks, and more moderately sensitive to annual average daily truck traffic (AADTT). It has been also found to be highly sensitive to curling/warp effective temperature difference, coefficient of thermal expansion and thermal conductivity.

- Base support condition plays an important role in achieving desired RCC slab density during construction and also for RCC pavement performance. Base erodibility also helps reducing pumping of fines through cracks and joints resulting in less faulting prediction. Results from the APT study also indicated similar findings. The currently available RCC thickness design procedure doesn't consider the base support condition for faulting potential. The proposed M-E design method considers the base support condition in the design consideration for faulting prediction. This will provide the design engineers to choose the right base type for RCC pavement design.

- Since RCC pavement showed outstanding performance under heavy loads, overlooking the load equivalency factor (LEF) and the influence of the pavement structure in damage quantification can provide an inaccurate assessment of the design service life. The fatigue based LEF obtained from this study will be beneficial for accurately predicting the true pavement life of RCC pavements subjected to heavy trafficking.

- The proposed M-E based RCC pavement design procedure was developed by following the current Pavement ME design procedure for a jointed plain concrete pavement (JPCP) design. The major modification lies in that a primary performance indicator proposed for an RCC M-E pavement thickness design is the "fatigue cracking, % total slab lane area" with a field developed transfer function, not the "Percent slabs with transverse cracks" used in JPCP design. It maintains the fundamental concepts as close as possible with the Pavement ME JPCP pavement design. Thus, the proposed M-E design procedure can be directly implemented into the Pavement M-E design software for RCC pavement design.

Recommendations

Louisiana has many miles of low- to medium-volume roadways currently used by a significantly large amount of heavy and over-loaded trucks from shale oil/gas industries, logging and agricultural activities. Due to the heavy trafficking, the pavements experienced significant pavement distresses that typical maintenance activities cannot sufficiently address. According to the finding from this study, RCC could be used as a design alternative for those heavy-duty low speed pavement applications. The developed RCC fatigue model and the M-E based thickness design procedure proposed in this study can be directly employed in prediction of the load-induced and/or erosion-related pavement distresses and performance for RCC-surfaced pavement applications in Louisiana. However, due to the limited data of RCC mix types and field performance considered in the study, the associated M-E fatigue and other distress models/transfer functions will be warranted to be further enhanced and calibrated when more RCC mix designs and in situ pavement performance become available, especially from those newly constructed RCC pavement applications nationwide.

Acronyms, Abbreviations, and Symbols

Term	Description
AASHTO	American Association of State Highway and Transportation Officials
ACI	American Concrete Institute
ACPA	American Concrete Pavement Association
ADT	Average Daily Traffic
ADTT	Average Daily Truck Traffic
AEA	Air Entraining Agent
ANN	Artificial Neural Network
APT	Accelerated Pavement Testing
ASTM	American Society for Testing and Materials
CBR	California Bearing Ration
CDOT	Colorado Department of Transportation
CRCP	Continuously Reinforced Concrete Pavements
CTB	Cement-Treated Base
CTE	Coefficient of Thermal Expansion
CTL	Construction Technology Laboratories
DOTD	Department of Transportation and Development
EALF	Equivalent Axle Load Factor
EICM	Enhanced Integrated Climate Model
ESALS	Equivalent Single Axle Load
FARCC	Fly Ash Roller Compacted Concrete
FHWA	Federal Highway Administration
FWD	Falling Weight Deflectometer
ICT	Illinois Center for Transportation
InTrans	Institute for Transportation
IRI	International Roughness Index
JDMD	Joint Deflection Measurement Device
JMF	Job Mix Formula

Term	Description
JPCP	Jointed Plain Concrete Pavement
LEF	Load Equivalency Factor
LGG	Lafayette Consolidated Government
LTPP	Long-Term Pavement Performance
LTRC	Louisiana Transportation Research Center
LVDT	Linear Variable Differential Transformer
M-E	Mechanical-Empirical
MnDOT	Minnesota Department of Transportation
MPEDG	Mechanistic-Empirical Pavement Design Guide
MR	Modulus of Rupture
Mr	Resilient Modulus
MTS	Material Testing System
NCHRP	National Cooperative Highway Research Program
NJDOT	New Jersey Department of Transportation
PCA	Portland Cement Association
PCC	Portland Cement Concrete
RCC	Roller Compacted Concrete
SR	Stress Ratio
TDR	Time Domain Reflectometer
TMK	Texas Measurements
UCS	Unconfined Compressive Strength
UCS	Unconfined Compressive Strength
USACE	United States Army Cops of Engineering

References

[1] ACI 325.10R-95. State-of-the-Art Report on Roller-Compacted Concrete Pavements, Manual of Concrete Practice, American Concrete Institute, 2004.

[2] Portland Cement Association. 2005. Roller-Compacted Concrete Pavements for Highways and Streets. Publication IS328. Skokie, IL: Portland Cement Association. http://www.cement.org/bookstore/download.asp?mediatypeid=1&id=7927&itemid=IS328

[3] Harrington, D., F. Abdo, W. Adaska, and C. Hazaree. Guide for Roller-Compacted Concrete Pavements. National Concrete Pavement Technology Center, Institute for Transportation (InTrans), Iowa State University, 2010.

[4] Zollinger, C. Recent Advances and Uses of Roller Compacted Concrete Pavements in the United States., Paving Solutions, CEMEX, Inc, Houston, TX USA, 2015

[5] Pittman, D., A. Gary. Characteristics of Roller-Compacted Concrete Pavements in the United States. MAIREPAV 7, Auckland, New Zealand, 2012

[6] LaHucik, J., & Roesler, J. Field and Laboratory Properties of Roller Compacted Concrete Pavements. Transportation Research Record: Journal of the Transportation Research Board, (2630), pp. 33–40, 2017

[7] Roden, R. RCC Fatigue Model Development by the American Concrete Pavement Association (ACPA) – Interim Report, 2013.

[8] Adamu M., Mohammed B. S., and Shahir M. Mechanical properties and performance of high-volume fly ash roller compacted concrete containing crumb rubber and nano silica. Construction and Building Materials, 17, pp. 521–538, 2018

[9] Ferrebee, E., Brand, A., Kachwalla, A., Roesler, J., Gancarz, D., & Pforr, J. Fracture properties of roller-compacted concrete with virgin and recycled aggregates. Transportation Research Record: Journal of the Transportation Research Board, 2441, pp. 128–134, 2014

[10] Portland Cement Association (PCA). Guide Specification for Construction of Roller Compacted Concrete Pavements. PCA Document IS009, 2004.

[11] ACPA, *StreetPave*, American Concrete Pavement Association, Skokie, IL, 2005.

[12] Wong, Henry HC, and Albert KH Kwan. Packing density: a key concept for mix design of high performance concrete. Proceedings of the materials science and technology in engineering conference, HKIE materials division, Hong Kong. 2005

[13] ASTM C 1040. Standard Test Methods for In-Place Density of Unhardened and Hardened Concrete, Including Roller Compacted Concrete, By Nuclear Methods, 2005

[14] ASTM C642. Standard Test Method for Density, Absorption and Voids in Hardened Concrete, American Society for Testing and Materials, 2013

[15] Khayat, K. H. N. A. Libre and Z. Wu. Roller compacted concrete for rapid pavement construction. Missouri Department of Transportation project no. TR201518, 2019

[16] Lee, S. W., Cho, Y.-H., & Park, C. Mechanical performance and field application of low cement based concrete under compaction energy. KSCE Journal of Civil Engineering, 18(4), pp. 1053–1062, 2014

[17] LaHucik, J., & Roesler, J. Field and Laboratory Properties of Roller Compacted Concrete Pavements. Transportation Research Record: Journal of the Transportation Research Board, (2630), pp. 33–40, 2017

[18] Khed, V. C, V. Gokulanadh and M. Hema Latha. A Review on Recent Advancement of Roller Compacted Concrete. International Journal of Inventive Engineering and Sciences (IJIES) ISSN: 2319-9598, Volume-5 Issue-12, 2020

[19] Neville, A. M. "Properties of Concrete," 4th ed., John Wiley & Sons Inc., London, United Kingdom, 1996.

[20] Mallela, J., Abbas, A., Harman, T., Chetana, R., Liu, R., and Darter, M. Measurement and Significance of the Coefficient of Thermal Expansion of Concrete in Rigid Pavement Design, Transportation Research Record: Journal of the Transportation Research Board No. 1919, 2005.

[21] Alungbe, G. D., Tia, M., and Bloomquist, D. G. "Effects of Aggregate, Water/Cement Ratio, and Curing on the Coefficient of Linear Thermal Expansion of Concrete," Transportation Research Record: Journal of the Transportation Research Board No. 1335, Washington D.C., pp. 44-51, 1992

[22] Hossain, M. S. and C. Ozyildirim. Use of Roller-Compacted Concrete Pavement in Stafford, Virginia, Virginia Department of Transportation (VDOT) report no. 15-R19, 2015

[23] Uygunoglu, T and Topcu, I. B. Thermal expansion of self-consolidating normal and lightweight aggregate concrete at elevated temperature. Construction and Building Materials, 23, pp. 3063–3069, 2009

[24] Mallela, J., Abbas, A., Harman, T., Chetana, R., Liu, R., and Darter, M. Measurement and Significance of the Coefficient of Thermal Expansion of Concrete

in Rigid Pavement Design, Transportation Research Record: Journal of the Transportation Research Board No. 1919, 2005.

[25] Simon, M. J., and Dallaire, M. P. "Taking Concrete to the Next Level," Public Roads, Vol. 66, No. 1, 2002. http://www.tfhrc.gov/pubrds/02jul/01.htm. Accessed April 10, 2021.

[26] Shin H.C and Y. Chung. Determination of Coefficient of Thermal Expansion Effects on Louisiana's PCC Pavement Design, Louisiana transportation Research Center (LTRC) Project Number: 07-2C, 2011

[27] Wu, Z., M. Mahdi, and T. D. Rupnow. Roller Compacted Concrete over Soil Cement under Accelerated Loading, Louisiana Department of Transportation and Development, LTRC Project No. 12-7P, 2017

[28] Chhorn, C., Hong, S. J., & Lee, S.-W. A study on performance of roller compacted concrete for pavement. Construction and Building Materials, 153, pp. 535–543, 2017

[29] Saucier, K. Roller-compacted concrete (RCC). In: Significance of Tests and Properties of Concrete and Concrete-Making Materials. ASTM International, 1994

[30] Donegan, J. P. Roller compacted concrete, chapter 48, ICE Manual of Highway Design and Management. Institution of Civil Engineers, 2011

[31] Zollinger, C. Recent Advances and Uses of Roller Compacted Concrete Pavements in the United States., Paving Solutions, CEMEX, Inc, Houston, TX USA, 2015

[32] WAPA. Washington Asphalt Pavement Association. https://www.asphaltwa.com/welcome-facts/ accessed on October, 2021

[33] AASHTHO. Guide for Design of Pavement Structures. Washington, D.C., American Association of State Highway and Transportation Officials (AASHTO), 1993

[34] Packard, R.G.; Thickness Design for Concrete Highway and Street Pavements. Portland Cement Association, Skokie, IL, 1984.

[35] Darter, M.I., Design of Zero-Maintenance Plain Jointed Pavements. Report FHWA-RD 77-111. Federal Highway Administration, U.S. Department of Transportation, Washington, D.C. 1977.

[36] Pickett, G., and G.K. Ray. Influence Charts for Concrete Pavements, Transactions of the American Society of Civil Engineers, Vol. 116, ASCE, Reston, VA. 1951.

[37] National Cooperative Highway Research Program (NCHRP). Guide for Mechanistic Empirical Pavement Design of New and Rehabilitated Pavement Structures, NCHRP Final Report, ARA, Inc. 2008

[38] Murdock, J. W., & Kesler, C. E. Effect of range of stress on fatigue strength of plain concrete beams. In Journal of the American Concrete Institute Proceedings, 55, 221–231, 1958

[39] Tayabji, S. D. and D. J. Halpenny. Thickness design of of Roller-Compacted Concrete Pavement, Transp. Res. Rec 1136, 1987.

[40] Tayabji, S. D. and P. A. Okamoto. Engineering Properties of Roller-Compacted Concrete, Transp. Res. Rec 1136, 1987.

[41] Titus-Glover, L., J. Mallela, M.I. Darter, G. Voigt, and S. Waalkes. Enhanced Portland Cement Concrete Fatigue Model for StreetPave. Transportation Research Record, 1919, pp. 29-37, 2005

[42] Calis, G. and S. A. Yildizel. Investigation of roller compacted concrete: Literature review, Challenge Journal of Concrete Research Letters 10 (3), pp. 63–74, 2019

[43] Delatte, N. Simplified Design of Roller-Compacted Concrete Composite Pavement. In Transportation Research Record: Journal of the Transportation Research Board, No. 1896, pp.57-65, 2004

[44] Wöhler, A. Versuche zur Ermittlung der auf die Eisenbahnwagenachsen einwirkenden Krafte und die Widerstandsfaihigkeit der Wagen-Achsen. Zeitschrift Fur Bauwesen, X, 583–616, 1860.

[45] Bauschinger J. Ueber die Veranderung der elasticitatsgrenge und der festigkeit des eisens und stahls durch strecken und quetschn, durch erwarmen und abkuhlen und durch oftmal wiederholte beanspruchung. Mitteilungen aus dem Mechanisch-Technischen Laboratorium der K. Technischen Hochschule in Munchen. 1886

[46] Paris PC. A rational analytic theory of fatigue. The trend in engineering. 1961

[47] Park, J. Y., S. W. Lee, S. H. Han, and Y. K. Kim, Fatigue Behavior of Roller-Compacted ConcretePavement Based on Full-Scale Fatigue Test, Journal of Testing and Evaluation 48, no. 4 pp. 2895–2907, 2020. https://doi.org/10.1520/JTE20170522

[48] Sengun, E., B. Alam, I. O. Yaman, H. Ceylan. A New Evaluation of the Fatigue Design Criteria of Roller Compacted Concrete (RCC) Pavements, Constr. Build. Mate, 289, 2021.

[49] Okamoto, P. A. Roller Compacted Concrete Pavement Properties. Portland Cement Association, Skokie, IL, 2008

[50] Sun, W., J. Liu, H. Qin, Y. Zhang, Z. Jin, and M. Qian. Fatigue Performance and Equations of Roller Compacted Concrete With Fly Ash, Cement and Concrete Research, 28(2), pp. 309–315, 1998

[51] Willis, J. R. A Synthesis of Practical and Appropriate Instrumentation Use for Accelerated Pavement Testing in the United States. International Conference on Accelerated Pavement Testing, Madrid, Spain, 2008

[52] Weinmann, T. L., A. E. Lewis, and S. D. Tayabji. Pavement Sensors Used at Accelerated Pavement Test Facilities. 2004

[53] Brown, S. F. State-of-the-Art Report on Field Instrumentation for Pavement Experiments. Transportation Research Record: Journal of the Transportation Research Board, No. 640, TRB, National Research Council, Washington, D.C., pp. 13-28, 1977

[54] Carr H.T., and Jeremy R. W. APT Instrumentation – Where Do I Begin? Accelerated Pavement Testing to Transport Infrastructure Innovation. Lecture Notes in Civil Engineering, vol 96. Springer, Cham, 2020.

[55] Steyn, W., L. Plessis, and E. Denneman. Technical Memorandum: Instrumentation for APT and LTPP. Contract Report, 2006

[56] Tabatabaee, N., and Sebaaly, P. State-of-the-art pavement instrumentation. Transp. Res. Rec. 1260, 246–255, 1990

[57] Leandri, P., Bacci, R., Natale, A.D., Rocchio, P.: Appropriate and reliable use of pavement instrumentation on in-service roads. In: Airfield and Highway Pavement 2013: Sustainable and Efficient Pavements, pp. 1424–1433, 2013

[58] Saghefar, M., Frink, E., Bortz, B.S., Hossain, M.: Instrumentation experience at the Kansas accelerated pavement testing facility. In: Airfield and Highway Pavement 2013: Sustainable and Efficient Pavements, pp. 1409–1423, 2013

[59] Sok, T., S. J. Hong, Y. K. Kim, and S. W. Lee. Evaluation of load transfer characteristics in roller-compacted concrete pavement, International Journal of Pavement Engineering, 2018 DOI: 10.1080/10298436.2018.1511782

[60] AASHTO T 166 Standard Method of Test for Bulk Specific Gravity (Gmb) of Compacted Asphalt Mixtures Using Saturated Surface-Dry Specimens, 2021

[61] ASTMC78/C78M, Standard Test Method for Flexural Strength of Concrete (Using Simple Beam with Third-Point Loading, American Society for Testing and Materials, 2018.

[62] AASHTHO. Guide for Design of Pavement Structures. Washington, D.C., American Association of State Highway and Transportation Officials (AASHTO), 1986

[63] S. Arora, S. P. Singh, Flexural Fatigue Analysis of Concrete made with 100% Recycled Concrete Aggregates, J. of Mater and Eng. Struct. 2, 2015, 77–89.

[64] S.P. Singh, S.K. Kaushik, Fatigue strength of steel fiber reinforced concrete in flexure. Cement Concrete Comp. 25, 2003, 779-786.

[65] Ramakrishnan, V; Wu G. Y and Hosalli, G. Flexural Fatigue Strength, Endurance Limit, and Impact Strength of Fiber Reinforced Concretes. Transportation Research Record, 1226, 17-24, 1989

[66] B. H. Oh, Fatigue Analysis of Plain Concrete in flexure, ASCE, 112(2), 1986, 273-288

[67] W. Weibull, A statistical distribution function of wide applicability, J. Appl. Mech. 18, 1951, 293–297

[68] S.R. Kasu, N. Mitra, A.R. Muppireddy, Influence of polyester microfiber reinforcement on flexural fatigue characteristics of concrete, Road Mater. Pavement Des. 2020, 1–17

[69] Rao, S. and Roesler, J. (2004) Cumulative Fatigue Damage Analysis of Concrete Pavement Using Accelerated Pavement Testing Results. Proceedings of the 2nd International Conference on Accelerated Pavement Testing, Minneapolis, September, 2004

[70] Hasan, T., and M. Jalali. Viscoelastic analysis of geogrid-reinforced asphaltic pavement under different tire configurations. International Journal of Geomechanics 18(7), 2018

[71] Yijuan, M., H. Kim, I. Kim, and Y. H. Cho. Development of a mechanistic-empirical prediction model for joint spalling distress in concrete pavements. Construction and Building Materials 44, pp. 276-286, 2013.

[72] Nassif, H., K. Ozbay, H. Wang, R. Noland, P. Lou, S. Demiroluk, D. Su, Chaekuk Na, J. Zhao, and M. Beltran. Impact of freight on highway infrastructure in New Jersey. No. FHWA-NJ-2016-004, 2015.

[73] Prozzi, J., M. Murphy, L. Loftus-Otway, A. Banerjee, M. Kim, Han Wu, J. P. Prozzi et al. "Oversize/overweight vehicle permit fee study". No. FHWA/TX-13/0-6736-2. 2012.

[74] Mechanistic-Empirical Pavement Design Guide-A Manual of Practice- AASHTO 2020.

[75] Lee, Y. H., Bair, J. H., Lee, C. T., Yen, S. T.and Lee, Y. M., Modified Portland Cement Association Stress Analysis and Thickness Design Procedures. Transportation Research Record 1568, TRB, National Research Council, Washington, D. C., U. S. A., pp. 77-88 (1997).

[76] Portland Cement Association (PCA). Thickness Design for Concrete Highway and Street Pavements, Engineering Bulletin EB109P, Skokie, Illinois, 1984

[77] Wu, Z., and D. X. Xiao. Development of DARWin-ME Design Guideline for Louisiana Pavement Design, Louisiana Department of Transportation and Development, LTRC Project No. 12-4P, 2016.

[78] Zhang, J., and Li, V. C. Influence of supporting base characteristics on the shrinkage induced stresses in concrete pavements, 127(6), pp. 455-463, 2001.

Appendix A

Typical Pavement Instrumentation Results

The typical RCC pavement responses under different load magnitudes are shown in Figure A1-A under both static and dynamic loading condition. The sensors are named as following: BV= Bottom Vertical; BT=Bottom Transverse; TV= Top Vertical; TT= Top Transverse. The number represents the sensor location as shown in Figure 12.

Figure A1. Dynamic bottom strain response at 9-kip loading (Section 4)
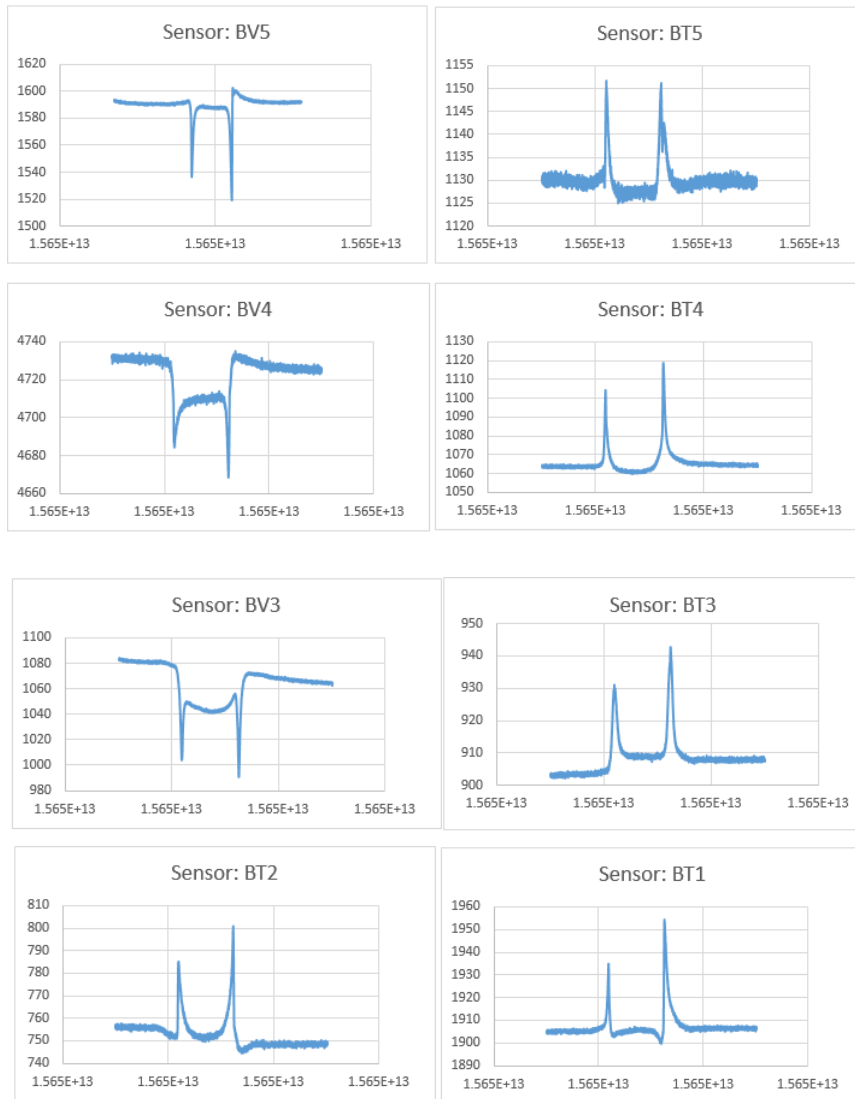
Figure A2. Dynamic bottom strain response at 16-kip loading (section 4)
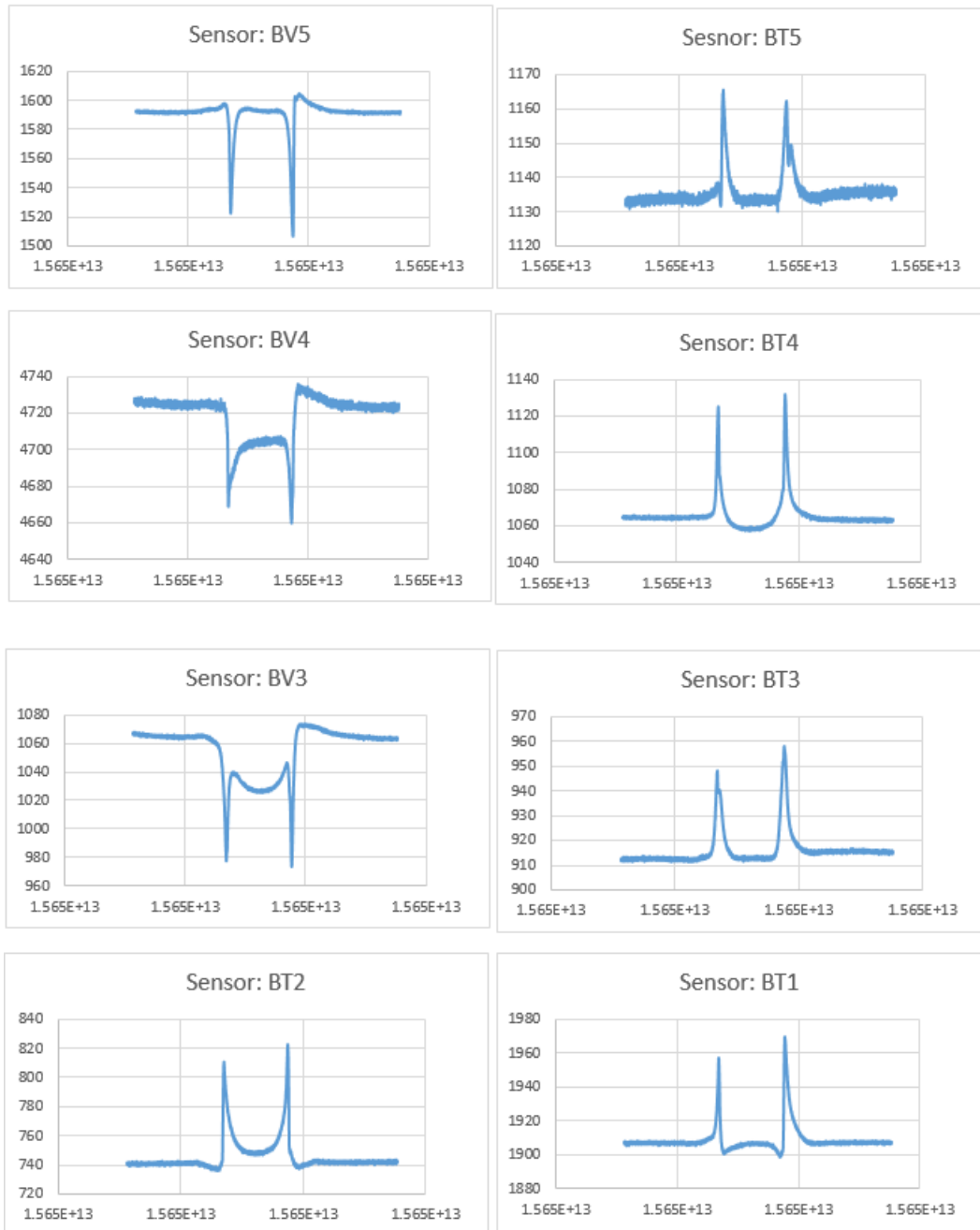
Figure A3. Dynamic bottom strain response at 20-kip loading (section 4)
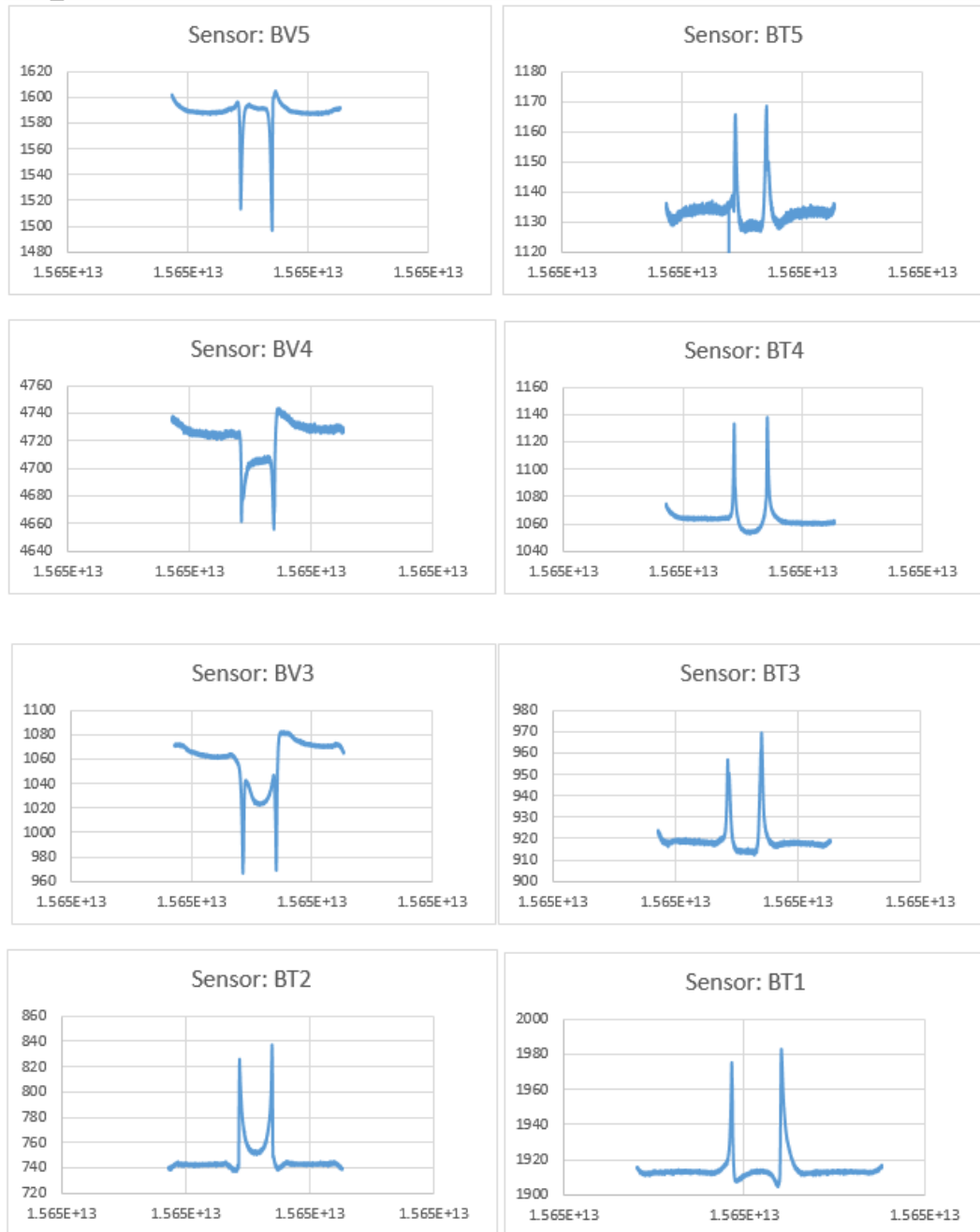
Figure A4. Dynamic bottom strain response at 25-kip loading (section 4)
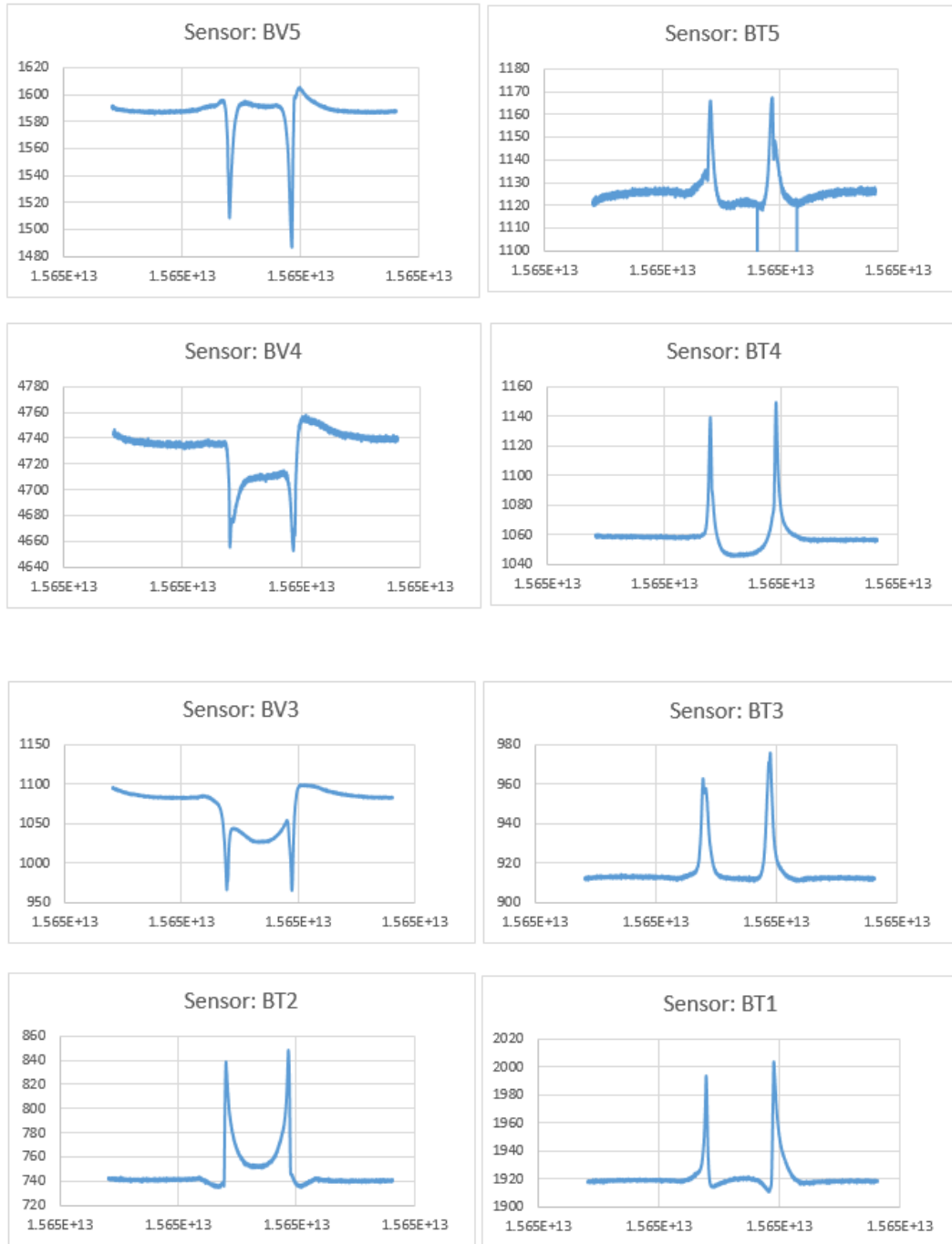
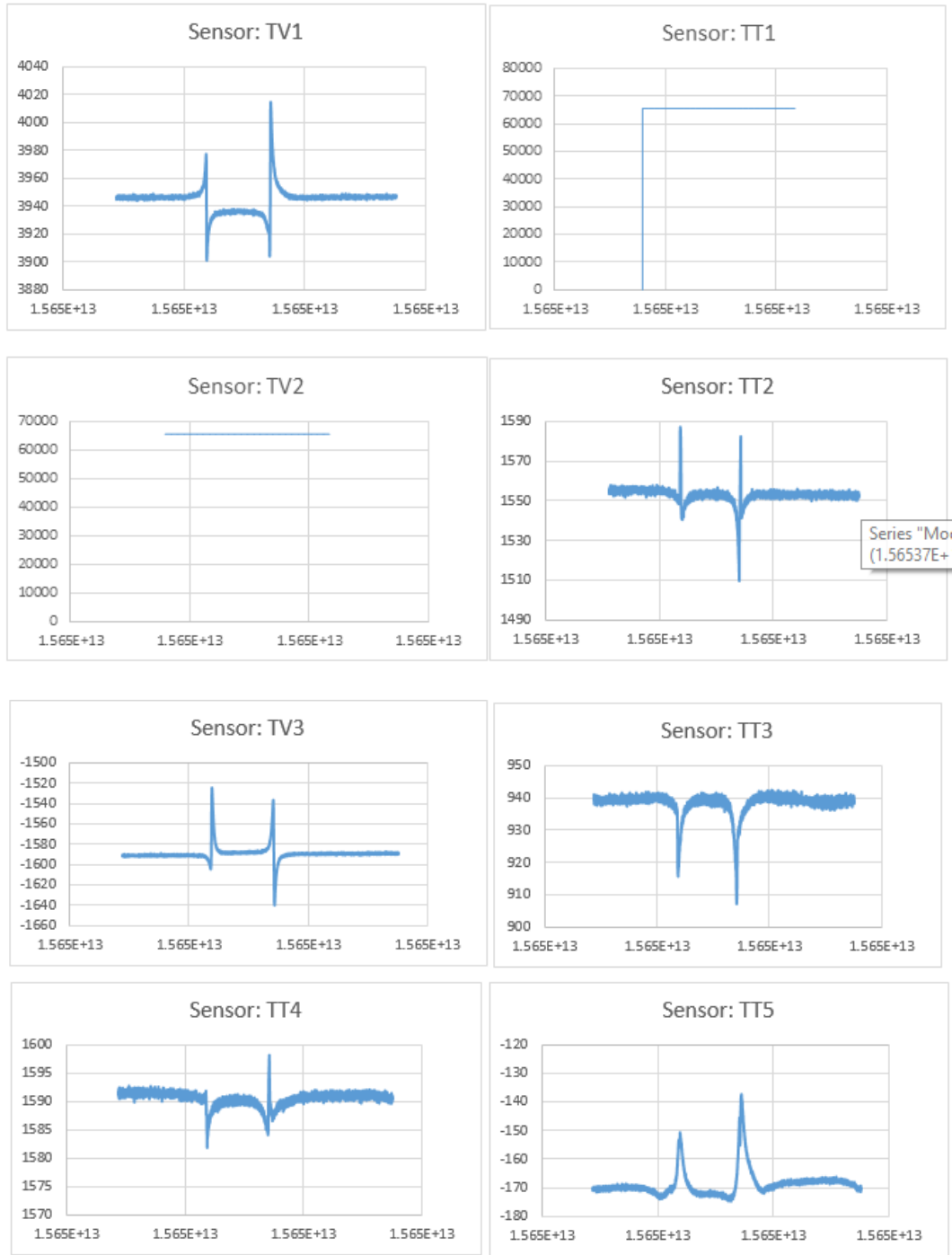**Figure A5. Dynamic top strain response at 9-kip loading (section 4)**

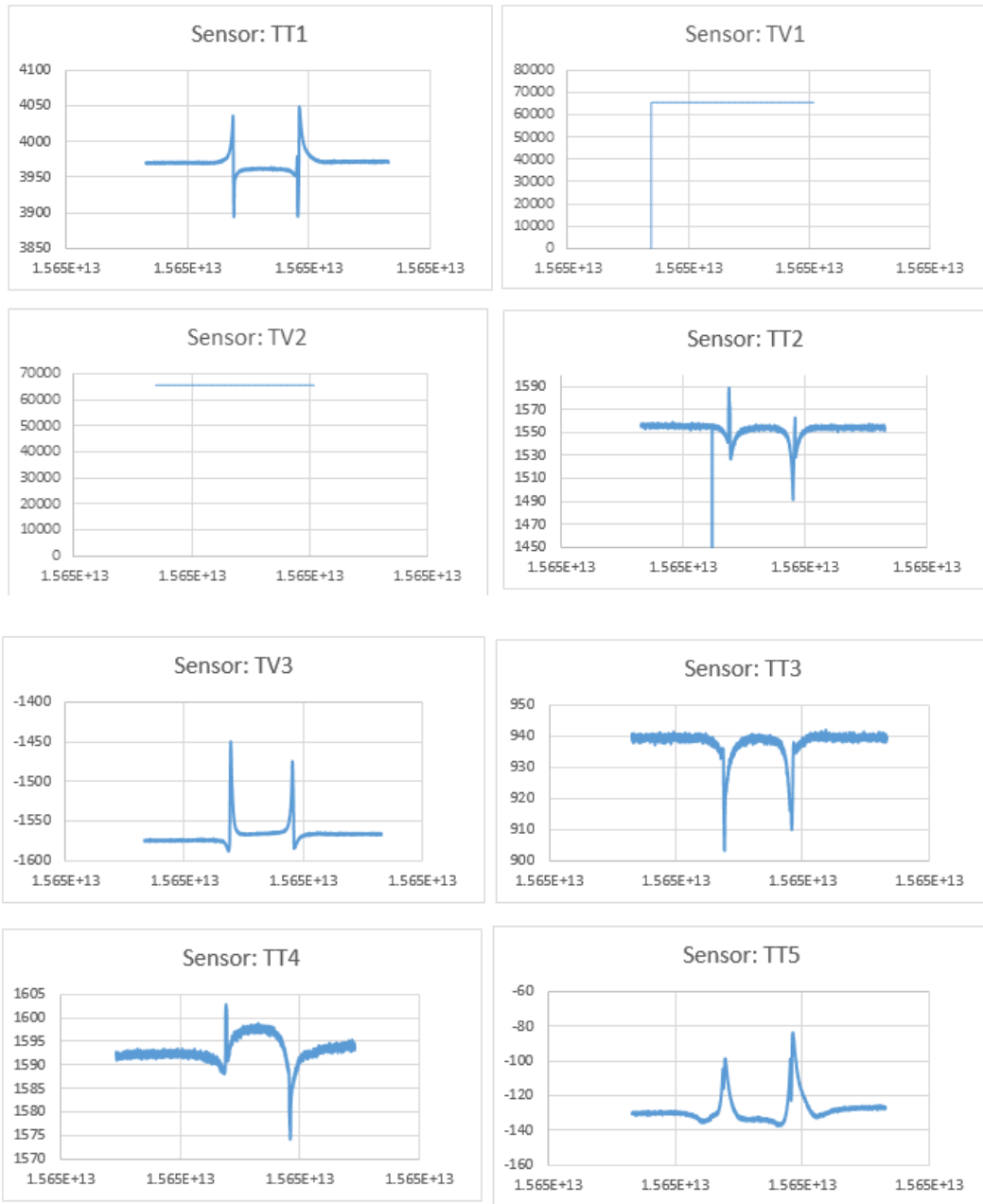**Figure A6. Dynamic top strain response at 16-kip loading (section 4)**

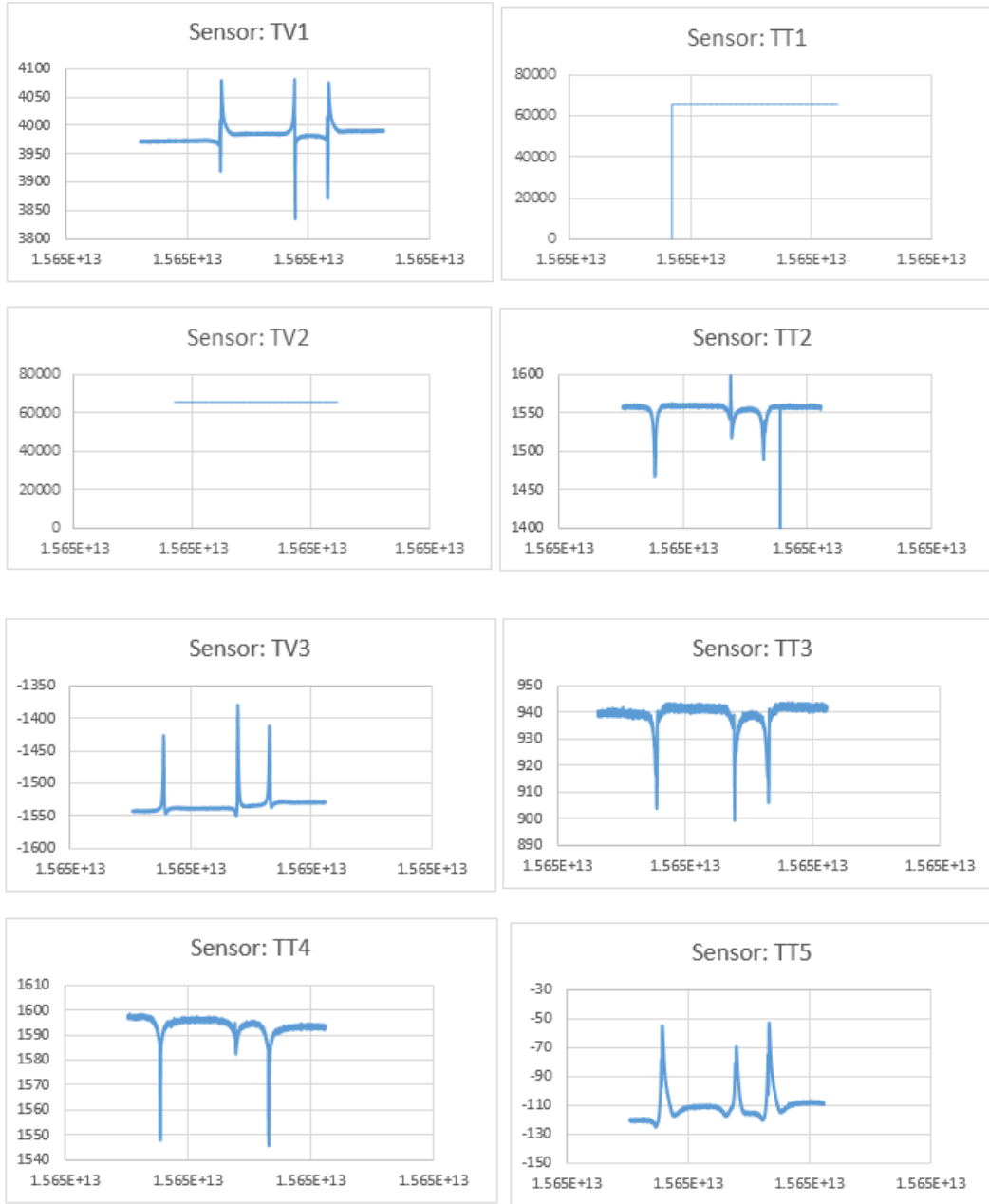**Figure A7. Dynamic top strain response at 20-kip loading (section 4)**

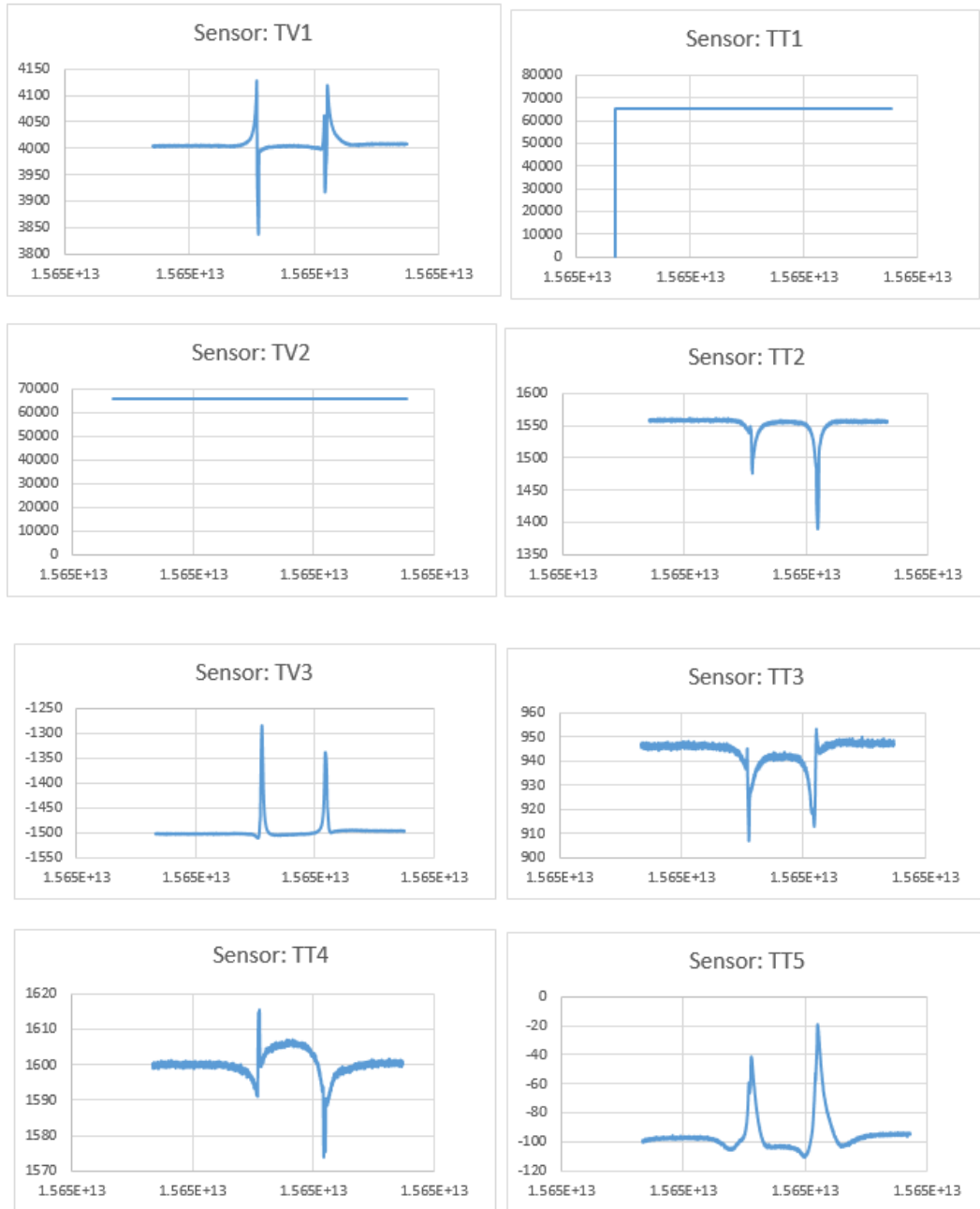**Figure A8. Dynamic top strain response at 25-kip loading (section 4)**

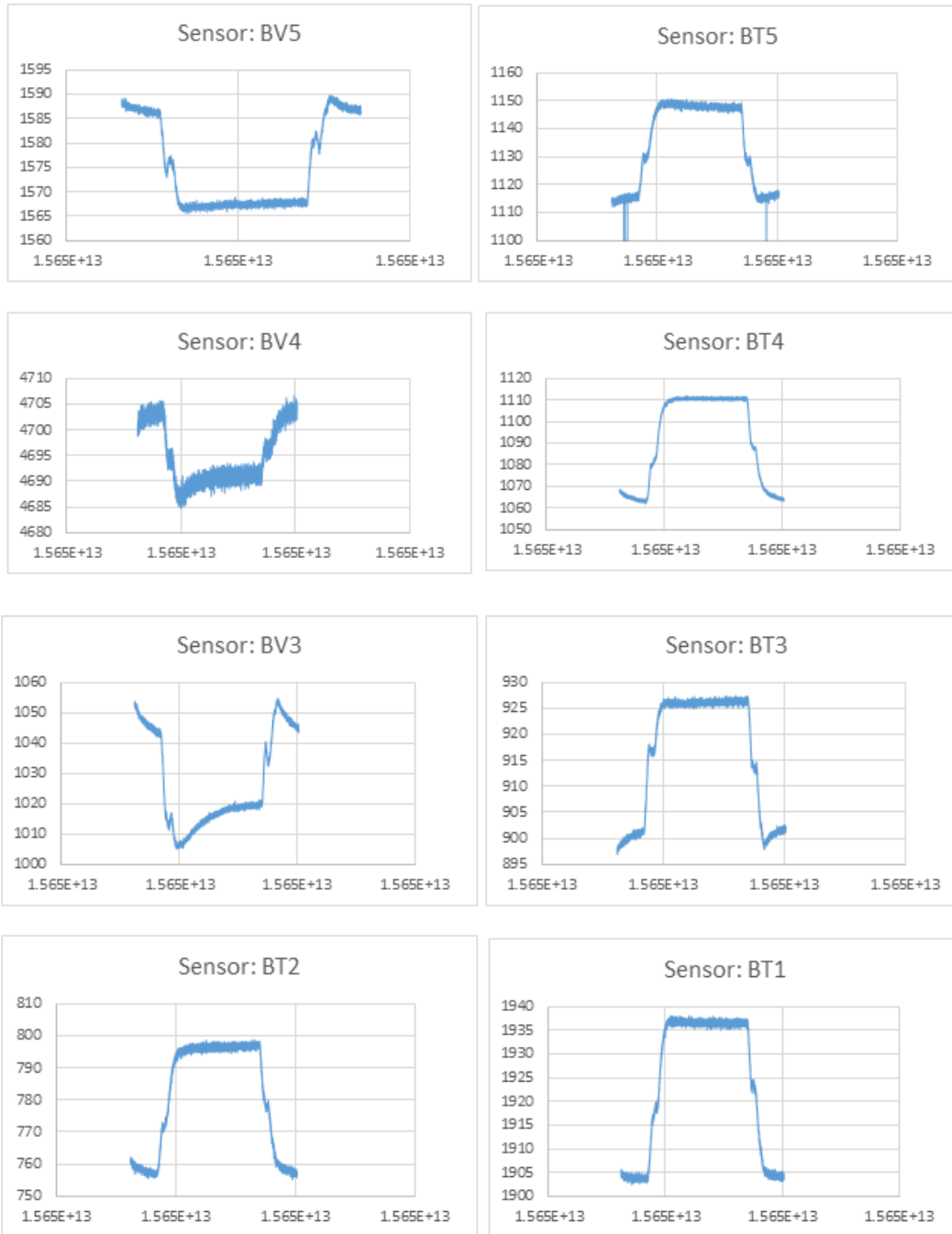**Figure A9. Static bottom strain response at 9-kip loading (section 4)**

Figure A10. Static bottom strain response at 16-kip loading (section 4)

Sensor: BV5

Sensor: BT5

Sensor: BV4

Sensor: BT4
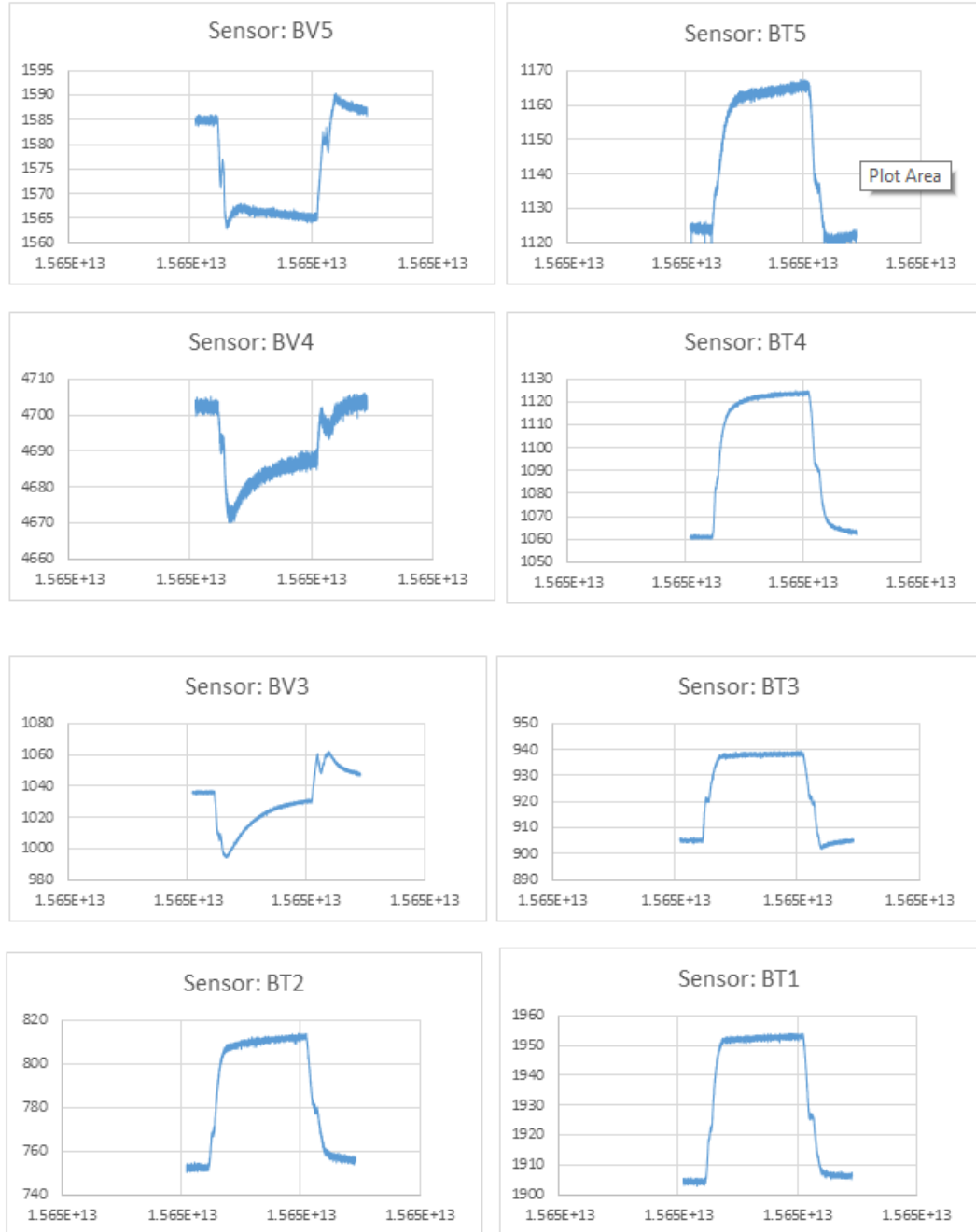
Sensor: BV3

Sensor: BT3

Sensor: BT2

Sensor: BT1

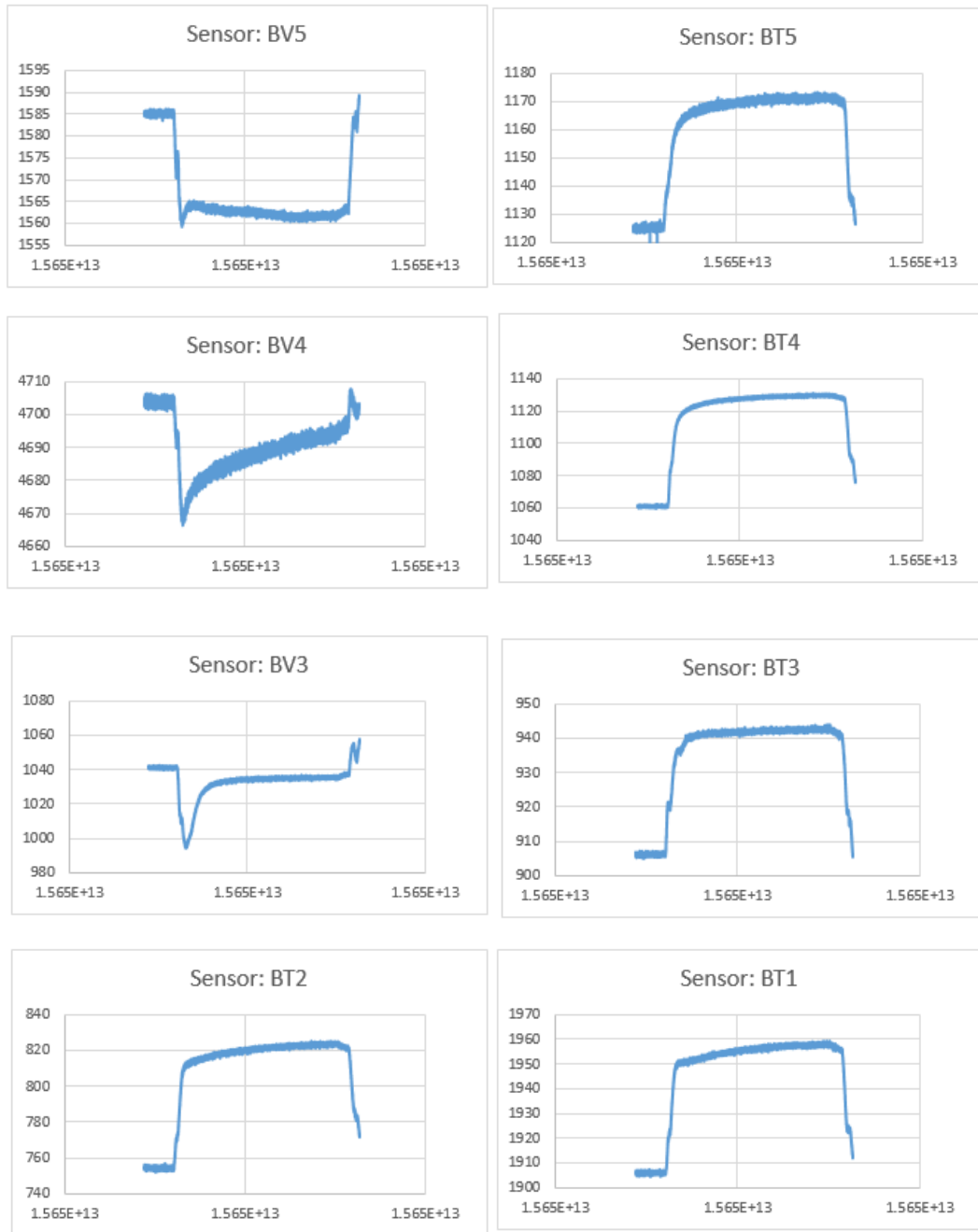**Figure A11. Static bottom strain response at 20-kip loading (section 4)**

Figure A12. Static bottom strain response at 25-kip loading (section 4)
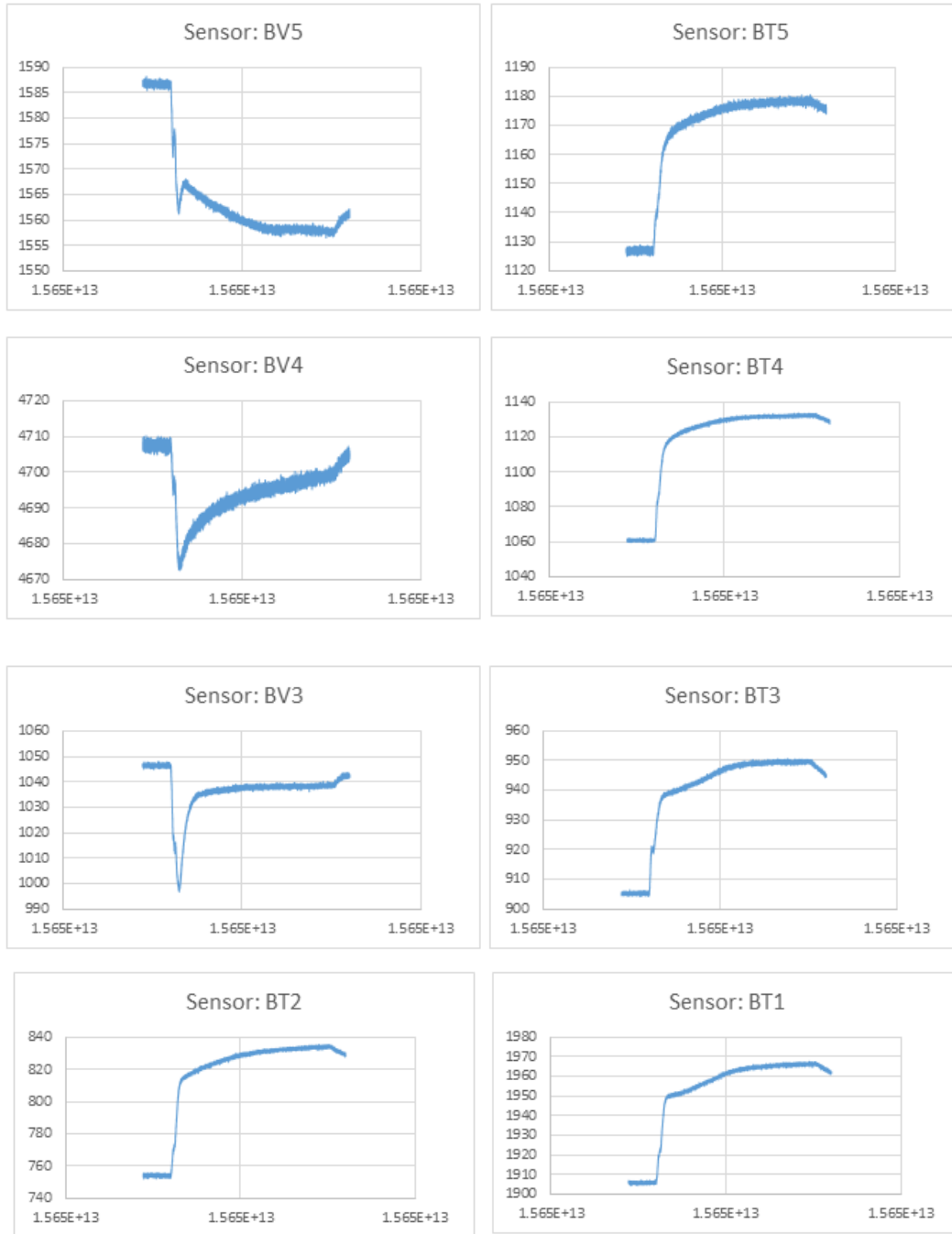
Figure A13. Static top strain response at 9-kip loading (section 4)
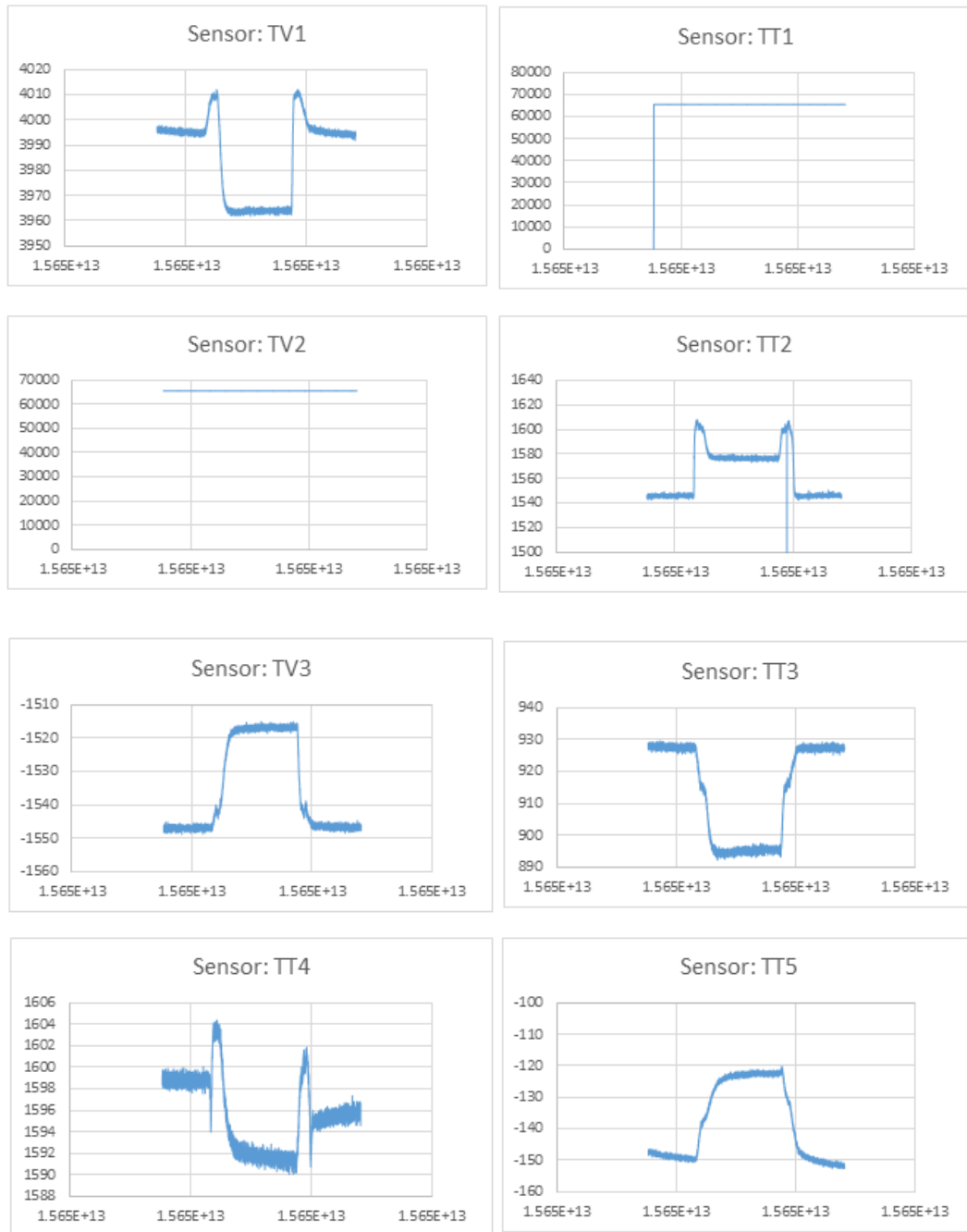
Figure A14. Static top strain response at 16-kip loading (section 4)

Figure A15. Static top strain response at 20-kip loading (section 4)

Figure A16. Static top strain response at 25-kip loading (section 4)
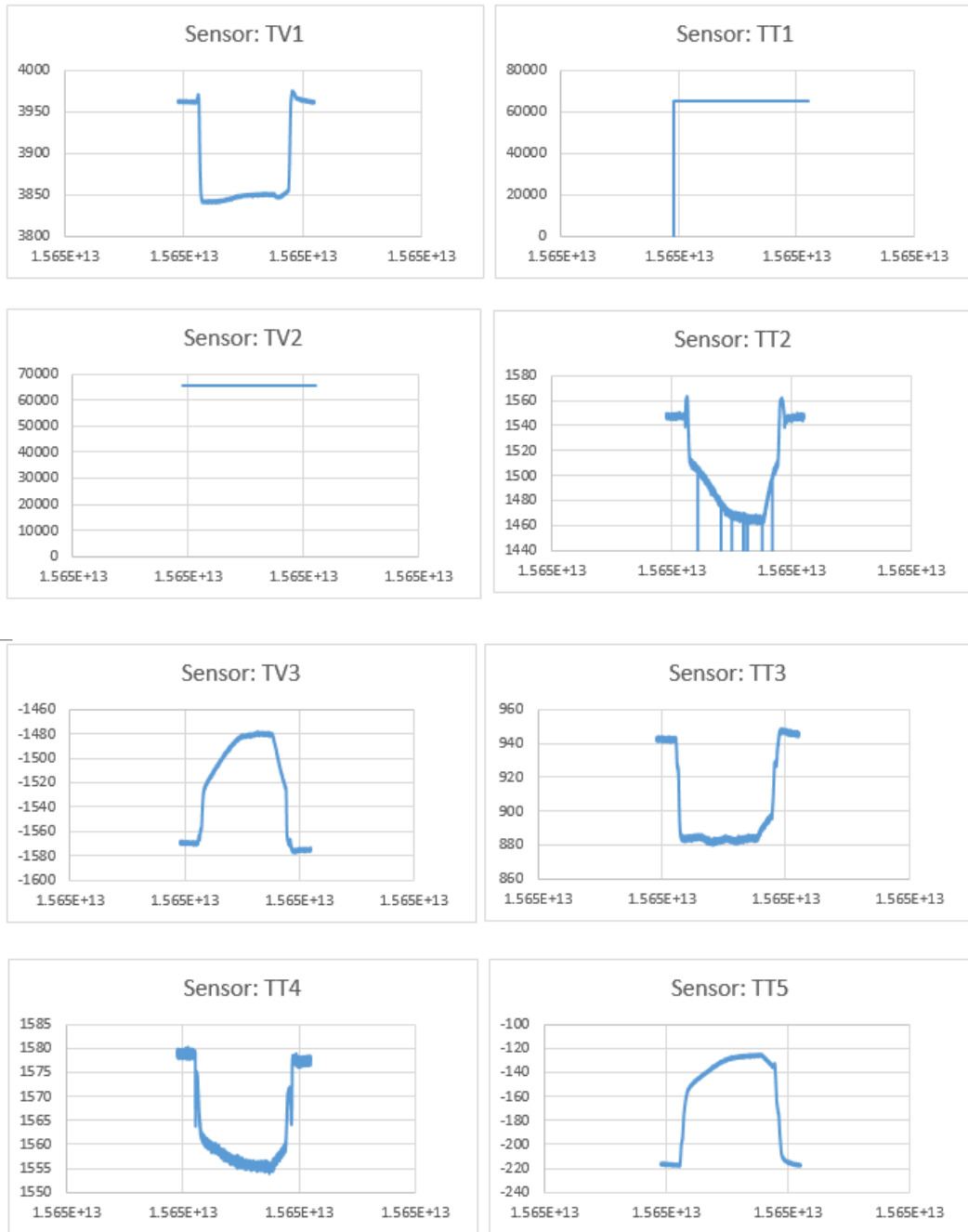
Figure A17. Dynamic bottom strain response at 9-kip loading (section 1)

Figure A18. Dynamic bottom strain response at 16-kip loading (section 1)

Figure A19. Dynamic bottom strain response at 20-kip loading (section 1)

Figure A20. Dynamic bottom strain response at 25-kip loading (section 1)

Figure A21. Dynamic top strain response at 9-kip loading (section 1)

Figure A22. Dynamic top strain response at 16-kip loading (section 1)

Figure A23. Dynamic top strain response at 20-kip loading (section 1)
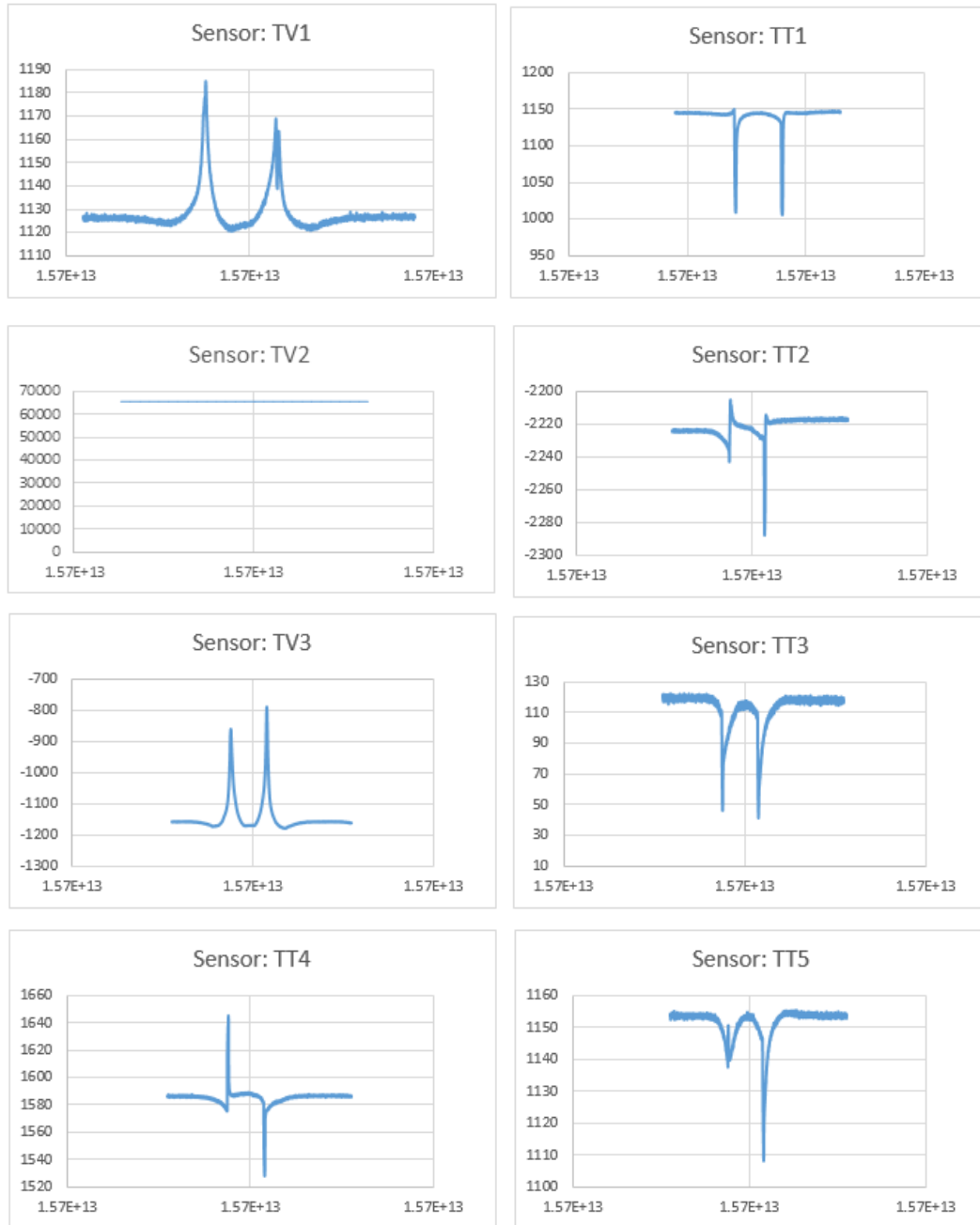
Figure A24. Dynamic top strain response at 25-kip loading (section 1)
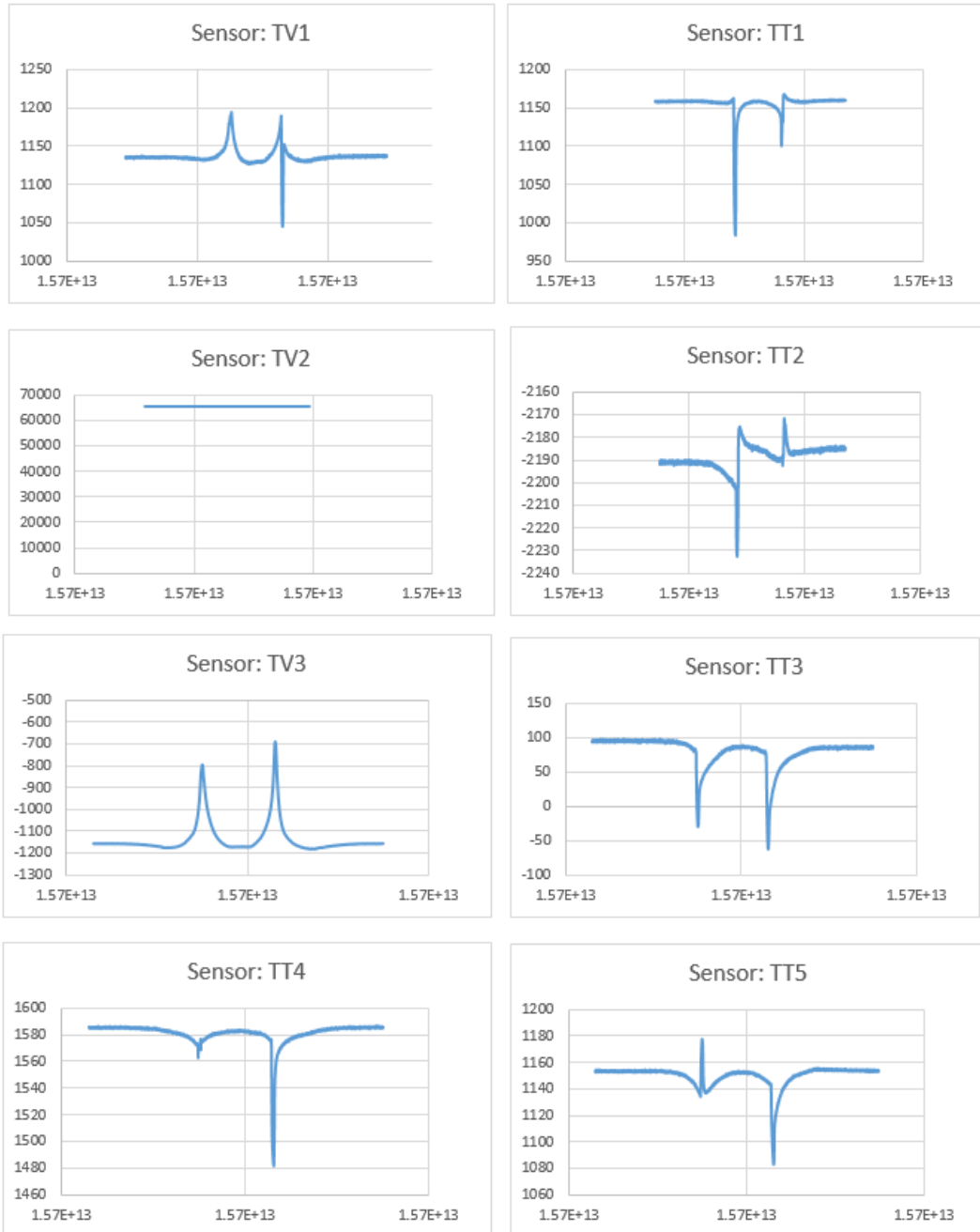
Figure A25. Static bottom strain response at 9-kip loading (section 1)
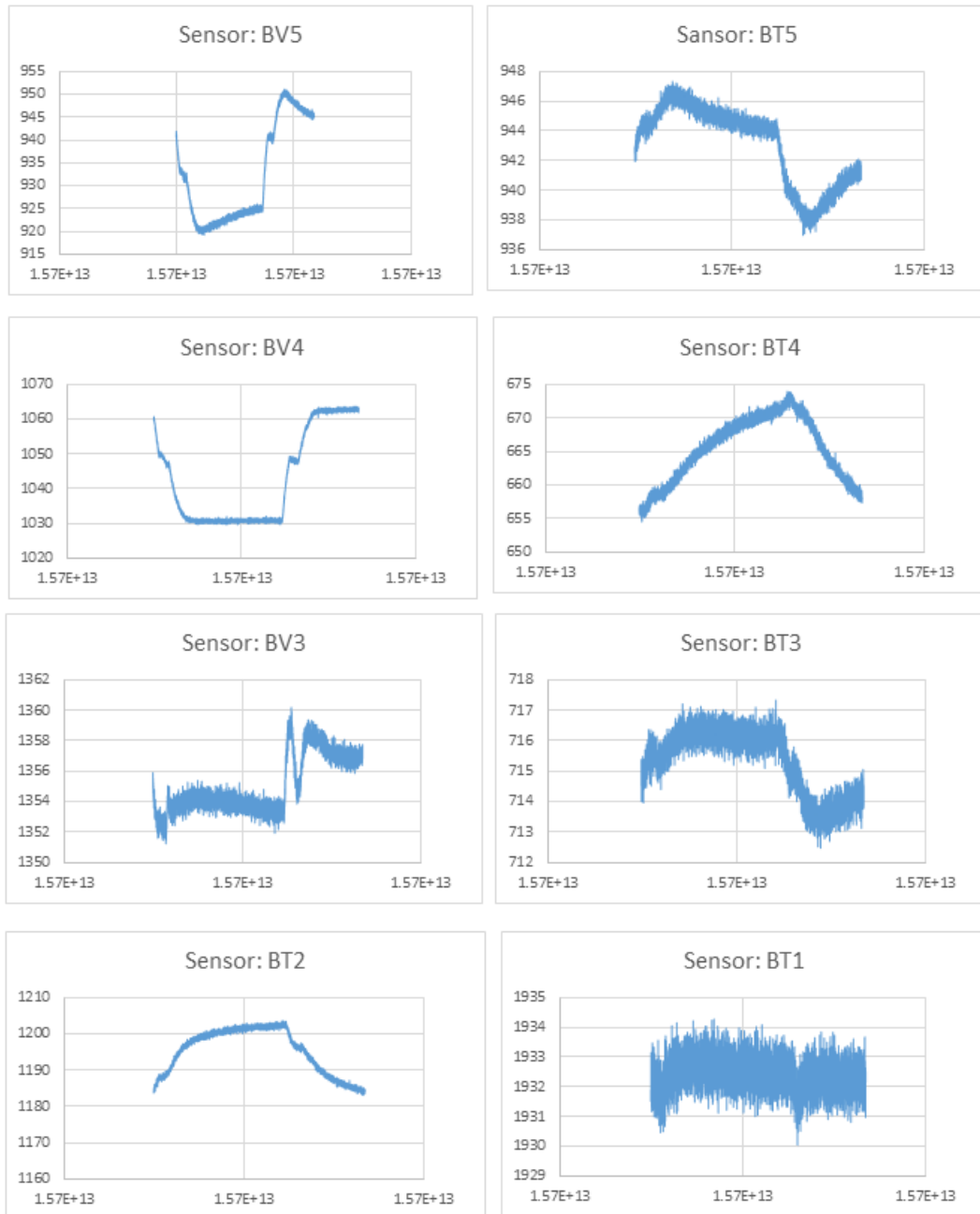
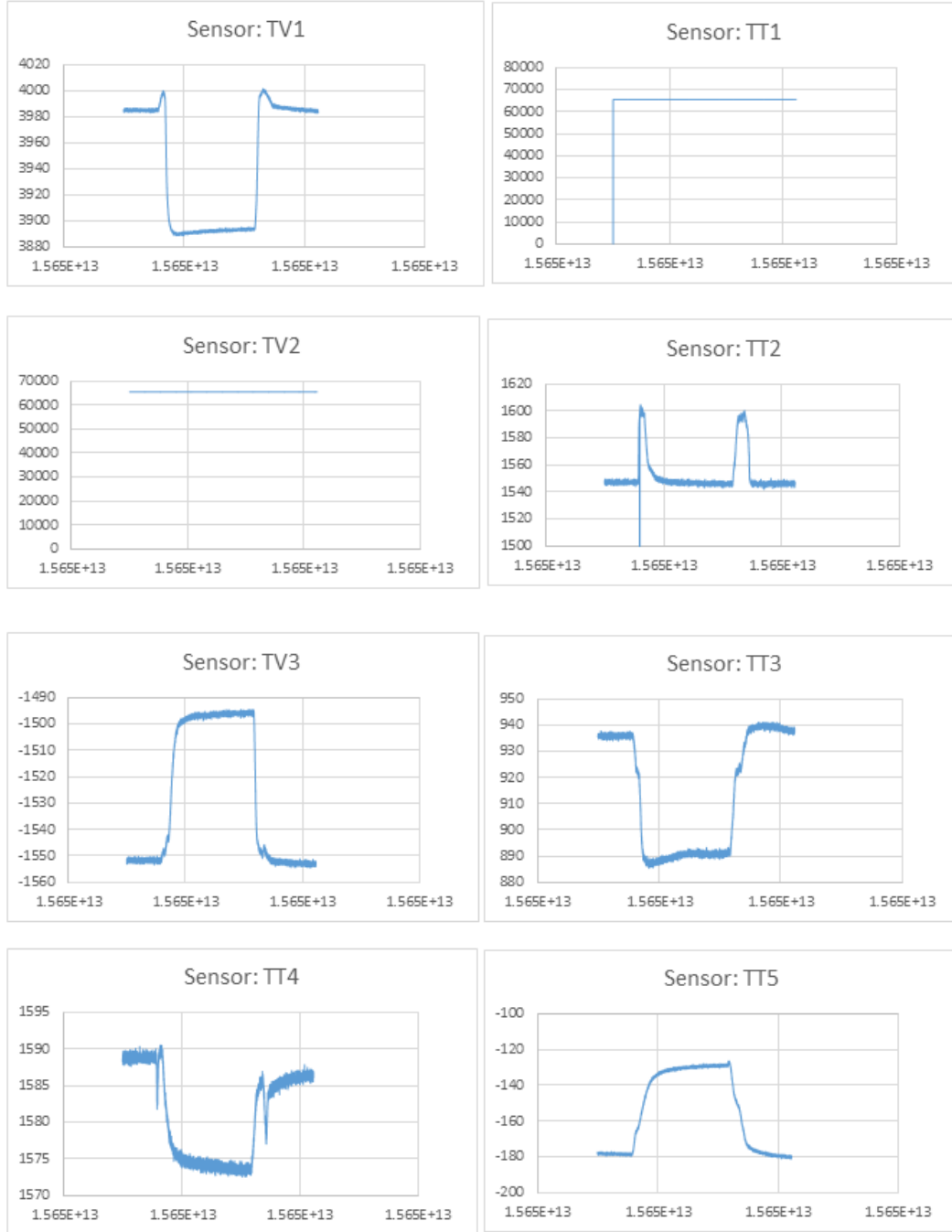**Figure A26. Static bottom strain response at 16-kip loading (section 1)**
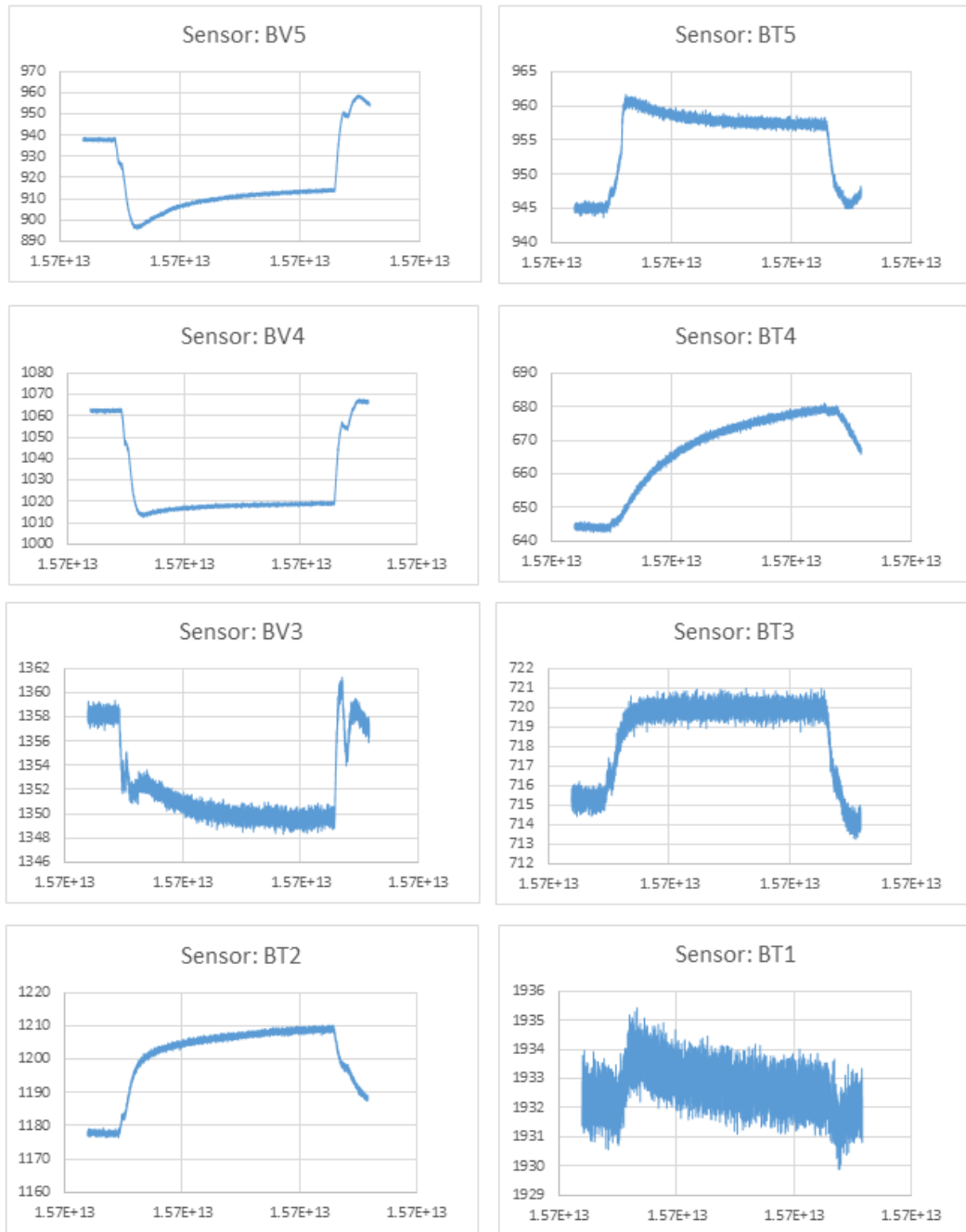
Figure A27. Static bottom strain response at 20-kip loading (section 1)
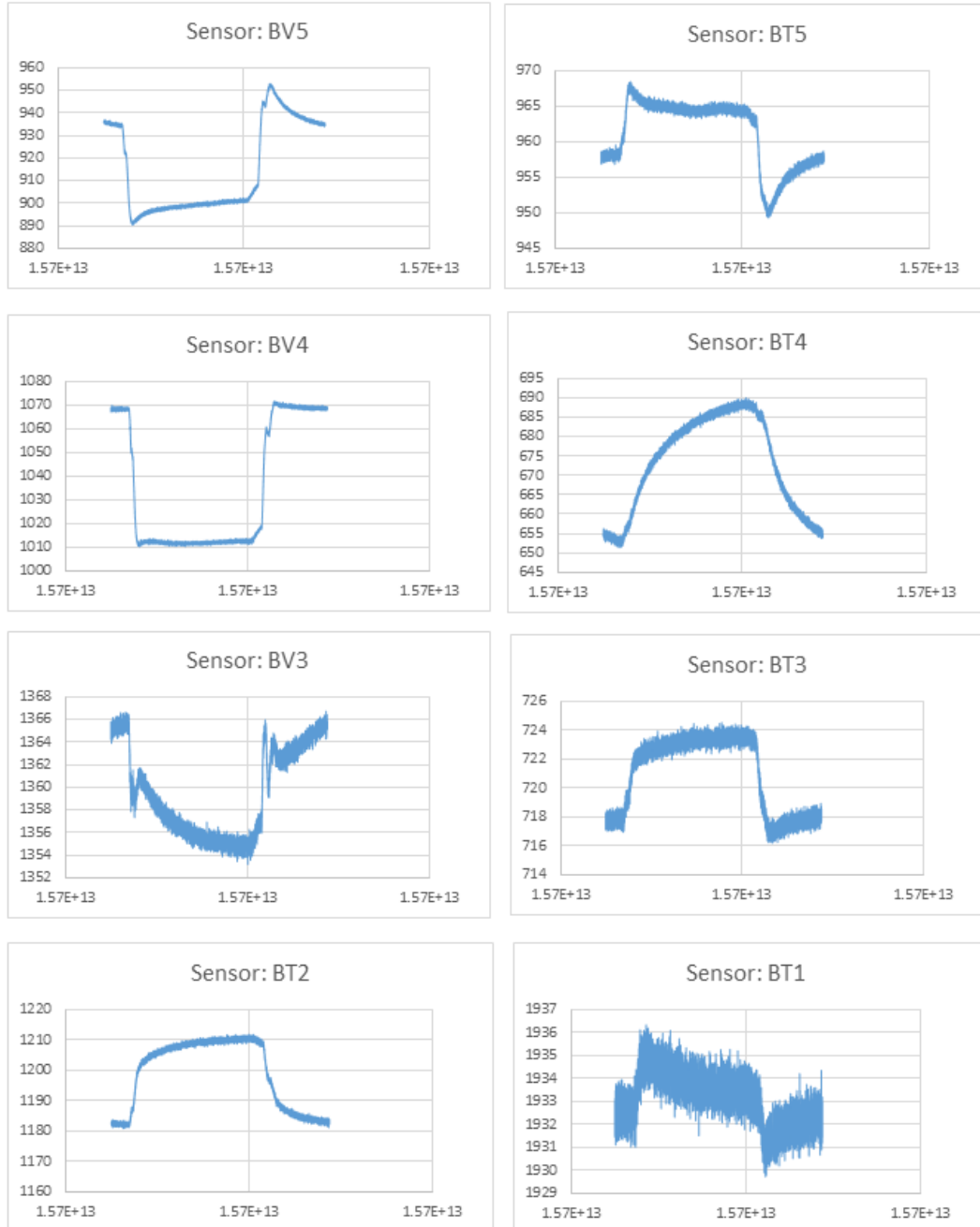
Figure A28. Static bottom strain response at 25-kip loading (section 1)
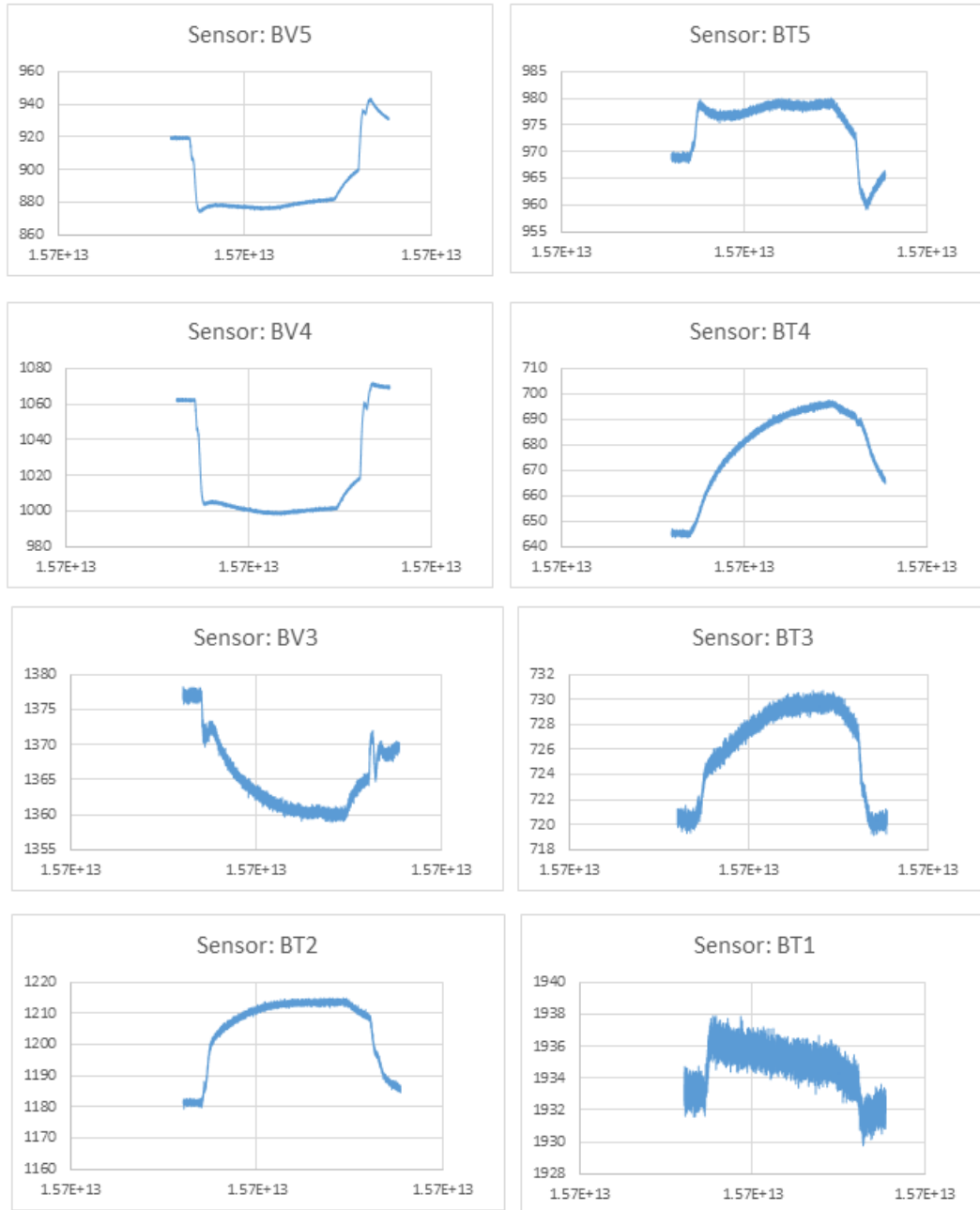
Figure A29. Static top strain response at 9-kip loading (section 1)
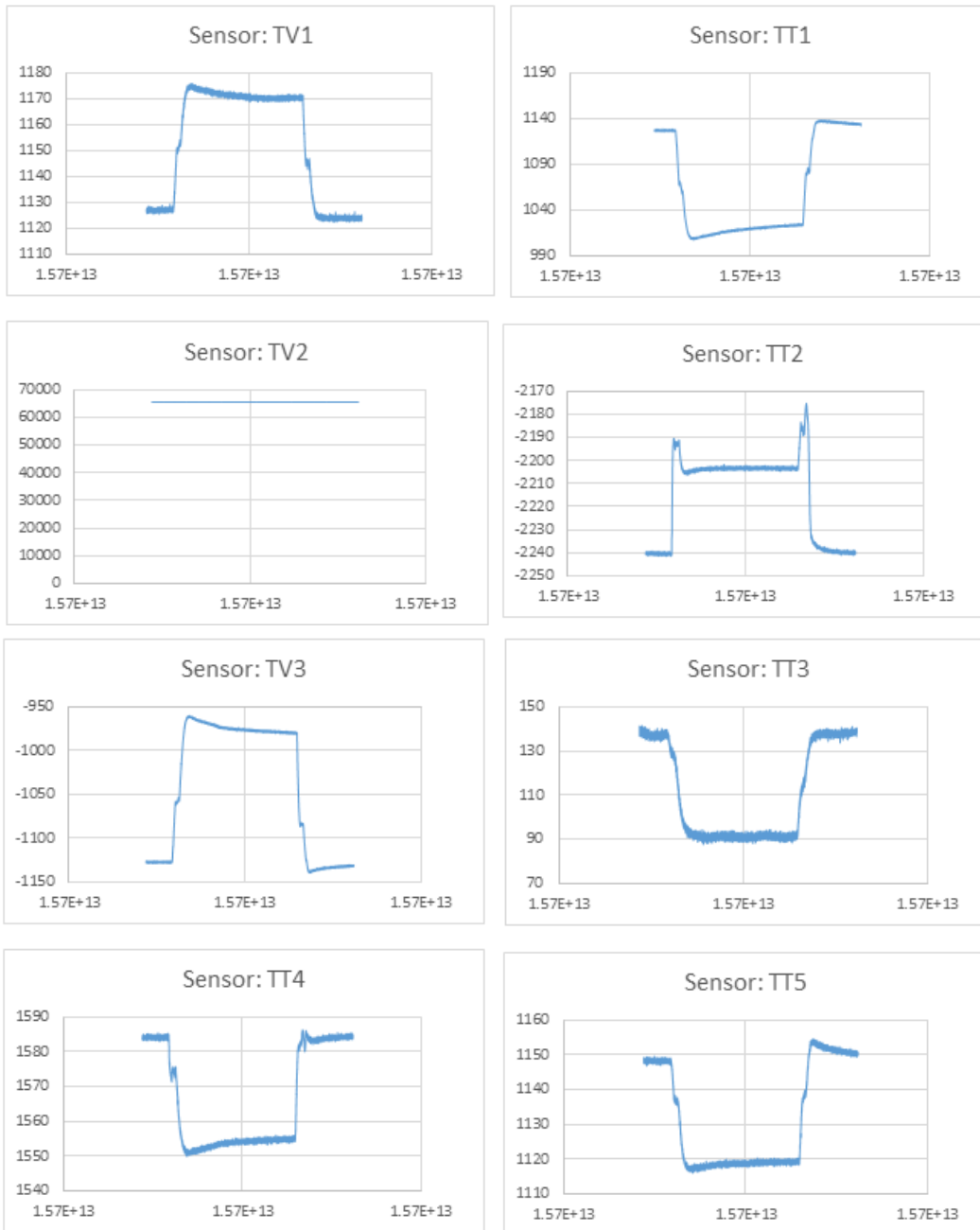
Figure A30. Static top strain response at 16-kip loading (section 1)
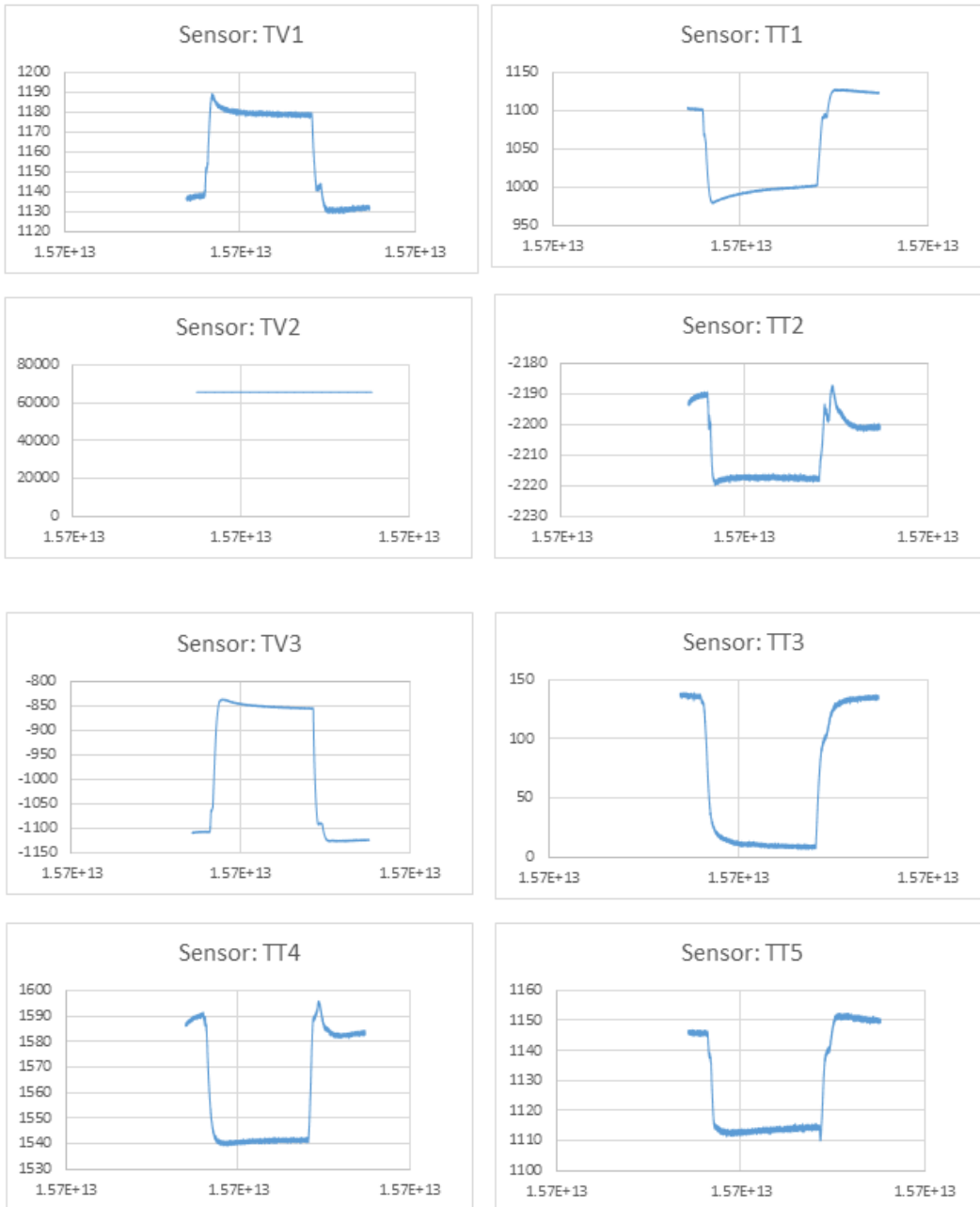
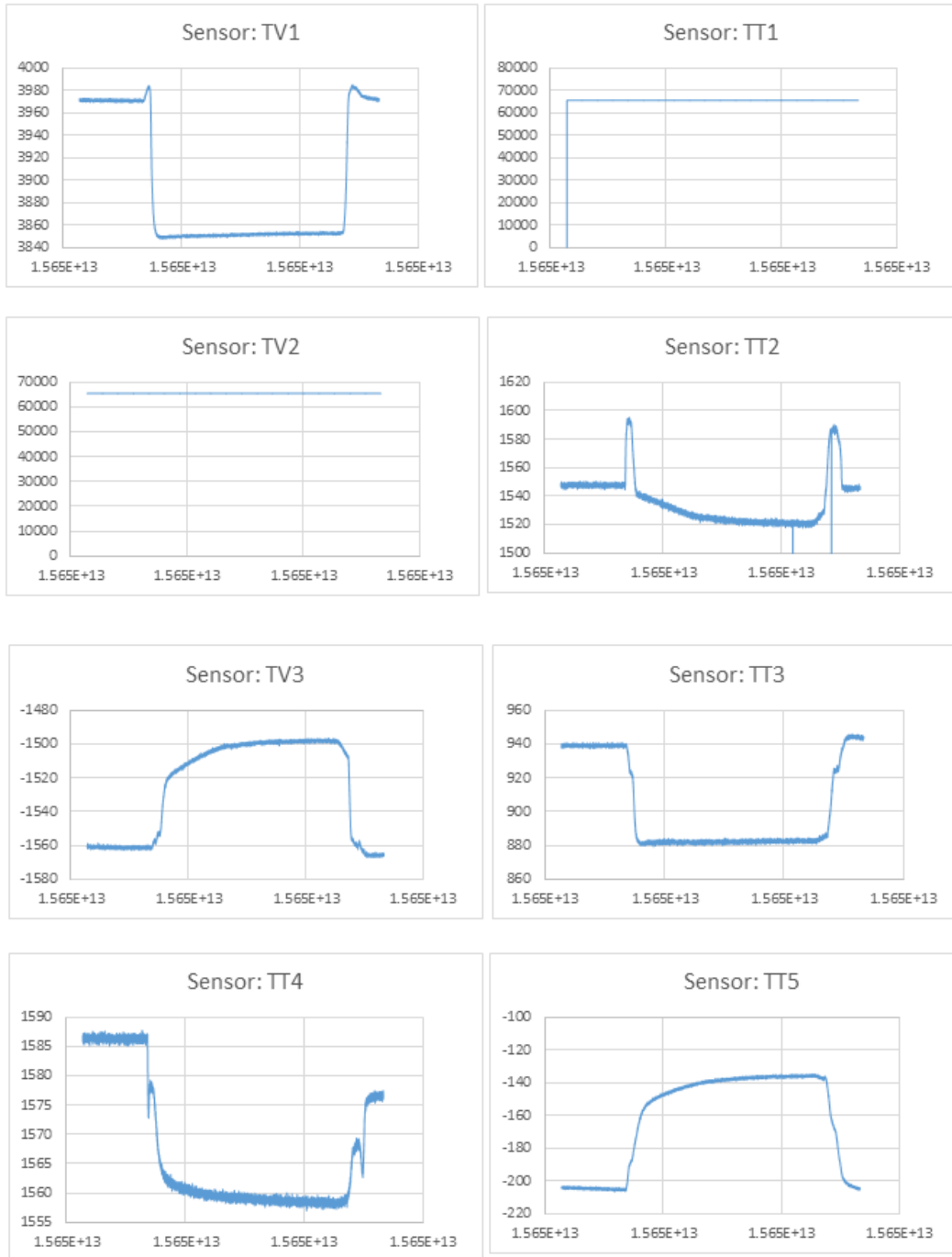**Figure A31. Static top strain response at 20-kip loading (section 1)**

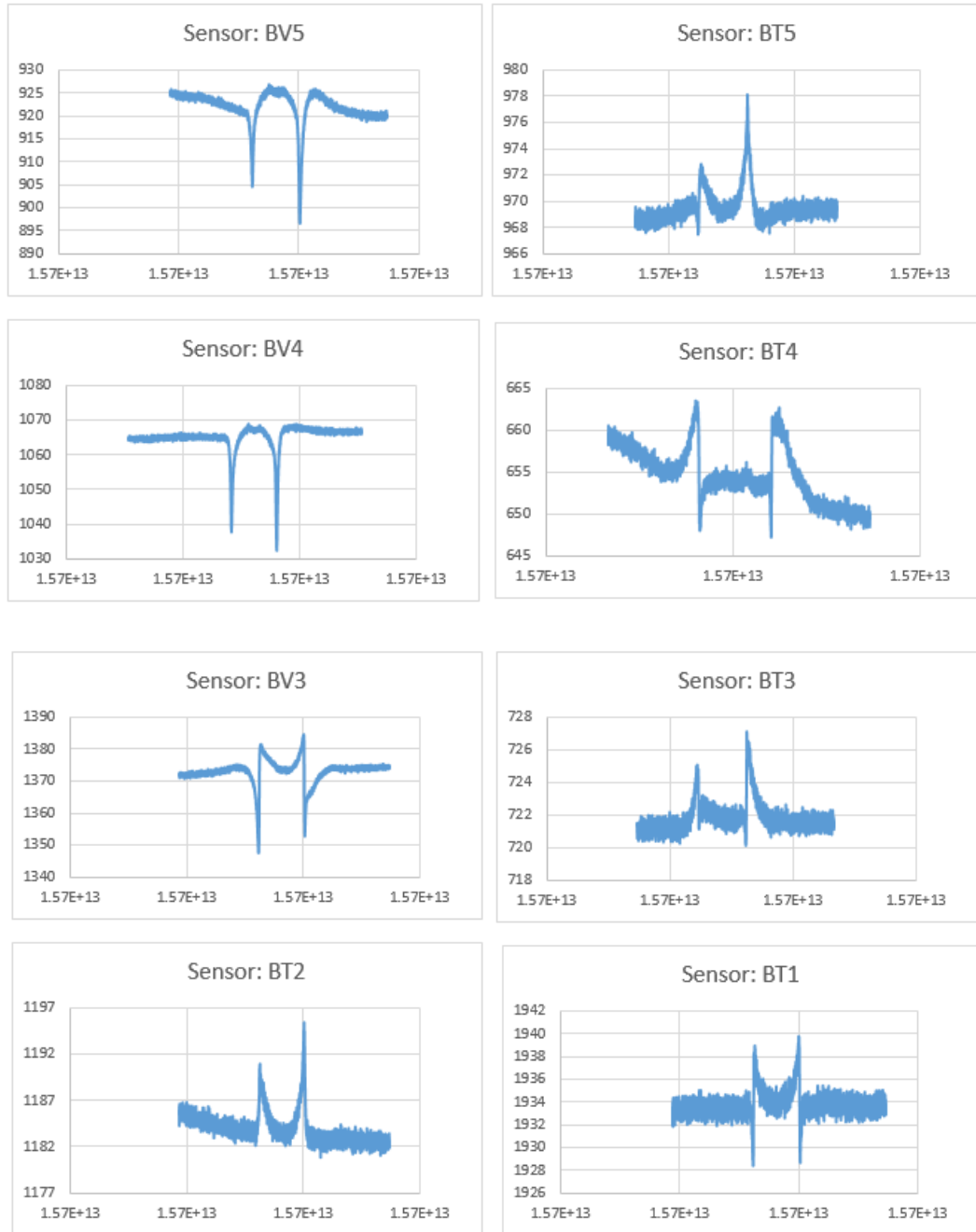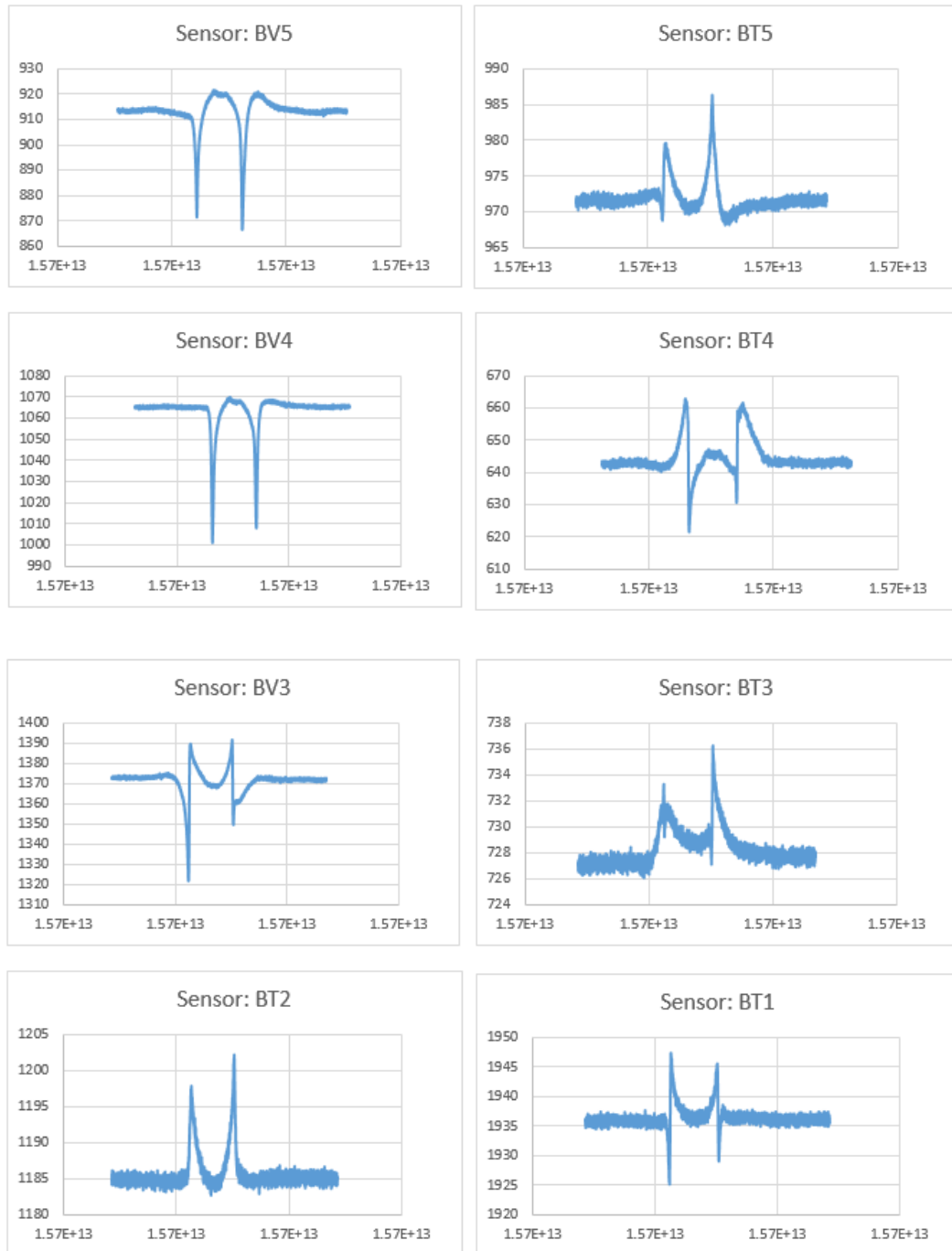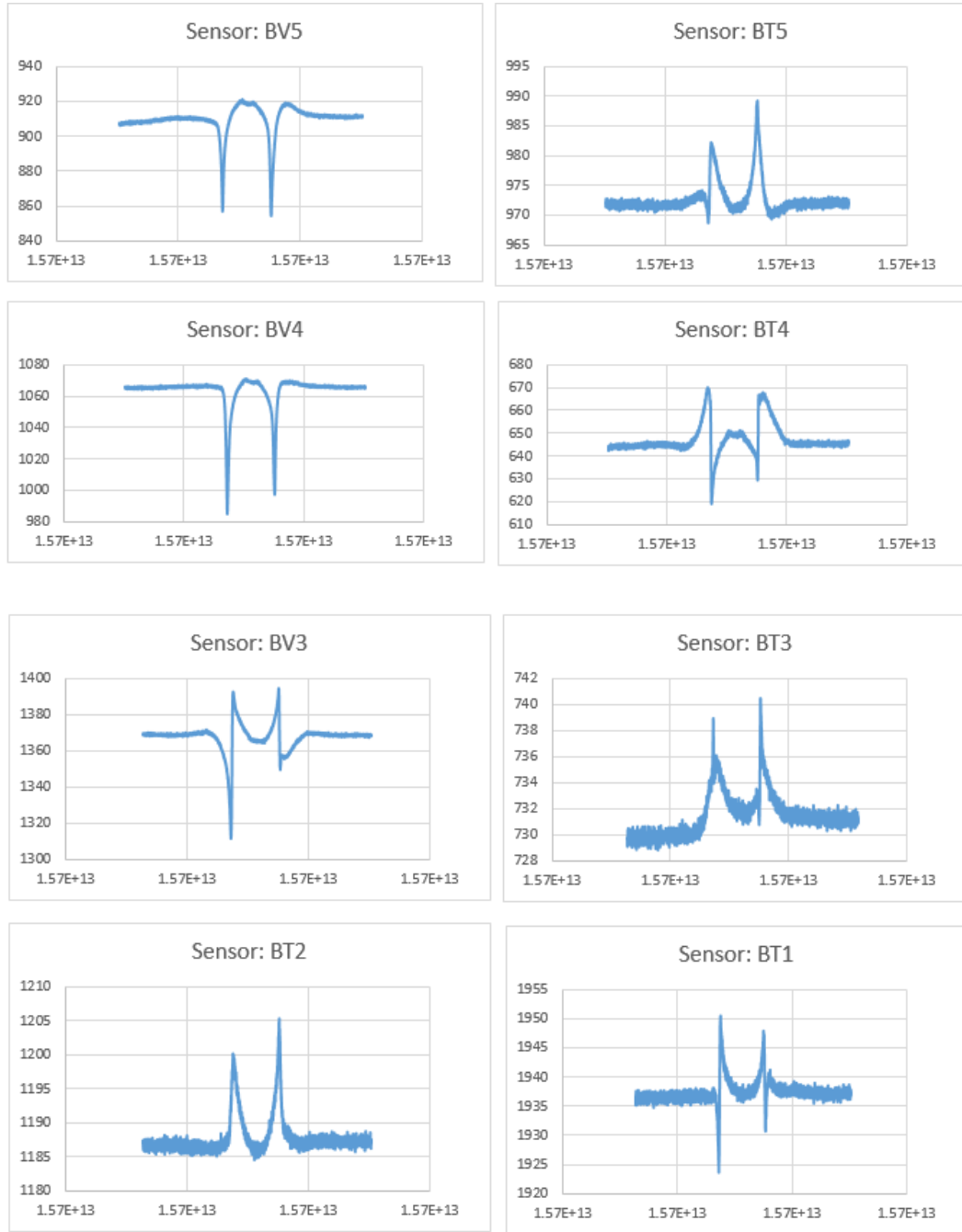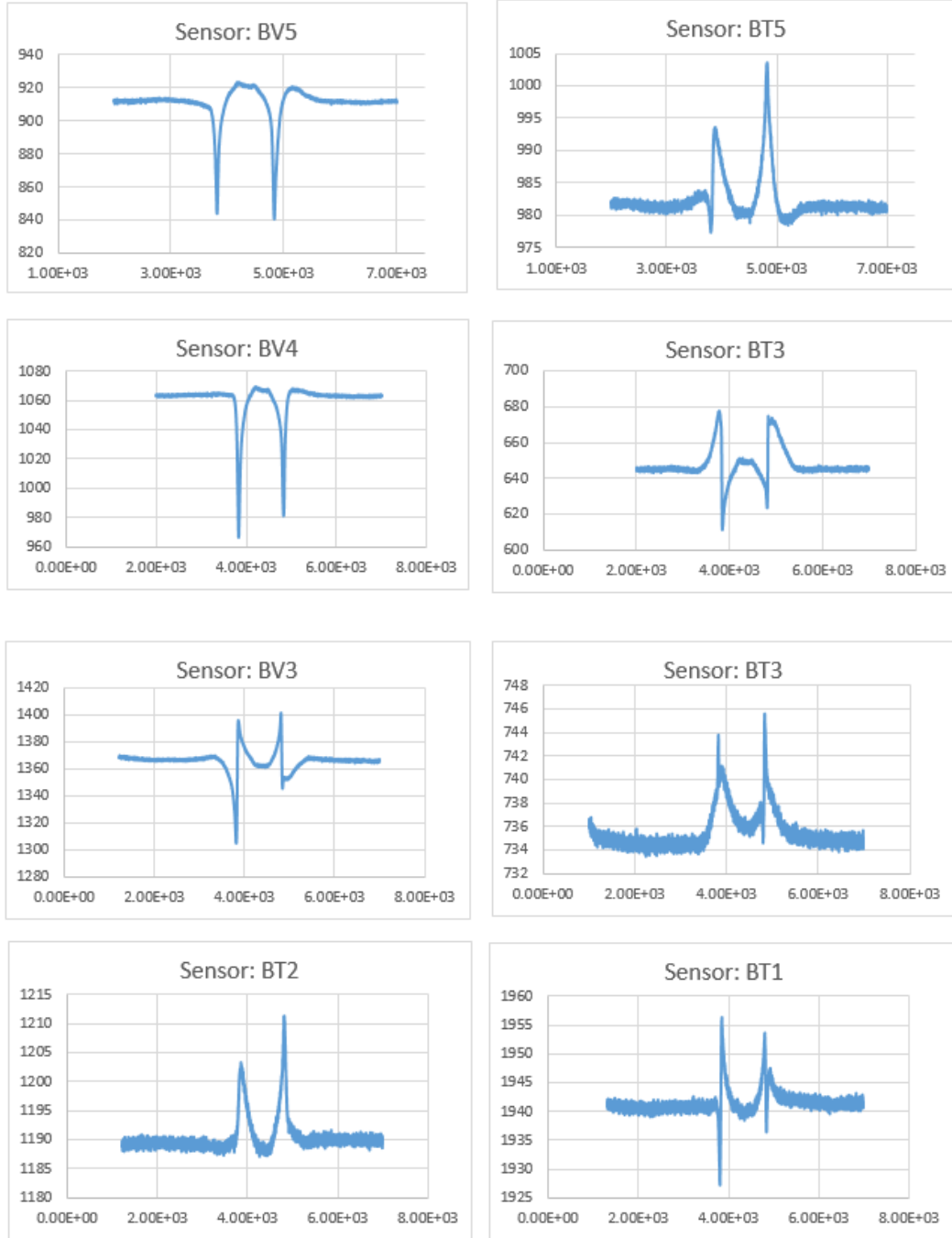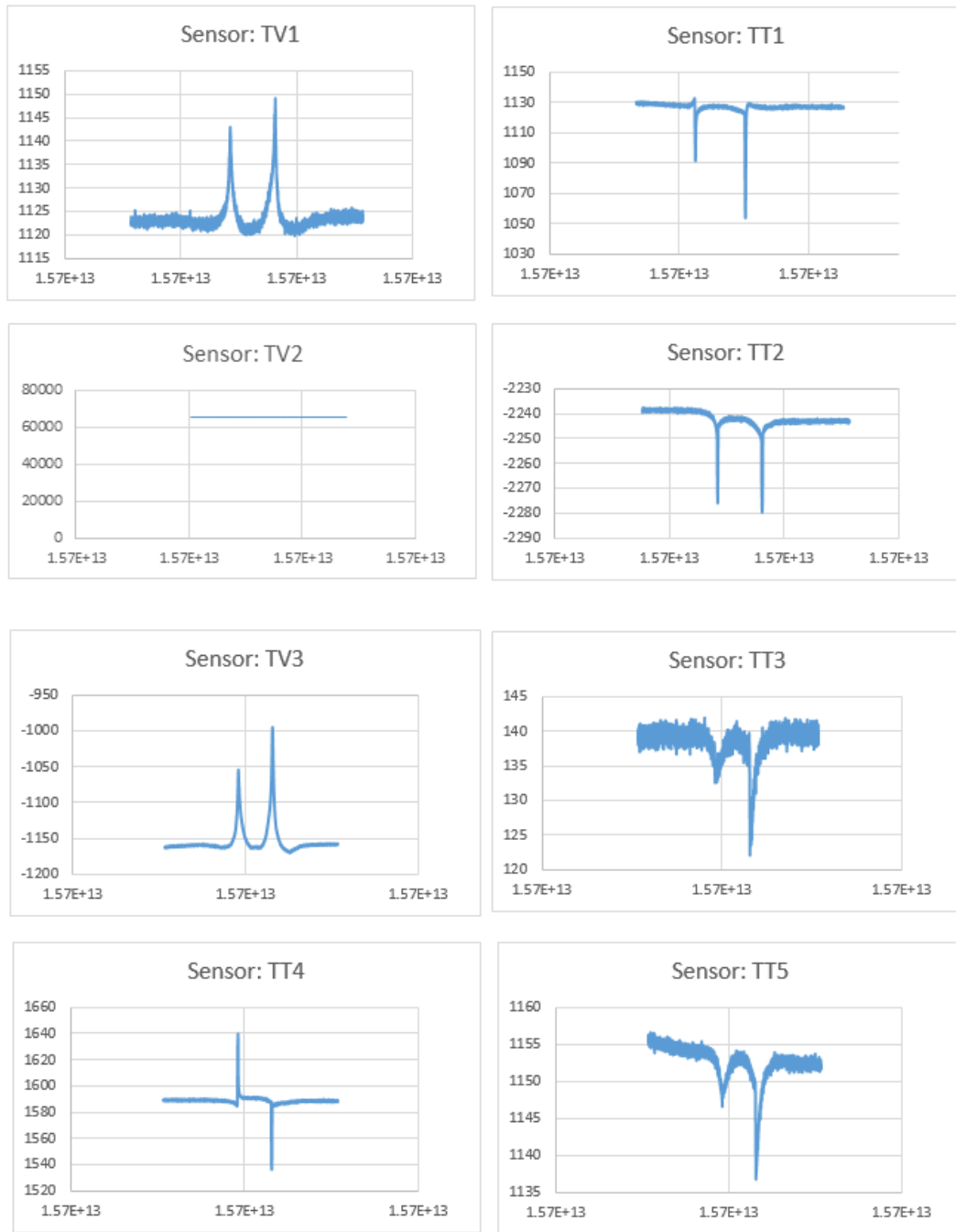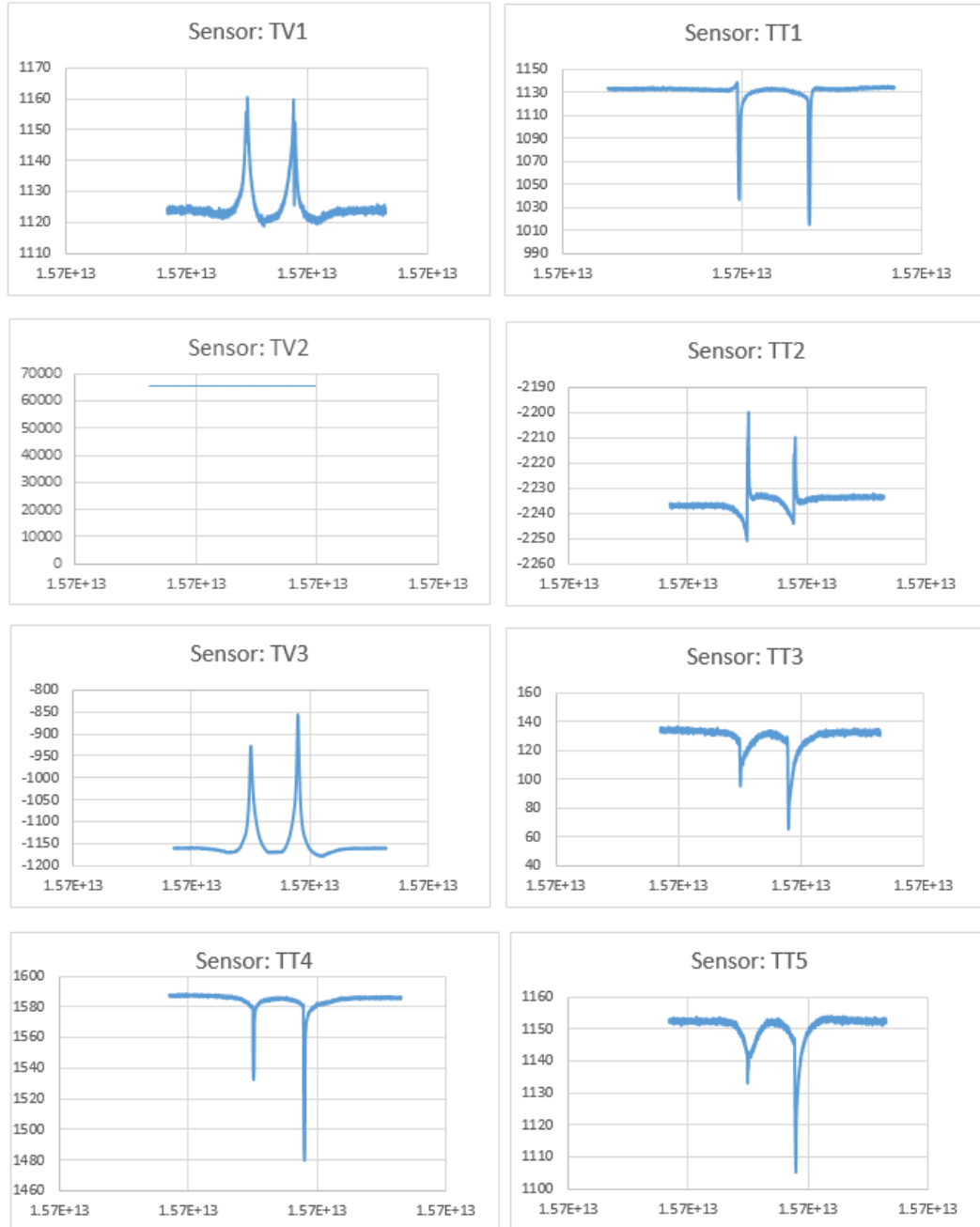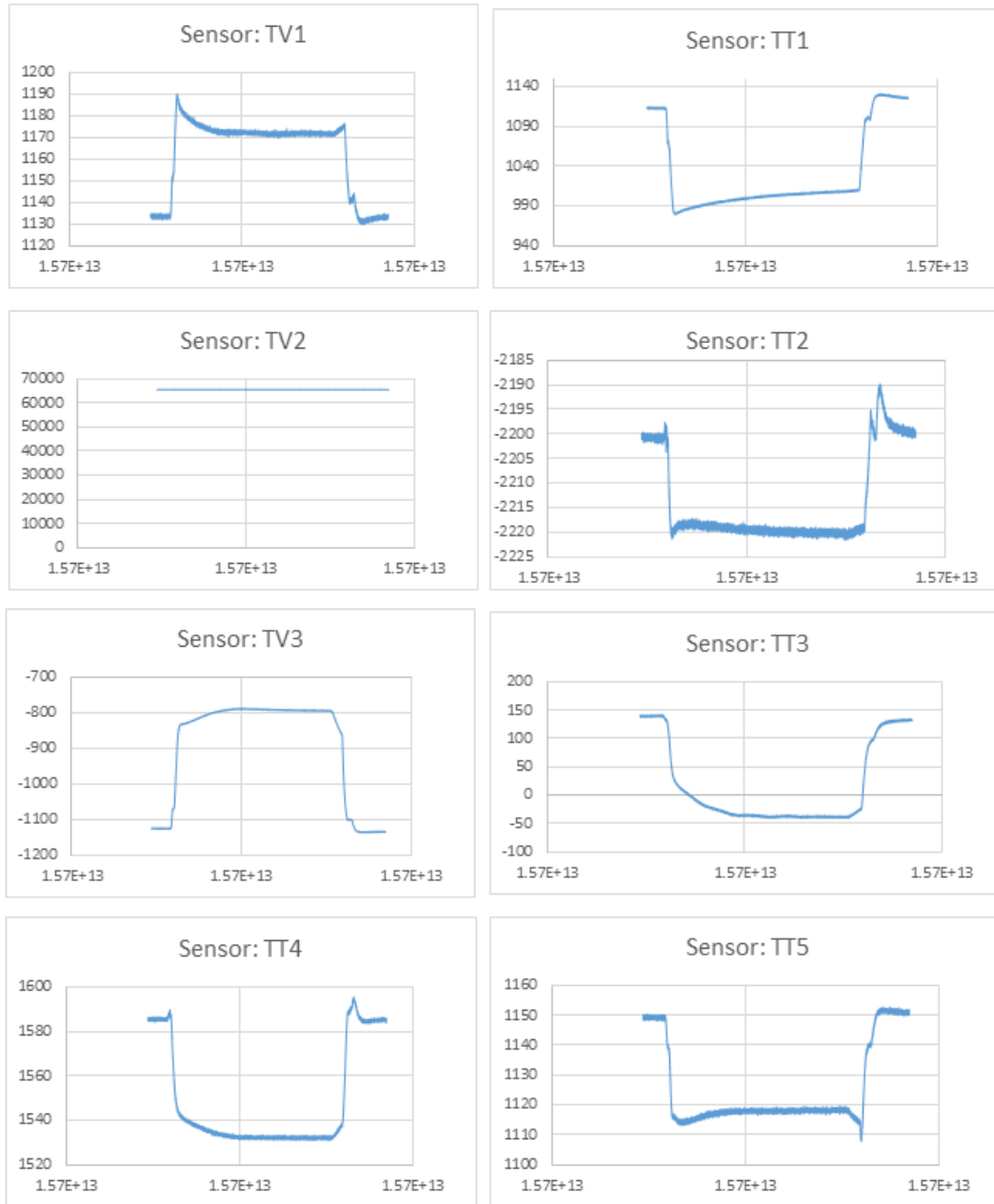**Figure A32. Static top strain response at 25-kip loading (section 1)**
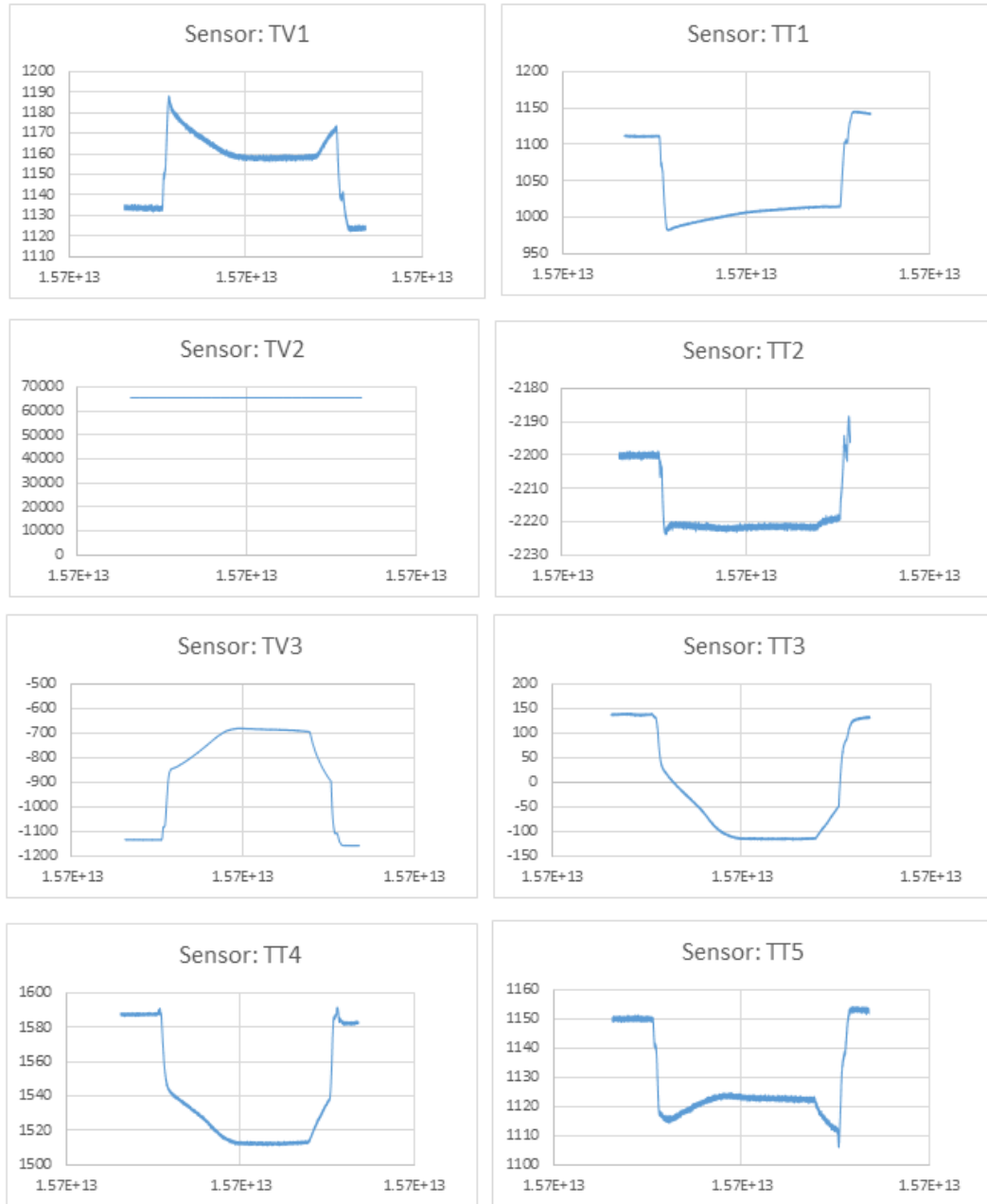
Appendix B

Analytical Steps for M-E Based RCC Thickness Design Procedure

To determine the appropriate design RCC thickness, a trial-and-error approach was performed using various input combinations with a trial thickness until the desired failure criterion is met. The following systematic procedure need to be considered to predict the pavement performance during the RCC thickness design:

- **Step 1:** Process input parameters

- **Step 2:** Determine saw-cut joint spacing

- **Step 3:** Determine loss of support along slab edge

- **Step 4:** Determine structural responses under traffic and environmental loading

- **Step 5:** Determine damage for each design increment

- **Step 6:** Determine pavement performance at the end of design life

Step 1: Process Input Parameters

- Process materials properties data

  — Determination of RCC modulus of elasticity, flexural strength for each monthly increment i throughout the design period based on level of user inputs

  — Determination of RCC relative humidity for each month

  — Determination of RCC drying shrinkage for each month

Figure B1. Change in PCC modulus of elasticity and flexural strength throughout the design period
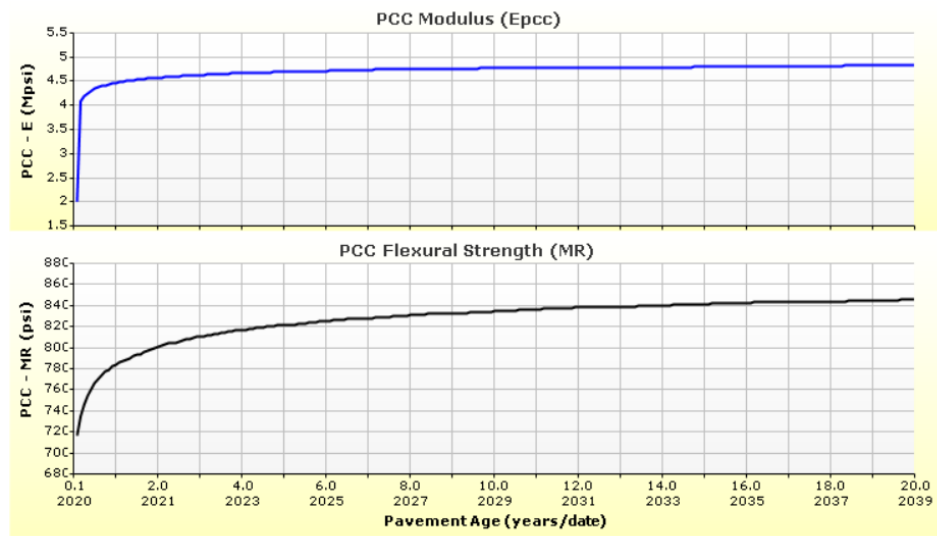
Figure B2. PCC material properties

PCC	
Thickness (in)	6.0
Unit weight (pcf)	150.0
Poisson's ratio	0.2

Thermal	
PCC coefficient of thermal expansion (in/in/°F x 10^-6)	4.9
PCC thermal conductivity (BTU/hr-ft-°F)	1.25
PCC heat capacity (BTU/lb-°F)	0.28

Mix		
Cement type		Type I (1)
Cementitious material content (lb/yd^3)		600
Water to cement ratio		0.42
Aggregate type		Dolomite (2)
PCC zero-stress temperature (°F)	Calculated Internally?	True
	User Value	-
	Calculated Value	76.9
Ultimate shrinkage (microstrain)	Calculated Internally?	True
	User Value	-
	Calculated Value	629.8
Reversible shrinkage (%)		50
Time to develop 50% of ultimate shrinkage (days)		35
Curing method		Curing Compound

PCC strength and modulus (Input Level: 3)	
28-Day PCC modulus of rupture (psi)	700.0
28-Day PCC elastic modulus (psi)	4000000.0

— Determination base modulus of elasticity for each month

— Determination subgrade k-value for each month

— Estimation base erodibility for each annual increment i
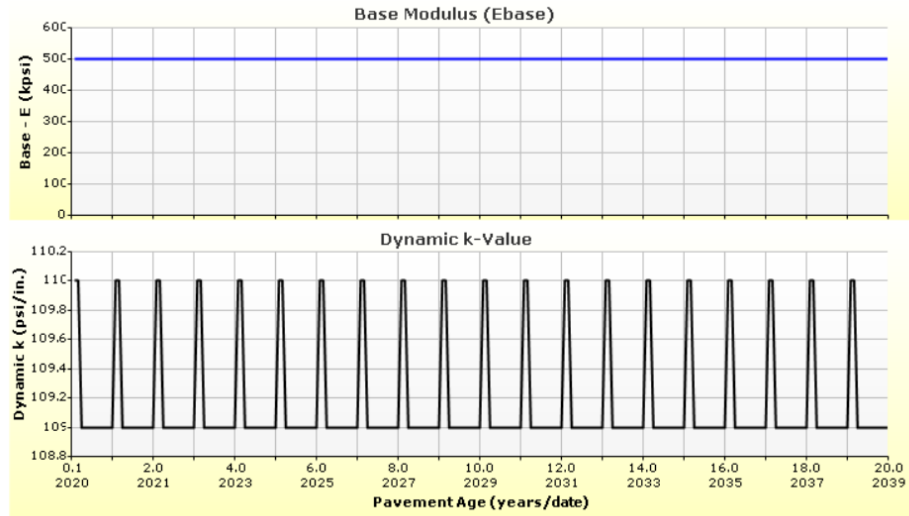
- Process traffic data

Determination of traffic parameters need to be similar to current pavement ME approach considering vehicle class distribution throughout the design period.

Figure B4. Vehicle class distribution

Month	Vehicle Class									
	4	5	6	7	8	9	10	11	12	13
January	1.0	1.0	1.0	1.0	1.0	1.0	1.0	1.0	1.0	1.0
February	1.0	1.0	1.0	1.0	1.0	1.0	1.0	1.0	1.0	1.0
March	1.0	1.0	1.0	1.0	1.0	1.0	1.0	1.0	1.0	1.0
April	1.0	1.0	1.0	1.0	1.0	1.0	1.0	1.0	1.0	1.0
May	1.0	1.0	1.0	1.0	1.0	1.0	1.0	1.0	1.0	1.0
June	1.0	1.0	1.0	1.0	1.0	1.0	1.0	1.0	1.0	1.0
July	1.0	1.0	1.0	1.0	1.0	1.0	1.0	1.0	1.0	1.0
August	1.0	1.0	1.0	1.0	1.0	1.0	1.0	1.0	1.0	1.0
September	1.0	1.0	1.0	1.0	1.0	1.0	1.0	1.0	1.0	1.0
October	1.0	1.0	1.0	1.0	1.0	1.0	1.0	1.0	1.0	1.0
November	1.0	1.0	1.0	1.0	1.0	1.0	1.0	1.0	1.0	1.0
December	1.0	1.0	1.0	1.0	1.0	1.0	1.0	1.0	1.0	1.0

Figure B5. Traffic parameters and hourly distribution

Distributions by Vehicle Class

Vehicle Class	AADTT Distribution (%) (Level 3)	Growth Factor	
		Rate (%)	Function
Class 4	1.3%	2%	Linear
Class 5	8.5%	2%	Linear
Class 6	2.8%	2%	Linear
Class 7	0.3%	2%	Linear
Class 8	7.6%	2%	Linear
Class 9	74%	2%	Linear
Class 10	1.2%	2%	Linear
Class 11	3.4%	2%	Linear
Class 12	0.6%	2%	Linear
Class 13	0.3%	2%	Linear

Truck Distribution by Hour

Hour	Distribution (%)	Hour	Distribution (%)
12 AM	2.3%	12 PM	5.9%
1 AM	2.3%	1 PM	5.9%
2 AM	2.3%	2 PM	5.9%
3 AM	2.3%	3 PM	5.9%
4 AM	2.3%	4 PM	4.6%
5 AM	2.3%	5 PM	4.6%
6 AM	5%	6 PM	4.6%
7 AM	5%	7 PM	4.6%
8 AM	5%	8 PM	3.1%
9 AM	5%	9 PM	3.1%
10 AM	5.9%	10 PM	3.1%
11 AM	5.9%	11 PM	3.1%
		Total	100%

Axle Configuration

Traffic Wander	
Mean wheel location (in)	18.0
Traffic wander standard deviation (in)	10.0
Design lane width (ft)	12.0

Axle Configuration	
Average axle width (ft)	8.5
Dual tire spacing (in)	12.0
Tire pressure (psi)	120.0

Average Axle Spacing	
Tandem axle spacing (in)	51.6
Tridem axle spacing (in)	49.2
Quad axle spacing (in)	49.2

Wheelbase			
Axle Type / Value Type	Short	Medium	Long
Average spacing of axles (ft)	12.0	15.0	18.0
Percent of Trucks (%)	17.0	22.0	61.0

Number of Axles per Truck

Vehicle Class	Single Axle	Tandem Axle	Tridem Axle	Quad Axle
Class 4	1.62	0.39	0	0
Class 5	2	0	0	0
Class 6	1.02	0.99	0	0
Class 7	1	0.26	0.83	0
Class 8	2.38	0.67	0	0
Class 9	1.13	1.93	0	0
Class 10	1.19	1.09	0.89	0
Class 11	4.29	0.26	0.06	0
Class 12	3.52	1.14	0.06	0
Class 13	2.15	2.13	0.35	0

- Process temperature profile data

Determination of the equivalent linear temperature gradient for each hour of every day over the design period need to be similar to EICM concept and using available data from weather station. These linear temperature gradients need to be extrapolated over the design life to compute combine temperature curling and load stresses of the RCC pavement.

Figure B6. Temperature data over the design period
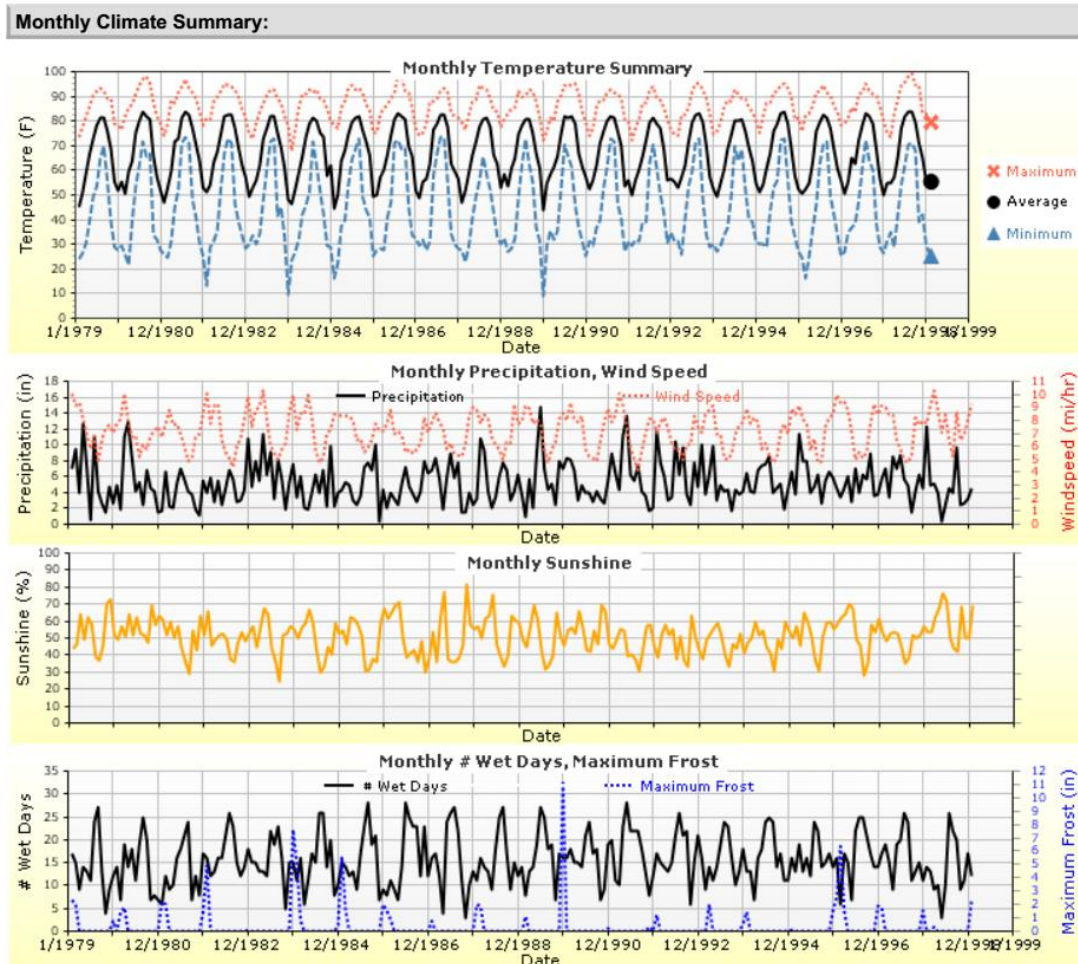
Step 2: Determine Saw-Cut Joint Spacing

The saw-cut joint spacing is to minimize thermal and moisture curling of the slab, but spacing the sawed joints too close together would result in higher construction and maintenance costs than necessary, thereby reducing some of the benefit of using RCC pavements. The saw-cut joint spacing will also significantly affect the long term joint movement and pavement performance. It is necessary to determine the saw-cut joint spacing for the prediction of the critical tensile stresses for fatigue accumulation and potential joint faulting. Drying shrinkage and coefficient of thermal expansion need to be primary contributors to early crack initiation at the saw cut joints in RCC pavement. The effect of slab curling on the development of cracking at saw-cut joints and long term joint movement in the RCC pavement need to be investigated in addition to joint deflections and load transfer efficiency (LTE). A separate algorithm can be used to determine the

optimum saw cut joint spacing based on the pavement structure, material properties and weather data.

To determine the spacing of naturally occurring cracks in RCC pavements, a cracking model is adopted considering the development of the axial stress due to uniform thermal contraction and drying shrinkage. The model uses a one-dimensional analysis that ignores the effects of stresses or strains in directions other than along the length of the slab, assuming that the RCC slab is linear elastic and the base beneath is a rigid material. A RCC slab with length (L), width (W) and thickness (H) is modeled, for which x is the direction parallel to the slab length and the end of the slab are located at x=0 and x=L. The slab will contract symmetrically about its center as its volume decreases either from drying shrinkage or thermal contraction. The sliding of the slab along the base course develops frictional forces along the interface, which are proportional to the movement of the slab. The basis of the model is characterized by a differential equation proposed by Zhang and Li (2001) [78] and the axial stress for two cases are obtained by solving the differential equations and can be directly use for calculating the maximum stress. The following two cases can be directly used for the prediction of the axial stress:

Case 1 : $|u(0)| \leq \delta_0$, thus

$$\sigma_{axial} = E\varepsilon_e \left(\frac{\cosh \beta (\frac{L}{2}-x)}{\cosh(\frac{\beta L}{2})} - 1 \right) + \sigma_o \frac{\cosh \beta (\frac{L}{2}-x)}{\cosh(\frac{\beta L}{2})}$$

When the $\frac{d\sigma_{axial}}{dx} = 0$ from above equation, and $x = L/2$. the maximum average stress σ_{am} occurs at $L/2$:

$$\sigma_{am} = E\varepsilon_e \left(\frac{1}{\cosh(\frac{\beta L}{2})} - 1 \right) + \sigma_o \frac{1}{\cosh(\frac{\beta L}{2})}$$

And $u(0) = -\frac{1}{\beta}(\frac{\sigma_o}{E} + \varepsilon_e) \frac{1-e^{-\beta L}}{1+e^{\beta L}}$

Case 2: $u(0) \geq \delta_0$ and $u(x_o) = \delta_0$, thus

$$\sigma_{axial} = E\varepsilon_e \left(\frac{\cosh(\beta(\frac{L}{2}-x))}{\cosh(\beta(\frac{L}{2}-x_o))} - 1 \right) + (E\beta^2 \delta_o x_o + \sigma_o) \frac{\cosh(\beta(\frac{L}{2}-x))}{\cosh(\beta(\frac{L}{2}-x_o))}$$

When the $\frac{d\sigma_{axial}}{dx} = 0$ from above equation, and $x = L/2$. Then, the maximum average stress σ_{am} at $L/2$:

$$\sigma_{am} = E\varepsilon_e \left(\frac{1}{\cosh(\beta(\frac{L}{2}-x_o))} - 1 \right) + (E\beta^2 \delta_o x_o + \sigma_o) \frac{1}{\cosh(\beta(\frac{L}{2}-x_o))}$$

Where, $\beta = \sqrt{\dfrac{\tau_o}{Eh\delta_o}}$ and σ_o: average axial stress at $x = 0$, usually considered zero at the crack face, and x_o is the coordinate value of x where the displacement $u(x)$ equals to δ_o, x_o can be determined by solving numerical equation below,

$$\delta_o = -\frac{1}{\beta}(\beta^2 \delta_o x_o + \varepsilon_e)\frac{e^{-\beta x_o} - e^{-\beta(L-x_o)}}{e^{-\beta x_o} + e^{-\beta(L-x_o)}}$$

The environment induced strain ε_e, consists of two components: $\varepsilon_e(t) = \varepsilon_T(t) + \varepsilon_{dry}(t)$, $\varepsilon_T(t) = \alpha \times \Delta T_{axial}$ is thermal strain due to uniform temperature change through the concrete slab thickness (mm/mm). $\Delta T_{axial} = (T_{axial} - T_{zs})$, where T_{zs}: zero stress temperature (°C) at which the stress is zero, and $\varepsilon_{dry}(t)$: uniform drying shrinkage strain of concrete slab (mm/mm).

The curling stress due to temperature gradient throughout the RCC pavement depth can be calculated based on the following equation.

$$\sigma_{curling} = \frac{E\alpha\Delta T_L}{2(1-v^2)}(C_x + vC_y)$$

Step 3: Determine Loss of Support along Slab Edge

The loss of support along the slab edge of the RCC pavement need to be calculated annually over the design life. If there is significant loss of support, the critical stress will increase resulting in more fatigue damage and eventually will affect the pavement performance. The critical deflection around the saw cut joint will also be influenced by the loss of support resulting in additional faulting related distresses. The estimation of the void or base erodibility need to be calculated for each annual increment.

Step 4: Determine Structural Responses under Traffic and Environmental Loading

Calculation of the critical slab stresses for all the cases that needs to be analyzed. The following factors should be considered during the analysis:

- Pavement Structure- slab size, shoulder type, slab base interface

- Load configuration- axle type

- Load level- different load magnitude based on axle type

- Temperature gradient- the effects of mean monthly temperature gradient, permanent curl/warp, and monthly variation in warping expresses as the effective temperature difference

- Lateral load positions- to consider traffic wandering

Finite element analysis program is required to predict the structural responses to incorporate all the factors mentioned above. The critical location for stress prediction in RCC pavement under both load and environmental effects needs to be evaluated as well.

Step 5: Determine Damage for each Design Increment

To evaluate accumulated fatigue damage due to slab bending, an incremental analysis need to be used in this procedure. The analysis period need to be subdivided into time increments based on pavement design life, concrete strength gains, subgrade support, and climatic conditions relative to their effect on pavement performance. Total fatigue damage will then be computed as a summation of fatigue damages developed during each analysis increment.

- Adjust base annual single and tandem annual axle load spectra for within year variations

- Adjust traffic for each within 24 hours probability of temperature gradients occurrence, seasonal cycle and annual traffic growth

- Determine probability of coverage function of a traffic passing at Gaussians points to account for traffic wander

- Determine number of axle load application at each Gaussian point based on probability of coverage function

- Obtain bending stresses at critical points using specified load offset position for each load level, progressive monthly and cyclic hourly increment.

- Calculate allowable load application for each cyclic hourly and seasonal increment

- Calculate fatigue damage at critical points due to axle load for progressive monthly and cyclic hourly increment, accounting for traffic wander

- Accumulate damage for each progressive monthly and cyclic hourly increment over all axle load level

Step 6: Determine Pavement Performance at the End of Design Life

In this Step, all the pavement performances and corresponding design reliability need to be determined to verify the design criterion. A sensitivity analysis will also be performed for prediction to calibration parameters.

- Calculate percent fatigue cracking from cracking model

- Calculate joint faulting due to erosion potential

- Calculate surface smoothness (IRI) at the end of design life

RCC pavement design need to be based on three performance criteria: fatigue cracking, erosion and smoothness. The designer can select some or all three performance criteria. For each selected performance measure, the designer must select the desired performance level at the end of design life (e.g., percent fatigue cracking, erosion damage, and IRI) and reliability level.

Considering the steps mentioned above, the table below was generated to predict the fatigue and erosion damage for the previously mentioned design example.

Table B1. Fatigue and erosion damage prediction for single axle

Single Axle					
Axle Load	Actual Traffic	Stress Ratio	Allowable traffic	% Fatigue	% Erosion
3000	8346.35	0.08	43108721140335	0.00	0.00
4000	6704.191	0.11	18470061633834	0.00	0.00
5000	10404.94	0.14	8015150821088	0.00	0.00
6000	9765.959	0.16	3513255579675	0.00	0.00
7000	11725.07	0.19	1552705407484	0.00	0.00
8000	16386.56	0.21	691043918924	0.00	0.00
9000	22608.12	0.24	309425649354	0.00	0.00
10000	26988.76	0.26	139293383128	0.00	0.00
11000	24711.74	0.28	63005977497	0.00	0.00
12000	17773.11	0.31	28622655421	0.00	0.07
13000	10763.13	0.33	13054168430	0.00	0.16
14000	7069.995	0.36	5975305787	0.00	0.24
15000	4636.308	0.38	2744250437	0.00	0.30
16000	3807.855	0.40	1264262987	0.00	0.41
17000	2886.271	0.43	584133058	0.00	0.49
18000	2341.522	0.45	270625218	0.00	0.59
19000	1802.843	0.47	125700582	0.00	0.66
20000	1372.081	0.50	58527077	0.00	0.69
21000	1000.773	0.52	27313116	0.00	0.69
22000	705.2248	0.55	12774101	0.01	0.64
23000	489.8759	0.57	5986716	0.01	0.58
24000	361.0106	0.59	2811284	0.01	0.55
25000	249.6657	0.61	1322637	0.02	0.48
26000	185.2244	0.64	623393	0.03	0.45
27000	150.0776	0.66	294331	0.05	0.45
28000	90.56534	0.68	139198	0.07	0.33
29000	74.67094	0.71	65937	0.11	0.34
30000	42.73333	0.73	31282	0.14	0.23
31000	38.82135	0.75	14863	0.26	0.26
32000	57.04667	0.78	7072	0.81	0.45
33000	24.01512	0.80	3370	0.71	0.22
34000	23.27329	0.82	1608	1.45	0.26
35000	10.84154	0.84	768	1.41	0.14
36000	19.53789	0.87	367	5.32	0.30
37000	6.041625	0.89	176	3.43	0.11
38000	7.351552	0.91	84	8.71	0.15
39000	5.42762	0.93	41	13.40	0.13
40000	5.446202	0.96	19	27.98	0.15
41000	0.00E+00	0.98	9	0.00	0.00

Table B2. Fatigue and erosion damage prediction for tandem axle

Tandem Axle					
Axle Load	Actual Traffic	Stress Ratio	Allowable traffic	% Fatigue	% Erosion
6000	7190.198	0.07	66510427356796	0.00	0.00
8000	8612.712	0.09	32603993143440	0.00	0.00
10000	14038.35	0.11	16155182137497	0.00	0.00
12000	16242.5	0.13	8072644098317	0.00	0.00
14000	16425.43	0.16	4061926751941	0.00	0.00
16000	14833.73	0.18	2055905348452	0.00	0.00
18000	12420.18	0.20	1045899026244	0.00	0.00
20000	11853.45	0.22	534479175833	0.00	0.00
22000	10947.71	0.24	274232506454	0.00	0.00
24000	10574.76	0.26	141216617144	0.00	0.01
26000	10911.65	0.28	72961198185	0.00	0.08
28000	11307.5	0.30	37811165712	0.00	0.24
30000	12434.41	0.32	19650340417	0.00	0.54
32000	12651.67	0.34	10238956184	0.00	0.97
34000	11360.56	0.36	5348126756	0.00	1.40
36000	8932.652	0.38	2799896769	0.00	1.68
38000	6343.474	0.40	1468987662	0.00	1.73
40000	4315.768	0.42	772285539	0.00	1.65
42000	2859.633	0.44	406793947	0.00	1.50
44000	1867.947	0.46	214667191	0.00	1.30
46000	1247.66	0.48	113478403	0.00	1.14
48000	821.2499	0.50	60087243	0.00	0.97
50000	554.0641	0.52	31866987	0.00	0.83
52000	366.6359	0.53	16926228	0.00	0.69
54000	245.8575	0.55	9003532	0.00	0.58
56000	179.2404	0.57	4795946	0.00	0.52
58000	112.7865	0.59	2558123	0.00	0.40
60000	72.03337	0.61	1366258	0.01	0.31
62000	53.23843	0.63	730615	0.01	0.27
64000	45.98003	0.65	391174	0.01	0.28
66000	44.74771	0.67	209681	0.02	0.33
68000	43.25873	0.69	112523	0.04	0.37
70000	24.16348	0.71	60450	0.04	0.25
72000	22.07321	0.73	32510	0.07	0.26
74000	20.54136	0.75	17502	0.12	0.29
76000	0.963729	0.76	9432	0.01	0.02
78000	0.464771	0.78	5088	0.01	0.01
80000	0.714657	0.80	2747	0.03	0.02
82000	0.00E+00	0.82	1485	0.00	0.00

Table B3. Fatigue and erosion damage prediction for tridem axle

Tridem Axle					
Axle Load	Actual Traffic	Stress Ratio	Allowable traffic	% Fatigue	% Erosion
12000	341.2185	0.13	8072644098317	0.00	0.00
15000	212.3451	0.17	2887830157133	0.00	0.00
18000	170.9857	0.20	1045899026244	0.00	0.00
21000	136.4286	0.23	382664145560	0.00	0.00
24000	117.8561	0.26	141216617144	0.00	0.00
27000	103.0555	0.29	52504603037	0.00	0.00
30000	104.2069	0.32	19650340417	0.00	0.00
33000	115.0316	0.35	7397763815	0.00	0.01
36000	141.3587	0.38	2799896769	0.00	0.03
39000	145.0193	0.41	1064855340	0.00	0.05
42000	138.047	0.44	406793947	0.00	0.07
45000	111.4405	0.47	156044028	0.00	0.09
48000	104.0504	0.50	60087243	0.00	0.12
51000	72.8217	0.53	23220404	0.00	0.12
54000	59.26818	0.55	9003532	0.00	0.14
57000	51.03563	0.58	3502079	0.00	0.16
60000	33.80499	0.61	1366258	0.00	0.14
63000	22.85476	0.64	534521	0.00	0.13
66000	22.00786	0.67	209681	0.01	0.16
69000	12.19963	0.70	82463	0.01	0.11
72000	14.36395	0.73	32510	0.04	0.17
75000	7.021216	0.75	12847	0.05	0.11
78000	5.738823	0.78	5088	0.11	0.11
81000	3.710436	0.81	2019	0.18	0.09
84000	2.993745	0.84	803	0.37	0.09
87000	1.695886	0.87	320	0.53	0.06
90000	1.240882	0.90	128	0.97	0.05
93000	1.303148	0.92	51	2.55	0.07
96000	0.616576	0.95	20	3.01	0.04
99000	0.417969	0.98	8	5.09	0.03
102000	0.529481	1.01	3	16.03	0.05